

Design and Development of a Next Generation Thermal Rock Bed Storage Experimental Facility

by

Stephanus Johannes Erasmus



*Thesis presented in partial fulfilment of the requirements
for the degree of Master of Engineering (Mechanical) in the
Faculty of Engineering at Stellenbosch University*

Supervisor: Prof. T.W. von Backström

Co-supervisor: Dr. M. Lubkoll
Prof. F. Dinter

April 2019

Declaration

By submitting this thesis electronically, I declare that the entirety of the work contained therein is my own, original work, that I am the sole author thereof (save to the extent explicitly otherwise stated), that reproduction and publication thereof by Stellenbosch University will not infringe any third party rights and that I have not previously in its entirety or in part submitted it for obtaining any qualification.

Date: April 2019

Copyright © 2019 Stellenbosch University
All rights reserved.



UNIVERSITEIT • STELLENBOSCH • UNIVERSITY
jou kennisvennoot • your knowledge partner

Plagiaatverklaring / Plagiarism Declaration

1. Plagiaat is die oorneem en gebruik van die idees, materiaal en ander intellektuele eiendom van ander persone asof dit jou eie werk is. *Plagiarism is the use of ideas, material and other intellectual property of another's work and to present it as my own.*
2. Ek erken dat die pleeg van plagiaat 'n strafbare oortreding is aangesien dit 'n vorm van diefstal is. *I agree that plagiarism is a punishable offence because it constitutes theft.*
3. Ek verstaan ook dat direkte vertalings plagiaat is. *I also understand that direct translations are plagiarism.*
4. Dienooreenkomstig is alle aanhalings en bydraes vanuit enige bron (ingesluit die internet) volledig verwys (erken). Ek erken dat die woordelike aanhaal van teks sonder aanhalingstekens (selfs al word die bron volledig erken) plagiaat is. *Accordingly all quotations and contributions from any source whatsoever (including the internet) have been cited fully. I understand that the reproduction of text without quotation marks (even when the source is cited) is plagiarism.*
5. Ek verklaar dat die werk in hierdie skryfstuk vervat, behalwe waar anders aangedui, my eie oorspronklike werk is en dat ek dit nie vantevore in die geheel of gedeeltelik ingehandig het vir bepunting in hierdie module/werkstuk of 'n ander module/werkstuk nie. *I declare that the work contained in this assignment, except where otherwise stated, is my original work and that I have not previously (in its entirety or in part) submitted it for grading in this module/assignment or another module/assignment.*

Studentenommer / Student number	Handtekening / Signature
Voorletters en van / Initials and surname	Datum / Date

Abstract

Design and Development of a Next Generation Thermal Rock Bed Storage Experimental Facility

S.J. Erasmus

*Department of Mechanical and Mechatronic Engineering,
University of Stellenbosch,
Private Bag X1, Matieland 7602, South Africa.*

Thesis: MEng (Mech)

April 2019

The value of concentrating solar power (CSP) plants lies in dispatchability, which is provided through an integrated cost-effective thermal energy storage system (TESS). Compared to current state of the art molten salt thermal energy storage systems, a rock bed thermal energy storage system has the potential to reduce both the capital costs and Levelized Cost of Electricity (LCOE) significantly. The Stellenbosch University (SU) first-generation rock bed thermal energy storage design served as a proof of concept while the second-generation rock bed design was designed for significant cost reduction. This work presents the third-generation rock bed TESS at SU, through partial re-design, predominantly aiming at maximizing the usable rock mass.

The rock bed thermal energy storage system is charged by air at a temperature of 650 °C. An existing experimental facility, based on the second-generation design, has recently been constructed. To modify the facility, a concept was developed with knowledge gathered from both the first and second-generation concepts. The new concept charges the rock bed from the top downwards, with a predicted near-linear thermocline progression, where the thermocline is defined as the transition layer from the high temperature to the low temperature within the rock bed. Although the concept has a higher capital cost, an improved performance is predicted for the entire system.

After development, the concept was adapted to the existing facility. Three experimental test campaigns were conducted, concluding with a multiple cycle test. This test consisted of three charge-discharge cycles, where the rock bed

was discharged to a minimum outlet temperature of 327 °C. Determining an accurate discharge mass flow rate was a challenge throughout testing, with flow leakages detected within the system. A flow loss assumption of 40 % was made after several cold air flow rates were tested. The second cycle within the multiple cycle test yielded a heating capacity of 336.67 kWh_{th}, a volumetric efficiency of 60.30 % and a thermal efficiency of 92.40 %. An overall efficiency of 94.24 % was achieved over the three cycles.

An analytical model was developed to be validated by the experimental results. From the validation, a possible prediction can be made on the performance of such a rock bed thermal energy storage system on an industrial scale. The thermal efficiency comparison yielded a maximum difference between the experimental and analytical results of +8.00 % for the first two cycles and +19.36 % for the third cycle. It is clear from this comparison that the model over-predicts the performance of the facility. Considering that the model is one dimensional and that it disregards both radiation and convection as heat transfer elements, as well as thermal losses, the model appears to be acceptable. However, it is recommended that further improvements be made to the model for a more accurate comparison.

The overall results show that there has been an improvement in performance of the rock bed after the design changes that were made. These design changes include the addition of insulation and introducing the high temperature air into the top of the rock bed, rather than at the bottom. Room for improvement on the design to achieve higher overall performance has been identified and possible solutions are presented within this project.

Uittreksel

Ontwerp en Ontwikkeling van 'n Volgende Generasie Termiese Klip Stoor Eksperimentele Fasiliteit

(“Design and Development of a Next Generation Thermal Rock Bed Storage Experimental Facility”)

S.J. Erasmus

*Departement Meganiese en Megatroniese Ingenieurswese,
Universiteit van Stellenbosch,
Privaatsak X1, Matieland 7602, Suid-Afrika.*

Tesis: MIng (Meg)

April 2019

Die waarde van gekonsentreerde sonkragaanlegte lê in versendbaarheid, wat deur 'n geïntegreerde koste-effektiewe termiese energie stoorstelsel voorsien word. 'n Termiese energie stoorstelsel wat bestaan uit 'n klipbed, het die potensiaal om die kapitaalkoste aansienlik te verminder in vergelyking met die huidige gesofistikeerde sout termiese energie stoorstelsels. Die tweede-generasie klipbed was ontwerp vir beduidende kostevermindering. Hierdie projek lê die derde-generasie klipbed termiese energie stoorstelsel by Stellenbosch UNiversiteit voor, en fokus op die gedeeltelike her-ontwerp van die tweede-generasie stelsel, wat hoofsaaklik daarop gemik is om bruikbare klipmassa te maksimeer.

Die klipbed termiese energie stoorstelsel maak gebruik van lug teen 'n temperatuur van 650 °C as hitteruilings vloeistof. 'n Ontwikkelde eksperimentele fasiliteit, gebaseer op die tweede-generasie ontwerp, bestaan reeds. Elemente van beide die eerste en tweede-generasie ontwerpe was in ag geneem om 'n verbeterde konsep te ontwerp. Die nuwe konsep laai die klipbed van bo na onder, met 'n voorspelde naby-lineêre termofront progressie. Alhoewel die konsep 'n hoër kapitaalkoste het, word 'n verbeterde prestasie vir die algehele stelsel voorspel.

Na die ontwerpfase is die konsep aangepas tot die bestaande eksperimentele fasiliteit. Na afloop van die konstruksie was drie eksperimentele toetse uitgevoer, met 'n meervoudige siklus toets die laaste en belangrikste. Hierdie toets het

bestaan uit drie laai-ontlaai siklusse, waar die stelsel elke keer ontlaai was tot \acute{n} minimum uitlaat temperatuur van $327\text{ }^{\circ}\text{C}$. Die bepaling van \acute{n} akkurate massa vloeitempo was \acute{n} uitdaging gedurende die eksperimentele toetse as gevolg van vloei lekkasies wat plaasgevind het in die sisteem. \acute{n} Vloei verlies van 40% was gebruik as aanname na verskeie koue lug vloeitempo toetse. Die tweede siklus van die toets het \acute{n} verhittingskapasiteit van $336.67\text{ kWh}_{\text{th}}$ gelewer, te-same met \acute{n} volumetriese effektiwiteit van 60.30% en 'n termiese effektiwiteit van 92.40% . Die meervoudige siklus toets het \acute{n} algehele doeltreffendheid van 94.24% bereik.

\acute{n} Analitiese model was ontwikkel vir die moontlike voorspelling rakende die prestasie van die nuwe konsep op \acute{n} industriële skaal. Die eksperimentele resultate was gebruik om die model te verifiër, deur die resultate te vergelyk. Die vergelyking het 'n maksimum verskil van $+8.00\%$ gelewer na die analitiese model se rigting vir die eerste twee siklusse en $+19.36\%$ vir die derde siklus. Hierdie verskil was tussen die eksperimentele resultate en analitiese model se termiese doeltreffendheid. Indien dit in ag geneem word dat die model slegs een-dimensioneel is en beide konveksie en radiasie ignoreer as hitteoordrag elemente, sowel as hitteverlies na buite elemente, is die model aanvaarbaar. Daar word wel aanbeveel dat verdere verbeteringe aangebring word tot die model om \acute{n} meer akkurate vergelyking te tref.

Die algehele resultate toon dat daar \acute{n} definitiewe verbetering is in terme van die prestasie van die stoorstelsel na die veranderinge wat plaasgevind het. Die toevoeging van insulasie en die laai van die klipbed van bo word gesien as positiewe veranderinge. Daar is egter nog baie ruimte vir verbetering om selfs hoër doeltreffendhede te bereik. Aanbevelings om die stoorstelsel te verbeter word binne hierdie projek gemaak.

Acknowledgements

I would like to express my sincere gratitude to the following people and organisations:

- Professor Theo von Backström for his expertise, guidance and project funding.
- Doctor Matti Lubkoll for asking the tough questions.
- Professor Frank Dinter for his expertise and the opportunity to work at Universidade de Évora.
- Jeannie Erasmus for language editing.
- Henk Laubscher for his ideas and expertise.
- Solar Thermal Energy Research Group (STERG) for project funding.

- Friends and family for their support throughout the project.
- Special thanks to those that helped during construction: Nico Erasmus, Stefan Kellerman, Charl du Toit, Jan Bouwer and the mechanical workshop at Stellenbosch University.

- My Mother, Father, Sister and Brother. Their unconditional love and support are instrumental to the person I am today.

Dedications

*Hierdie tesis word opgedra aan Ons Hemelse Vader en my familie. Sonder
Hulle onvoorwaardelike liefde, geduld en leiding is ek waarlik niks.*

Psalm 95:1-4.

*Kom, laat ons jubel tot eer van die Here, laat ons juig oor die rots by wie ons
redding vind, laat ons Hom toejuig met lofsange, want die Here is die magtige
God, die groot koning oor al die gode.*

Contents

Declaration	i
Abstract	iii
Uittreksel	v
Acknowledgements	vii
Dedications	viii
Contents	ix
List of Figures	xii
List of Tables	xiv
List of Symbols	xv
1 Introduction	1
1.1 General Introduction	1
1.1.1 Solar Energy	1
1.1.2 SUNSPOT Cycle	3
1.1.3 Rock Bed TESS at Stellenbosch University	4
1.2 Methodology	6
1.2.1 Problem Statement	6
1.2.2 Aims	7
1.3 Motivation and Objectives	7
1.3.1 Motivation	7
1.3.2 Objectives	8
1.4 Research Scope	8
1.4.1 Project Scope	8
1.4.2 Experimental Testing Scope	8
1.4.3 Analytical Model Scope	9
2 Literature Review	10

2.1	Introduction	10
2.2	Previous Rock Bed Research	10
2.2.1	Liquid	11
2.2.2	Gas	12
2.3	Rock bed TESS at Stellenbosch University	14
2.4	Techno-Economic Study	16
2.5	Chapter Summary	17
3	Development of Next-Generation System	19
3.1	Introduction	19
3.2	Concept Criteria	19
3.3	Concept Generation	20
3.4	Concept Evaluation	22
3.5	Design	23
3.6	Chapter Summary	25
4	Experimental Facility Construction and Test Setup	26
4.1	Introduction	26
4.2	Construction	26
4.3	Experimental Setup	32
4.4	Experimental Equipment	33
4.4.1	Temperature Measurement	34
4.4.2	Data and Flow Measurement	35
4.5	Efficiencies	37
4.5.1	Thermal Efficiency	37
4.5.2	Volumetric Efficiency	37
4.5.3	Overall Efficiency	37
4.6	Capital Cost	38
4.7	Chapter Summary	38
5	Experimental Campaigns and Results	39
5.1	Introduction	39
5.2	Procedure	39
5.3	Experimental Campaigns	39
5.3.1	Initial Test	40
5.3.2	Single Charge-Discharge Test	43
5.3.3	Multiple Cycle Test	46
5.4	Chapter Summary	56
6	Analytical Model and Results Comparison	57
6.1	Introduction	57
6.2	Methodology	57
6.2.1	Model Restrictions	58
6.2.2	Heat Transfer	58

6.2.3	Energy Balance	61
6.2.4	Pressure Drop	62
6.3	Simulation and Result Comparison	62
6.3.1	Simulation	63
6.3.2	Comparison of Results	68
6.4	Chapter Summary	72
7	Conclusion and Recommendations	73
7.1	Conclusion	73
7.2	Recommendations	74
	Appendices	75
A	Material Specification	76
A.1	Insulation	76
A.2	Stainless Steel	82
B	Safety Report	83
C	Operation Manual	91
C.1	Components	91
C.2	Charge Cycle Procedure	92
C.3	Discharge Cycle Procedure	99
D	Lessons Learned	101
D.1	Tarpaulin Cover	101
D.2	Flow Measurement	101
D.3	Hot Air Pipe	102
D.4	Mesh Frame	102
	List of References	103

List of Figures

1.1	DNI of South Africa	2
1.2	Parabolic trough CSP plant system layout	3
1.3	The SUNSPOT cycle	4
1.4	First rock bed experimental facility at SU	5
1.5	Second rock bed experimental facility at SU	6
2.1	Schematic of a laboratory-scale experimental facility	12
2.2	Schematic of first industrial pilot-scale facility	13
2.3	Ait Baha packed rock bed facility	13
2.4	Kröger’s packed bed concept	14
2.5	Gauchè’s packed bed concept	15
2.6	Charging cycle	16
2.7	Discharging cycle	16
2.8	Cost comparison	17
3.1	Concept illustration	21
3.2	Insulation layers	22
3.3	Adapted concept	23
3.4	One section of the spider web structure	24
3.5	Complete spider web structure	25
4.1	Hot air outlet pipe modified	28
4.2	Installation of the frame sections	29
4.3	Shaping of the rock pile	29
4.4	Insulation installation phase	30
4.5	Cold air outlet/inlet	30
4.6	Flow leak test results	31
4.7	Rock bed with dimensions	32
4.8	Experimental facility located at SUNREC	32
4.9	Charge cycle flow diagram	33
4.10	Discharge cycle flow diagram	33
4.11	Schematic of the thermocouple layout	34
4.12	Position of the thermocouples	34
4.13	Data logger	35

4.14	Pressure transducer and its specifications	36
4.15	Bell-mouth pressure drop over air flow rate	36
5.1	Rock bed temperature distribution - Charge cycle	41
5.2	End of the idle period of 60 hours	42
5.3	Thermal losses identified at the hot air inlet/outlet elbow	42
5.4	Initial temperature distribution - Test 2	43
5.5	Rock bed temperature distribution - Charge cycle	44
5.6	Discharge temperature over time - Second test	45
5.7	Scaffolding erected over the facility	46
5.8	Leakage areas	47
5.9	Leakage areas fixed	47
5.10	Initial temperature distribution - Multiple cycle test	48
5.11	Rock bed temperature distribution - First cycle	49
5.12	Rock bed temperature distribution - First idle period	50
5.13	Rock bed temperature distribution - Second cycle	51
5.14	Rock bed temperature distribution - Second idle period	52
5.15	Rock bed temperature distribution - Third cycle	53
5.16	Discharge temperature over time - Multiple cycle test	54
6.1	Computational domain of the cross-sectional area progression	58
6.2	Temperature distribution over position - Cycle 1	64
6.3	Temperature distribution over position - Cycle 2	64
6.4	Temperature distribution over position - Cycle 3	65
6.5	Biot number	66
6.6	Nusselt number	67
6.7	Pressure gradient	68
6.8	Discharge temperature over time comparison	71
6.9	Improved discharge temperature over time comparison	71
C.1	The electrical box housing all main switches	93
C.2	Vaporizer Switch	93
C.3	The main setup that runs the cycles	94
C.4	The valve setup for a charge cycle	94
C.5	VSD that controls the centrifugal fan	95
C.6	Gas train	96
C.7	Gashouse housing the LPG bottles	96
C.8	The vaporizer	97
C.9	Gas valve 1	97
C.10	Gas valve 2	98
C.11	Valve 3	98
C.12	Burner Control Panel	99
C.13	Hatch	100

List of Tables

1.1	Experimental results from the previous-generation facility	6
2.1	Relevant rock bed TESS research	11
3.1	Concept development criteria	20
3.2	Concept evaluation	22
4.1	Construction procedure	27
4.2	Updated capital cost of the facility	38
5.1	Test campaigns.	40
5.2	Results - Initial test.	43
5.3	Results - Second test	46
5.4	Multiple cycle results	55
5.5	Comparison of second-and third-generation results	56
6.1	Initial parameters	63
6.2	Comparison of the first charge-discharge cycle.	68
6.3	Comparison of the second charge-discharge cycle.	69
6.4	Comparison of the third charge-discharge cycle.	70
C.1	TESS components	92

List of Symbols

SYMBOL	DESCRIPTION	UNITS
A_{cs}	cross-sectional area	[m ²]
c_p	heat capacity	[J/(kg K)]
D_v	rock diameter	[m]
E	energy	[kJ]
f_v	friction factor	[–]
G	mass flux	[kg/(m ² s)]
h	height	[m]
h_v	heat transfer coefficient	[W/(m ² K)]
k	thermal conductivity	[W/(m K)]
L	progression length	[m]
ΔL	segment thickness	[m]
$LCOE$	levelized cost of electricity	[–]
MWh_{th}	thermal energy	[MWh]
\dot{m}	mass flow rate	[kg/s]
NTU	number of transfer units	[–]
Nu	Nusselt number	[–]
p	pressure	[Pa]
ΔP	pressure drop	[Pa]
\dot{Q}	energy rate	[kJ/s]
r	radius	[m]
Δ_r	radius difference	[m]
Re	Reynolds number	[–]
SM	solar multiple	[–]
T	temperature	[°C, K]
t	time	[s]
Δt	time step	[s]
v	superficial velocity	[m/s]

x	x-position	[m]
y	y-position	[m]

GREEK SYMBOLS

α	progression angle	[°]
β	rock bed surface angle	[°]
ε	void fraction	[–]
η	heat transfer efficiency	[–]
μ	air viscosity	[kg/m.s]
π	pi	[.]
ρ_a	air density	[kg/m ³]
ρ_r	rock density	[kg/m ³]
τ	time constant	[–]

SUBSCRIPTS

a	air
amb	ambient
i	inside
in	input
o	outside
out	output
p	particle(rock)
r	rock
s	surface
st	stored
th	thermal
v	volumetric

ABBREVIATIONS

CSP	concentrating solar power
DHI	Direct Horizontal Irradiation
DNI	Direct Normal Irradiation
e-NTU	effective number of transfer units
GHI	Global Horizontal Irradiation
HTF	heat transfer fluid
PCM	phase change material
SNL	Sandia National Laboratories
STERG	Solar Thermal Energy Research Group
SU	Stellenbosch University
SUNSPOT	Stellenbosch UNiversity Solar POver Thermodynamic cycle
SUNREC	Stellenbosch UNiversity Renewable Energy Center
TESS	thermal energy storage systems

Chapter 1

Introduction¹

1.1 General Introduction

The value of CSP, compared to Photovoltaic (PV), lies in dispatchability through TESS. Kolb *et al.* (2011) estimates that 13 % of capital costs within a CSP plant is contributed by thermal energy storage systems (TESS) and it has been targeted as an area for future cost reduction. Currently, the primary method of storing energy in concentrating solar power (CSP) plants is two-tank molten salt TESS. According to a capital cost estimation of 8-15 US\$/kWh_{th} by Allen *et al.* (2016), Rock bed TESS has the potential to reduce storage capital costs significantly, with current state of the art two-tank molten salt TESS contributing 22-30 US\$/kWh_{th} to the capital cost (Herrmann *et al.*, 2004).

1.1.1 Solar Energy

According to the latest statistics by the International Renewable Energy Agency (IRENA) (2018), the current total renewable energy capacity of South Africa is 4 959 MW. Of the total capacity, 2 014 MW is contributed by solar energy, of which only 14.8 % is concentrated solar power. Of all the renewable sources, the potential of solar energy is the greatest. In the case where solar energy reaches its potential, all electricity used in the world will be generated by solar energy alone (Wait But Why, 2014).

The resource for solar energy is irradiation from the sun, with Direct Normal Irradiation (DNI) being the main contributor (Stine and Geyer, 2001). DNI is irradiation that directly reaches the surface of the earth. Other irradiation types include; Diffuse Horizontal Irradiation (DHI), which is indirect irradiation that reaches the earth's surface due to clouds, and Global Horizontal Irradiation (GHI), which is the total irradiation that reaches the earth's

¹Parts of this chapter have been published in Erasmus *et al.* (2018a) and Erasmus *et al.* (2018b)

surface. Figure 1.1 depicts the intensity of DNI in South Africa, showing that the country has great potential for the use of solar energy.

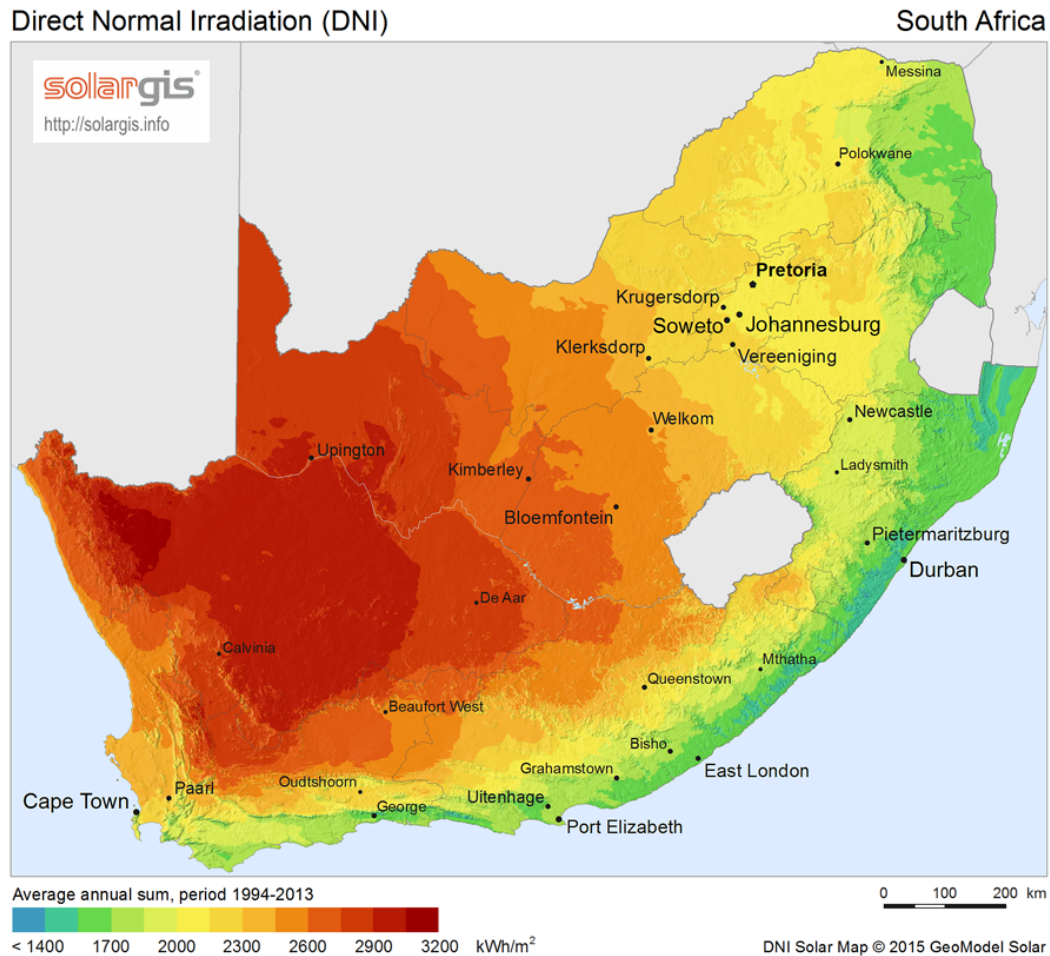


Figure 1.1: DNI of South Africa (SolarGIS, 2015)

CSP plants are used in industry to generate electricity from the solar resources for everyday use. In concept, the DNI is concentrated by either heliostats or parabolic troughs, to a focus point or line, to heat up a heat transfer fluid (HTF). This fluid is then used in a heat exchanger, transferring heat from the fluid to steam. In turn the steam is then used for generating electricity through a steam turbine.

Due to the solar resource being accessible only during daytime, a thermal storage system is introduced into the above explained process. The plant is designed in such a way, by using Solar Multiple (SM), that enough solar

energy is captured to ensure that the storage receives heat during peak irradiation hours of the day. Solar Multiple is defined as the aperture area of a solar field in relation to the capacity of the power cycle (Trieb *et al.*, 2009). For example, a SM of 1 would entail that the solar field is big enough to meet the capacity of the power cycle during peak irradiation. Thus, by increasing the solar multiple, excess thermal energy can be stored.

The system for a parabolic through CSP plant is illustrated in Figure 1.2. Here oil is used as heat transfer fluid within the solar field, with a heat exchanger situated between the molten salt, which is used for thermal storage, and oil cycles. Steam is used in the power block cycle as working fluid. Between the solar field cycle and the power block cycle there are various heat exchangers to ensure that the maximum amount of heat available is transferred between the cycles.

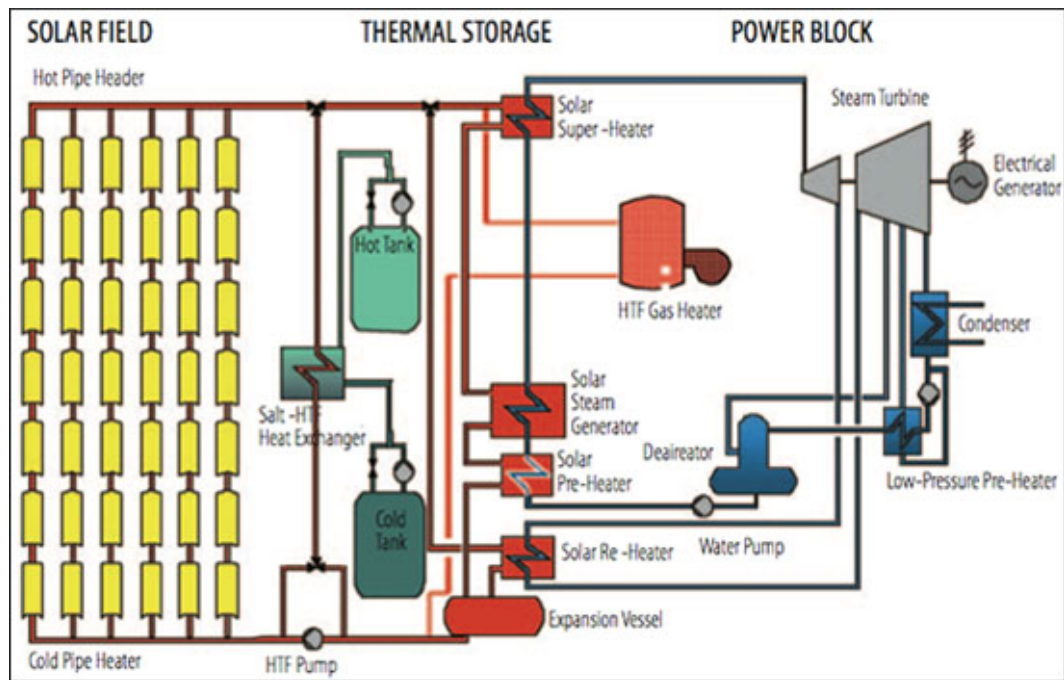


Figure 1.2: Parabolic trough CSP plant system layout (EAI, 2017)

1.1.2 SUNSPOT Cycle

Currently at Stellenbosch University's Mechanical and Mechatronic Engineering Department research is being conducted on the development of different solar thermal power generating plants. Stellenbosch University Solar Power Thermodynamic cycle (SUNSPOT) is one such concept, which was proposed by Professor Kröger in 2008. Figure 1.3 illustrates the SUNSPOT cycle.

The SUNSPOT cycle focuses on using ambient air as heat transfer fluid. In the cycle a packed rock bed is used for thermal energy storage. Each component of the cycle is being extensively researched at Stellenbosch University's Solar Thermal Energy Group (STERG) and developed in tandem with the goal of introducing a low-cost solar thermal power option to the industry.

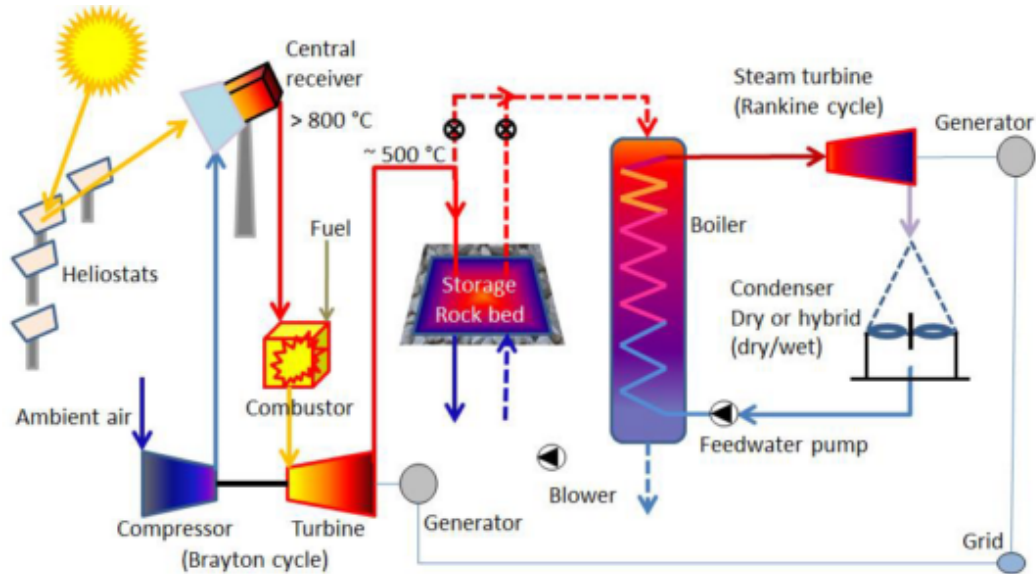


Figure 1.3: The SUNSPOT cycle (Kröger, 2011)

1.1.3 Rock Bed TESS at Stellenbosch University

Two rock bed TESS experimental facilities have been developed at Stellenbosch University (SU), the first by Allen *et al.* (2015) and the second by Laubscher (2017).

The first facility, known as the Sauna, is a small 3-ton packed rock bed as seen in Figure 1.4. The facility was used by Allen *et al.* (2015) to develop and validate the heat transfer and pressure drop theory for packed rock bed TESS. This theory will be used within this project to develop an analytical model, which will be validated by experimental results. Visible in Figure 1.4 is the rock type that is used, namely dolerite. The facility consists of three layers of rock, with the hot air being introduced at the top during charge. The hot air is supplied by a diesel burner and fan. This facility allows for the testing of various shapes and sizes of rock and other materials.



Figure 1.4: First rock bed experimental facility at SU (Allen *et al.*, 2015)

The second experimental facility, erected by Laubscher (2017), is based on a concept introduced by Gauché and Louw (2014). A discussion of the concept can be found in section 2.2. This 65-ton facility is shown in Figure 1.5. The facility makes use of Dolerite and Hornfels as material, with an approximate rock size of 50 mm in width and 25 mm in height. The purpose of the facility is to conduct experiments on a much larger scale, investigating the behavior of the temperature distribution and thermocline during charge-discharge cycles. Key findings of Laubscher (2017) are listed in Table 1.1 and will be used as a benchmark. This project proposes a next-generation concept of the facility, improving the performance of the previous-generation rock bed TESS concept, through partial re-design, predominantly aiming at maximizing both the thermal and volumetric efficiencies.



Figure 1.5: Second rock bed experimental facility at SU

Table 1.1: Experimental results from the previous-generation facility (Laubscher, 2017)

Property	Value	SI Unit
Average charge mass flow rate	0.48	kg/s
Average charge temperature	638	°C
Charge duration	3.50	h
Charging capacity	0.318	MW _{th}
Energy input	1.031	MWh _{th}
Average discharge mass flow rate	0.48	kg/s
Discharge duration	2.75	h
Useful energy output	0.619	MWh _{th}
Total pressure drop	280.00	Pa
Thermal efficiency	60.00	%
Volumetric efficiency	33.00	%
Minimum discharge temperature	327	°C

1.2 Methodology

1.2.1 Problem Statement

Within the Renewable Energy community, research on improving solar energy systems has taken the front seat not only in South Africa, but across the world. The focus was firstly to develop systems that can harvest the energy from the

sun to generate electricity for everyday use. These include systems such as PV and CSP. Unfortunately, these systems had one big flaw: They cannot be used to generate electricity when the sun is unavailable (cloudy days and at night).

This big flaw was solved by the introduction of TESS into the CSP industry, setting the industry apart from the rest. Although TESS are a necessity to ensure electricity generation during non-sun circumstances, these storage systems increased the capital costs of CSP plants. This created an opportunity for low-cost TESS concepts to be developed.

To achieve a low-cost TESS, innovation must take the forefront. Expensive elements such as the material, heat transfer fluid, filler and construction should be investigated for cost reduction opportunities. The TESS should still be efficient in performance, thus an optimized design must be reached. Efficiency in a TESS is defined as the recovery of heat from the TESS, where energy input is compared to useful energy output.

1.2.2 Aims

This project's research aim is to develop an efficient and cost-effective TESS concept through partial re-design of the previous-generation concept, experimental test campaigns and the development of an analytical model. The model will be validated by results obtained from the experimental test campaigns. The model will be based on theory developed and validated by Allen (2014). Validation of the model will enable the ability to predict the performance of an industrial-scale TESS in the future. The objectives and the motivation behind the project is described in Section 1.3. Dependent on the outcome of this project, recommendations on improvements can be made.

1.3 Motivation and Objectives

1.3.1 Motivation

The motivation is to generate and build a concept that is more cost-effective than molten salt storage, without decreasing the efficiency of the system (Allen, 2010). After the completion of the previous project, the outcomes indicated that there is still progress to be made regarding the research of thermal rock bed storage.

By taking the current facility and introducing an alternative concept, the facility is expected to reach higher efficiencies regarding thermal and volumetric efficiency, with the capital expenditure and levelized cost of electricity (LCOE) being reduced.

1.3.2 Objectives

The objectives of the project are:

1. Reduce the thermal losses of the existing facility.
2. Improve the facility to operate with an idle period.
3. Improve the heat recovery efficiency.
4. Improve the volumetric efficiency.
5. Maintain an economic feasible TESS.
6. Develop an analytical model that that will be validated by the experimental results.

The objectives can be summed in one main objective: To improve the performance of the facility, while remaining economically feasible.

1.4 Research Scope

1.4.1 Project Scope

The project entails the design and development of a next generation thermal rock bed storage experimental facility. Factors that will play a significant role in the facility include economical restrictions to remain cost-effective, as well as the improvement of the thermal efficiency of the facility. The primary focus will be to develop a concept that will be able to satisfy the objectives set out in Section 1.3.2.

The project will include an analytical model, for both charging and discharging cycles, of the next generation concept. The analytical model will be validated through experimental testing on the facility. Completion of both the model and experimental testing is expected to yield results that are sufficient to predict the performance of the facility on an industrial scale.

The project, which builds on work by Laubscher (2017), is developed in the context of application to the Stellenbosch UNiversity Solar POver Thermodynamic (SUNSPOT) cycle, discussed in Section 1.1.2, and the renewable energy community as a whole.

1.4.2 Experimental Testing Scope

Experimental testing on the facility will be conducted. The testing will vary between two scenarios, which a typical TESS will experience when active in

a CSP plant. The first scenario will be a single charge-discharge cycle from cold rock bed conditions. The second will be a multiple cycle test, consisting of a minimum of three charge-discharge cycles. The results of these tests will be compared to the analytical model to validate the model results. The focus of these tests will be to determine thermal losses, thermal and volumetric efficiency and possible improvements to the facility setup for future experimental use.

1.4.3 Analytical Model Scope

A one-dimensional (1-D) analytical model is to be developed which will focus on simulating the next generation concept by making use of heat transfer and pressure drop theory developed by Allen *et al.* (2015). The model will be used to determine various specifications of the rock bed TESS for experimental testing namely charge and discharge durations, temperature distribution in the rock bed, thermal capacity and thermocline behavior. The limitation of the 1-D model is that the effect of buoyancy cannot be taken into account. The methodology of the analytical model is discussed in Chapter 6.

The aim of the model is to be able to ultimately use the model for prediction of the performance of an industrial scale rock bed TESS that is based on the next generation concept.

Chapter 2

Literature Review¹

2.1 Introduction

The literature review discusses previous rock bed research. It includes a discussion on the first- and second-generation rock bed concepts developed at SU. The chapter concludes with a discussion on a techno-economic study on the previous-generation concepts.

2.2 Previous Rock Bed Research

Rock bed TESS has been a topic of interest in many projects, with the most relevant listed in Table 2.1. Liquid and gas features as the two types of heat transfer fluid (HTF) used for thermal energy storage.

The first research on liquid/solid packed bed TESS was conducted by Hallet and Gervais (1977), with a pilot-scale 5.7 MWh_{th} storage in preparation for the first industrial TESS at Solar One where oil is used as HTF with a maximum temperature of 290 °C. Pacheco *et al.* (2002) tested a 2.3 MWh_{th} rock bed storage, using molten salt as HTF, work which has been widely referenced in rock bed research, specifically to validate numerical models developed by the authors. (Esence *et al.*, 2017)

Gas/solid rock bed TESS was researched for the first time by Shewen *et al.* (1978) as well as Hollands and Sullivan (1984). The research focused on the pressure drop over a packed rock bed, as well as the possibility of using a rock bed as a subsystem to solar energy for the purpose of thermal storage.

¹Parts of this chapter have been published in Erasmus *et al.* (2018a) and Erasmus *et al.* (2018b)

Table 2.1: Relevant rock bed TESS research

Author	HTF	Solid	Temperature Range, [°C]
Hallet and Gervais (1977)	Oil	Granite rock and silica sand	218 - 302
Hollands and Sullivan (1984), Shewen <i>et al.</i> (1978)	Air	River gravel	20 - 67
Faas <i>et al.</i> (1986), McDonnell Douglas Astronautics Company (1986)	Oil	Rocks and sand	200 - 290
Pacheco <i>et al.</i> (2002)	Molten salt	Quartzite rock and silica sand	290 - 390
Zanganeh <i>et al.</i> (2012)	Air	Sedimentary rocks	20 - 500
Hoffmann <i>et al.</i> (2016)	Rapeseed oil	Quartzite rock	160 - 210

From the above list, the most recent and complete research is discussed in Section 2.2.1 and Section 2.2.2.

2.2.1 Liquid

The most recent and complete research on liquid/solid packed bed TESS was by Hoffmann *et al.* (2016). A laboratory-scale experimental facility was developed for experimental testing purposes and a schematic of the setup can be seen in Figure 2.1. Here rapeseed oil is used as HTF, with Quartzite rock as filler material. Hoffmann *et al.* (2016) developed two numerical models, which were then compared with the experimental results as well as two industrial-scale storage systems, namely those at Solar One and Sandia National Laboratories (SNL). The first model was single-phase one-dimensional, based on theory developed by Schumann (1929). The second model involved a two-phase one-dimensional approach.

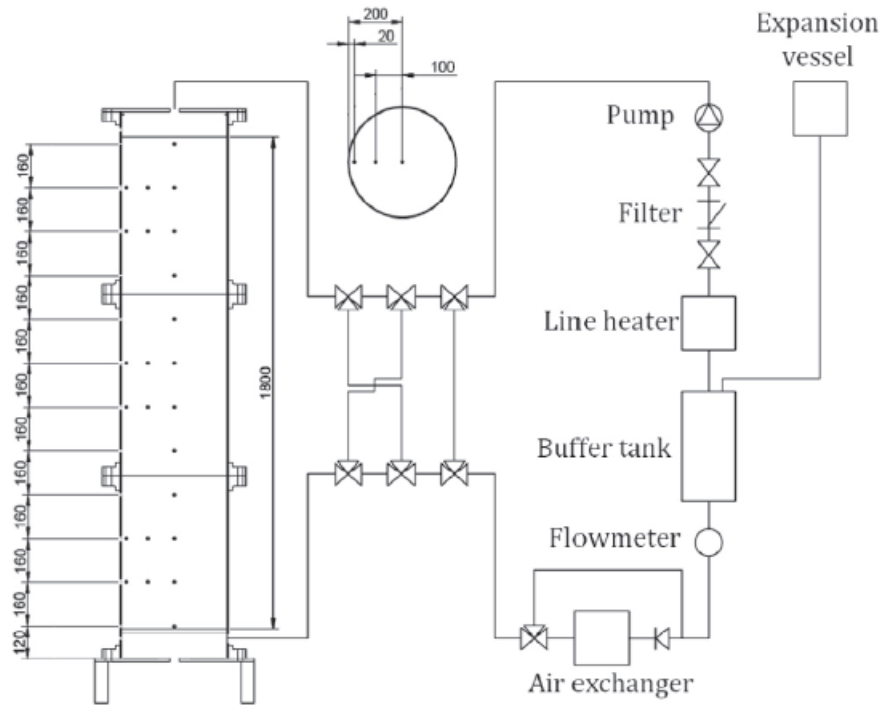


Figure 2.1: Schematic of small-scale experimental facility by Hoffmann *et al.* (2016)

It was concluded by Hoffmann *et al.* (2016) that the technology of rock bed TESS can reduce the costs of CSP plants, but to achieve this a thorough understanding of its behavior is required. Due to this necessity, numerous numerical models have been developed and compared to experimental data from relatively small systems.

2.2.2 Gas

Zanganeh *et al.* (2012) investigated a design of a rock bed in a truncated conical shape, as illustrated in Figure 2.2. The concept makes use of air as heat transfer fluid and a packed bed of rocks as storage material. A 6.5 MWh_{th} pilot-scale experimental facility was developed and constructed for test purposes.

2.3 Rock bed TESS at Stellenbosch University

The search for a more economical solution regarding storage has been an on-going topic at Stellenbosch University. This includes detail studies on various elements of thermal storage that include the pressure drop over a packed rock bed for various shapes, formations, void fractions and sizes (Allen *et al.*, 2013).

Further analysis regarding the thermal contraction and expansion of the rocks within the rock pile identified ratcheting as a potential problem. In 2013, Kröger proposed the concept illustrated in Figure 2.4. This concept was then provisionally patented on the design and layout of a thermal rock bed storage system (Allen *et al.*, 2013). The concept addressed the effect of thermal ratcheting, when the container and the rocks in the bed expand at different rates through temperature cycles which increases the void volumes and therefore allows for incremental rock settling, preventing ultimate failure (Von Backström *et al.*, 2012).

Kröger's concept requires both insulation and a roof structure, which is a large contributing factor to the cost of the concept. The roof is shielded from 650 °C air on the inside by the insulation, and in turn shields the insulation from weather from the outside. The concept shows that the thermocline would be structured that the hot section will be on top and the cold section at the bottom of the structure. This allows the thermocline profile to be the same for both the charge and discharge cycles.

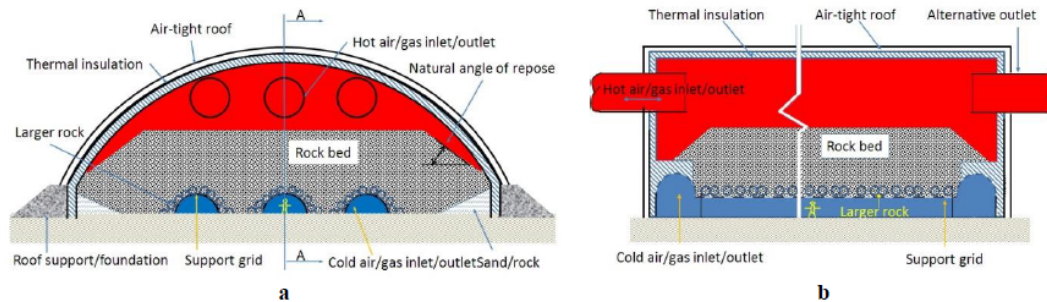


Figure 2.4: Kröger's packed bed concept (Kröger, 2013)

A second concept was developed by Gauché and Louw (2014). It is a modified version of Kröger's concept and is illustrated in Figure 2.5. This entailed simplifying Kröger's concept to make it a more economical option. Gauché and Louw (2014) removed the roof structure and insulation from the concept, thus cutting a large portion of the costs in Kröger's concept. Another change sees the hot air being administered at the bottom to the center of the rock

pile. This causes an inverted thermocline. The hot section of the thermocline would be on the inside of the rock bed, with the cold section on the outside. The temperature would thus gradually decrease from the center of the rock bed to close to ambient temperature on the outside layer of the rock bed. This would allow for the absence of insulation, since the outside layer that is part of the cold section would act as the insulation of the hot section. The concept also contains an optional tarpaulin cover over the rock pile to seal it off from outside elements such as rain and wind. As seen in Figure 1.5, the optional tarpaulin cover is included in the current facility.

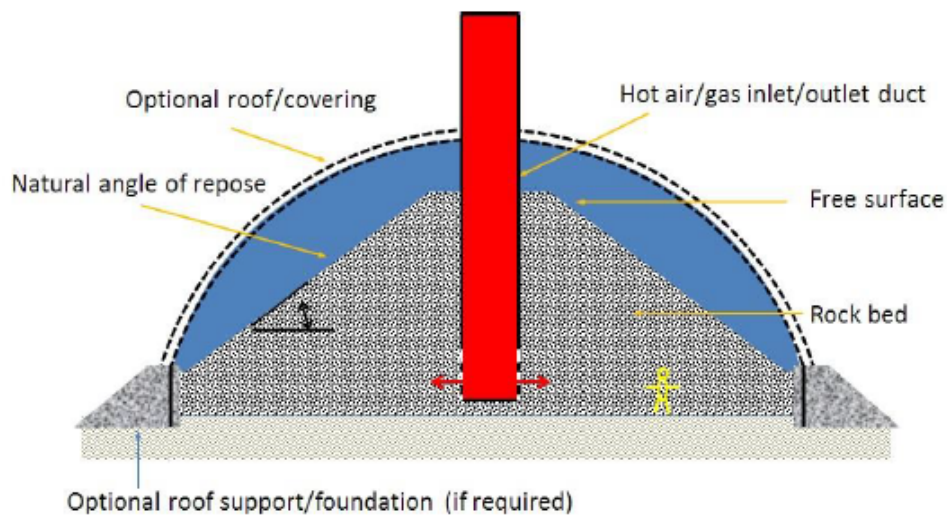


Figure 2.5: Gauché's packed bed concept (Gauché and Louw, 2014)

Buoyancy, due to natural convection caused by the temperature difference, would cause the hot air to rise, due to the pressure drop over the packed bed, during idling. The discharging of the hot air would entail reversing the flow direction of the air, forcing the air back into the duct and out into the pipe that previously supplied the hot air into the rock pile. Figures 2.6 and 2.7 illustrate these cycles.

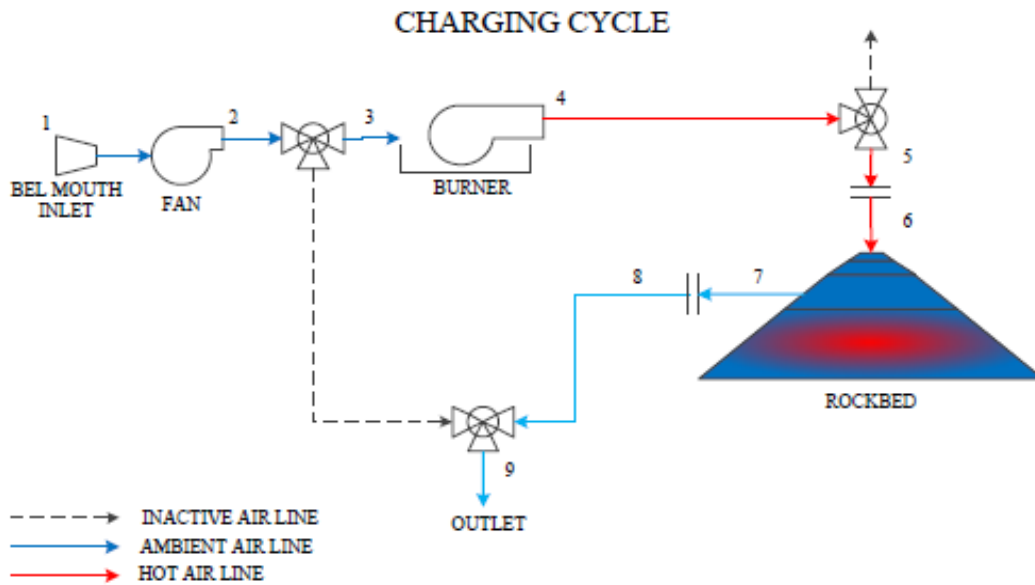


Figure 2.6: Charging cycle (Laubscher, 2017)

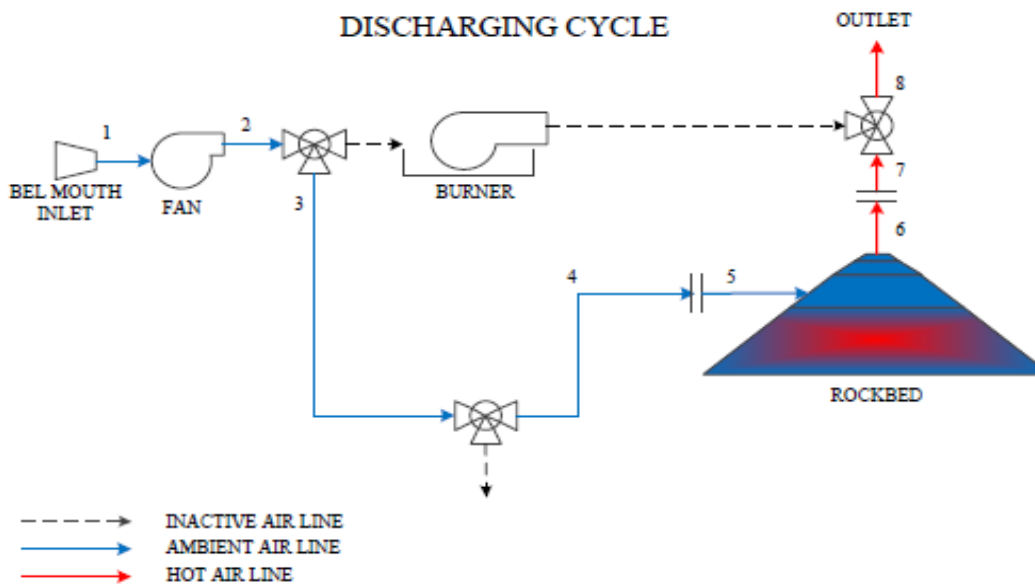


Figure 2.7: Discharging cycle (Laubscher, 2017)

2.4 Techno-Economic Study

A thorough techno-economic study on first- and second-generation concepts was conducted by Allen *et al.* (2016). A comparison was made between two-tank molten salt TESS and the SU's rock bed concepts. The study focused on

the capital cost of each system, with a capacity range between 10 MWh_{th} and 10 000 MWh_{th}. From Figure 2.8 it is evident that both Kröger and Gauché's concepts are significantly, 50-66 %, less expensive than that of a two-tank molten salt TES system.

The capital expenditure (CAPEX) of a molten salt TES system equates to 22-30 US\$/kWh_{th}. On the other hand, the study concluded that both rock bed concepts, depending on the design and cost of containment, has a CAPEX range of 8-15 US\$/kWh_{th} (Allen *et al.*, 2016). The difference in costs are related to the types of storage material and containment structure used. For two-tank molten salt TES systems, two tanks are used for containment, with molten salt acting as storage material. According to EPRI *et al.* (2010), molten salt has a cost of 1.17 US\$/kg. In comparison, the storage material for a rock bed TESS, in this case dolerite, is 0.02 US\$/kg (1 US\$ = 13.2 ZAR, July 2018).

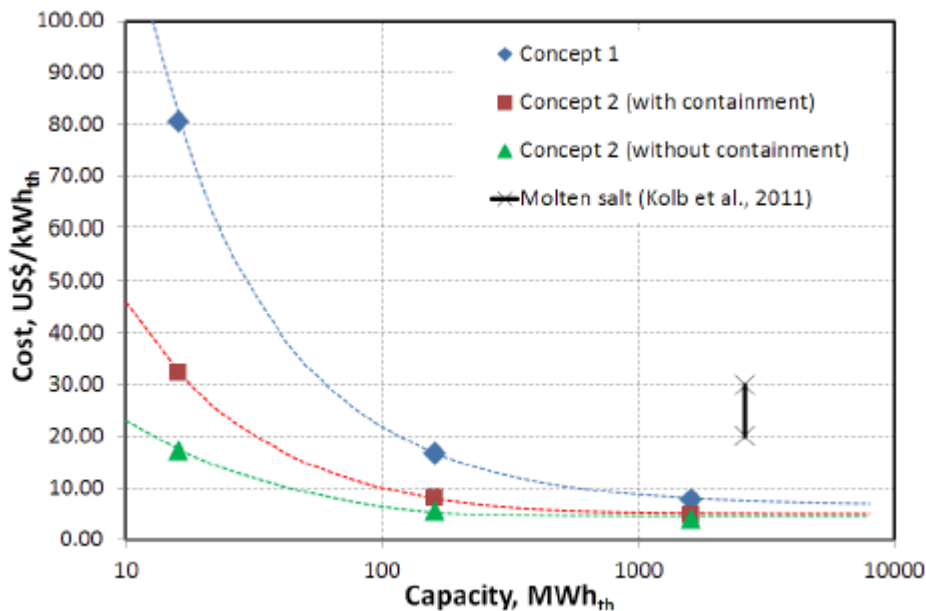


Figure 2.8: Cost comparison (Allen *et al.*, 2016)

A storage system within a CSP plant contributes up to 13 % of the plants capital costs, thus reducing the cost of a TES system will have a measurable effect in cost reduction of a CSP plant's LCOE (Kolb *et al.*, 2011).

2.5 Chapter Summary

This chapter presented a literature review. A background on solar energy is discussed, followed by a discussion on previous rock bed research, which

included projects where either liquid or gas features as heat transfer fluid. This is followed by a discussion on rock bed research at Stellenbosch University with a specific focus on the two concepts that precede this project. A techno-economic study is presented as conclusion of the literature review.

Chapter 3

Development of Next-Generation System¹

3.1 Introduction

This chapter discusses the concept development phase of the project. It gives insight into the criteria, constraints, generation and selection process of the concept. An adaptation of the chosen concept is then presented and discussed to be able to implement it onto the existing facility.

3.2 Concept Criteria

Knowledge of the previous rock bed concepts, discussed in Section 2.3, led to the development of a specific set of criteria for a new concept. The criteria, both of the nature of technical limitations or scientific interest, enabled the generation of new concepts for selection.

There are certain limitations that come with the existing facility, and these must be considered. The presence of the tarpaulin cover, cold air fan and hot air pipe that leads to the bottom of the rock bed sets specific technical limitations. The tarpaulin cover further introduces a temperature limitation, not being able to withstand temperatures above 90 °C. Should a concept be generated that disregards these limitations, it would require vast modification for maximum representation of a feasible concept. Furthermore, the concept must make use of the current heat source, being the combustion of liquid petroleum gas (LPG) within a burner heating up cold air. However, it is possible to generate a concept that disregards these limitations, which can then be modified to include these limitations.

¹Parts of this chapter have been published in Erasmus *et al.* (2018a) and Erasmus *et al.* (2018b)

Regarding heat transfer, the concept should enable the facility to make use of as much rock mass as possible, thus increasing the volumetric efficiency and as a result translated to a reduction in costs. By increasing the volumetric efficiency, the heating capacity of the facility will also be increased. The facility should also be able to idle for a long period, to both test the effectiveness of the insulation and thermocline behavior under idle conditions. Reduction of thermal losses is an important criterion, which will increase the thermal efficiency of the facility. The full criteria are listed in Table 3.1. The criteria are also ranked in importance, where 'L' is low, 'M' is medium and 'H' is high.

Table 3.1: Concept development criteria

Criteria	Limitations/Improvement	Importance
Tarpaulin cover	L	L
Hot air pipe	L	H
Cold fan	L	L
Heat source	L	L
Increase volumetric efficiency	I	H
Long idle period	I	H
Reduce thermal losses	I	H

3.3 Concept Generation

After identification of the concept criteria, the generation of a new concept commenced. Firstly, current concepts that achieve the outcome needed were evaluated, followed by the evaluation of the current facility and lastly, experts in different areas of discipline that have knowledge of their specific parts of the concepts were consulted. All the information gathered was then evaluated, and from this, possible improvements and new ideas were generated.

From this process the concept illustrated in Figure 3.1 stemmed. The concept was generated without considering the limitations. Hot air is introduced at the top of the rock bed with the cold air exiting at the bottom, which is expected to relatively evenly distribute the heat through the rock bed, causing the thermocline to progress linearly downwards. Secondly, insulation is added to the rock bed to reduce thermal losses. To extract the thermal energy from the rock bed, air is sucked through the rock bed via the hot air outlet with a high temperature fan, consequently cold air enters through the cold air inlet.

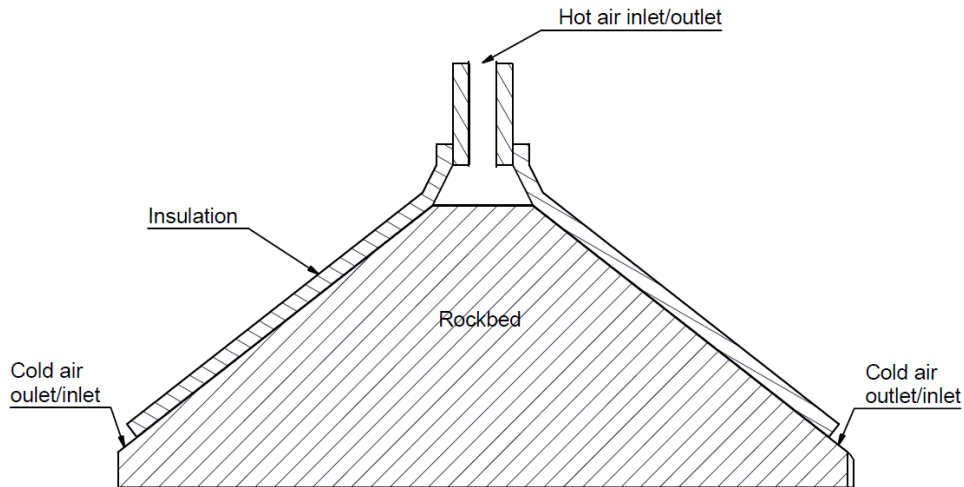


Figure 3.1: Concept illustration

This concept will ensure that the whole rock bed is used for thermal energy storage by being able to charge until $T_{out} = T_{in}$. In a functioning CSP plant this is ideal, since the hot air that exits the rock bed during charge can either be sent back to the tower or troughs to be heated or, in the case where the temperature is high enough, be sent directly to the power cycle. Of course, in the experimental facility the outlet air is only dumped back into the atmosphere.

Insulation is an important component toward achieving the set criteria, mainly to reduce thermal losses. The insulation will be layered as shown in Figure 3.2. Working from the right to the left of the figure, the mesh lies directly on top of the rock bed. This is followed by 3 layers of insulation (Appendix A), each stacked on the other to better insulate the rock bed. Stacking of the layers will also prevent any direct path to ambient conditions for flow through the insulation. By adding cladding to the outside of the third layer, the insulation is protected from ambient elements.

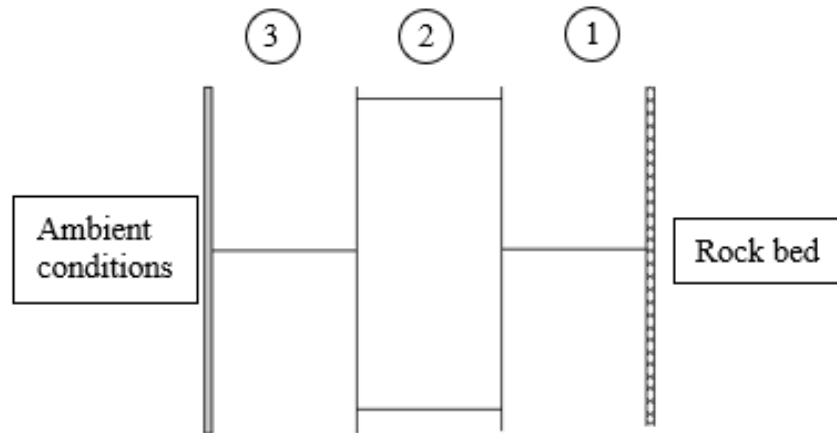


Figure 3.2: Insulation layers

3.4 Concept Evaluation

The selection process was based on the criteria discussed in Section 3.2. Table 3.2 shows whether the concept achieves the criteria. A "-" sign implicates that the criteria is not met, a "0" that the criterion is not met but can be with adjustments, "+" means the criterion is met, but can be adjusted to meet the "++" which means the concept fully satisfies the criteria.

Table 3.2: Concept evaluation

Criteria	Evaluation
Tarpaulin cover	0
Hot air pipe	+
Cold fan	0
Heat source	++
Increase volumetric efficiency	++
Long idle period	++
Reduce thermal losses	++

Table 3.2 shows that a total of 5 out of the 7 criteria are met by the concept. The concept will make use of the heat source and with the introduction of the insulation will be able to increase the volumetric efficiency, reduce thermal losses and allow a long idle period. By means of modification, the existing hot air pipe can be altered in such a way that the hot air is introduced into the top of the rock bed, achieving "++" status. The rest of the pipe will be kept in place to offer support to the rest of the hot air pipe assembly.

The evaluation shows that the concept does not make use of both the tarpaulin cover and cold air fan. Although these elements can be replaced by a hot air fan, in terms of cost it would make sense to rather adapt the concept to satisfy the criteria. A hot air fan is an expensive subsystem and the will increase construction cost. An adapted concept is illustrated in Figure 3.3, which does satisfy all criteria. It illustrates the charge cycle, with the discharge cycle being the reverse thereof. Hot air will still enter the rock bed at the top and pushed downwards through the rock bed. The cold air will then exit the rock bed at the bottom, flow upwards between the tarpaulin cover and the exit the system through a cold air pipe situated at the top. The cold air pipe is isolated from the hot air pipe, thus these two has no influence on one another. During discharge cold air will be blown into the cold air pipe, reversing the flow direction that takes place during charge.

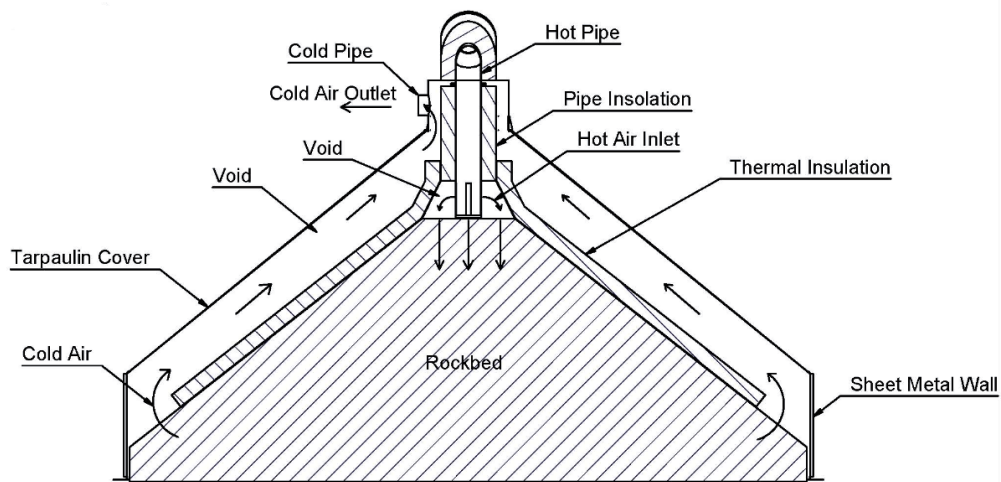


Figure 3.3: Adapted concept (Von Backström *et al.*, 2017)

Due to the modification the outside of the insulation will always be colder than the inside. In case of a flow leak through the insulation, this will be an advantage. The tarpaulin cover unfortunately does introduce the temperature limitation, which will restrict the charge outlet temperature. The concept has been provisionally patented by Von Backström *et al.* (2017).

3.5 Design

After finalizing the concept and its layout, more detail went into construction specifics. To ease construction and make sure that the insulation will be secure on top of the rock bed, it was decided to incorporate a spider web structure. This structure consists of 12 framed sections, each filled with stainless steel mesh. The insulation would then be fastened onto the mesh and structure

via wires and nails. The design of these sections is illustrated in Figure 3.4, with a complete frame structure illustrated in Figure 3.5. These sections were individually manufactured and then assembled on-site.

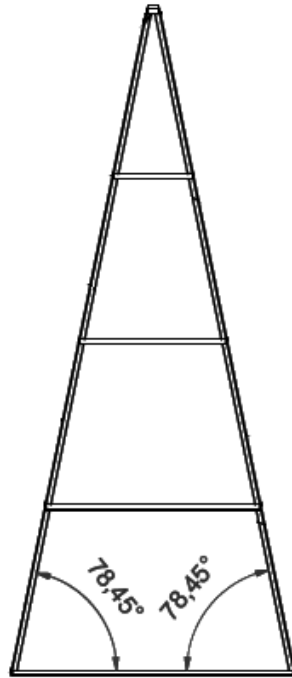


Figure 3.4: One section of the spider web structure

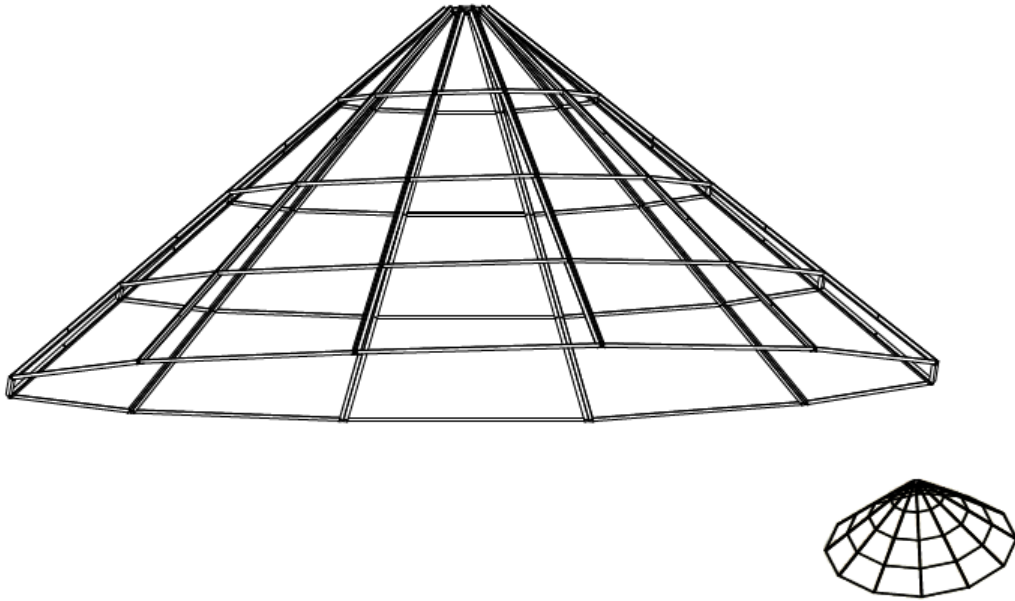


Figure 3.5: Complete spider web structure

3.6 Chapter Summary

Concept criteria were identified with knowledge from previously developed concepts by Kröger (2013) and Gauché and Louw (2014). With the criteria in mind, the concept generation phase led to the development of a concept that would possibly satisfy the given criteria. After an evaluation process, the concept was modified to satisfy the criteria fully, with the final concept illustrated in Figure 3.3. A schematic flow diagram of both the charge and discharge cycles, depicting the flow directions of each cycle was supplied. The chapter concludes with a design of the spider web structure which forms part of the insulation that will be on top of the rock bed.

Chapter 4

Experimental Facility Construction and Test Setup¹

4.1 Introduction

Construction of the developed concept onto the initial experimental facility is discussed in this chapter. The existing facility was completed and commissioned mid-2017, where-after experimental test campaigns were completed and analyzed. The setup of the initial facility and experimental results prior to modification can be found in Laubscher (2017).

4.2 Construction

Before the construction phase began, the construction procedure plan was determined. The procedure is listed in Table 4.1. The Table lists each task in order of completion together with a description of each task.

¹Parts of this chapter have been published in Erasmus *et al.* (2018a) and Erasmus *et al.* (2018b)

Table 4.1: Construction procedure

Task	Description
Modification of hot air pipe	The hot air pipe is modified to allow the air to exit the pipe into the top of the rock bed. The rest of the pipe downwards of the flow direction is sealed off
Installation of frame sections	The spider web structure is assembled onto the rock bed
Shaping rock pile	Rocks are shifted into the cavities between the spider web structure and rock bed surface to limit preferential air flow between these two elements
Installation of insulation	Cutting the insulation into sections and securing it onto the spider web structure
Evaluation	Evaluate the quality of construction. Ensure there is no flow leak through the insulation or into the bottom of the rock bed
Re-installation of cover	After evaluation, the tarpaulin cover closes the rock bed and allows discharging to take place

Modification of the hot air pipe is illustrated in Figure 4.1. Figure 4.1a illustrated the first phase where the cladding and insulation had to be removed. The second phase, which was to cut slits into the pipe for the hot air to exit, is illustrated in Figure 4.1b. The last phase of this task was to seal the pipe below the slits. This was done by installing two steel discs with 50 mm of insulation in-between. Rock wool is used as insulation in the facility and the properties can be viewed in A. Figure 4.1c shows that the pipe is sealed.



(a) Cladding and insulation removed



(b) Slits cut into steel pipe



(c) Sealed pipe

Figure 4.1: Hot air outlet pipe modified

Next, the spider web structure had to be installed. Firstly it was important to test whether the design of the frames was correct. The reason for this is that, due to the rock bed not being a solid structure, initial measurements can change. Figure 4.2a shows the fitment procedure. The frame sections were then installed onto the rock bed by linking the sections with each other using stainless steel bolts and nuts. The fully installed structure can be seen in Figure 4.2b.



(a) Frame fitment

(b) Completed spider web structure

Figure 4.2: Installation of the frame sections

After completion of the spider web structure the rock pile had to be shaped. As explained, it was done to limit preferential air flow in voids between the structure and the rock bed surface. The cavity between these two elements existed due to the frames designed to be at 40° , while the rock bed angle was measured to be 37° . The frames were designed to be at 40° to minimize the effect of thermal ratcheting by preventing rocks from rolling into open lower spaces. Figure 4.3 illustrates the rock bed before and after the rock pile was shaped. Shaping of the rock pile caused the entrance area into the rock bed at the top to increase. After shaping was completed, the cavity was greatly reduced, although it was expected that there will still be some bypass flow, the effect of this was later evident in the experimental results.



(a) Before shaping the rock bed

(b) Shaping complete

Figure 4.3: Shaping of the rock pile

The last step in the construction procedure was the installation of the insulation layers. The insulation, which was supplied in rolls with a width of 1.2 m, was cut into sections and secured to the structure. The first layer is illustrated in Figure 4.4a and the second in Figure 4.4b.



(a) First layer

(b) Second layer

Figure 4.4: Insulation installation phase

Figure 4.5 shows the gap where the cold air will exit the rock bed during charge and enter the rock bed during discharge. This gap is approximately 0.15 m wide.



Figure 4.5: Cold air outlet/inlet

Before the installation of the third layer, the installed insulation layers were inspected to make sure that there are no direct flow leaks. This was done by introducing hot air into the rock bed and then taking pictures with a thermal camera. In the event of a leak, the camera would identify it by illustrating

a hot spot. As seen in Figure 4.6 three spots were identified by the thermal camera. After closer inspection, it was confirmed that at these locations, there were direct flow paths through the insulation. These spots were filled with insulation, before the third layer was added.

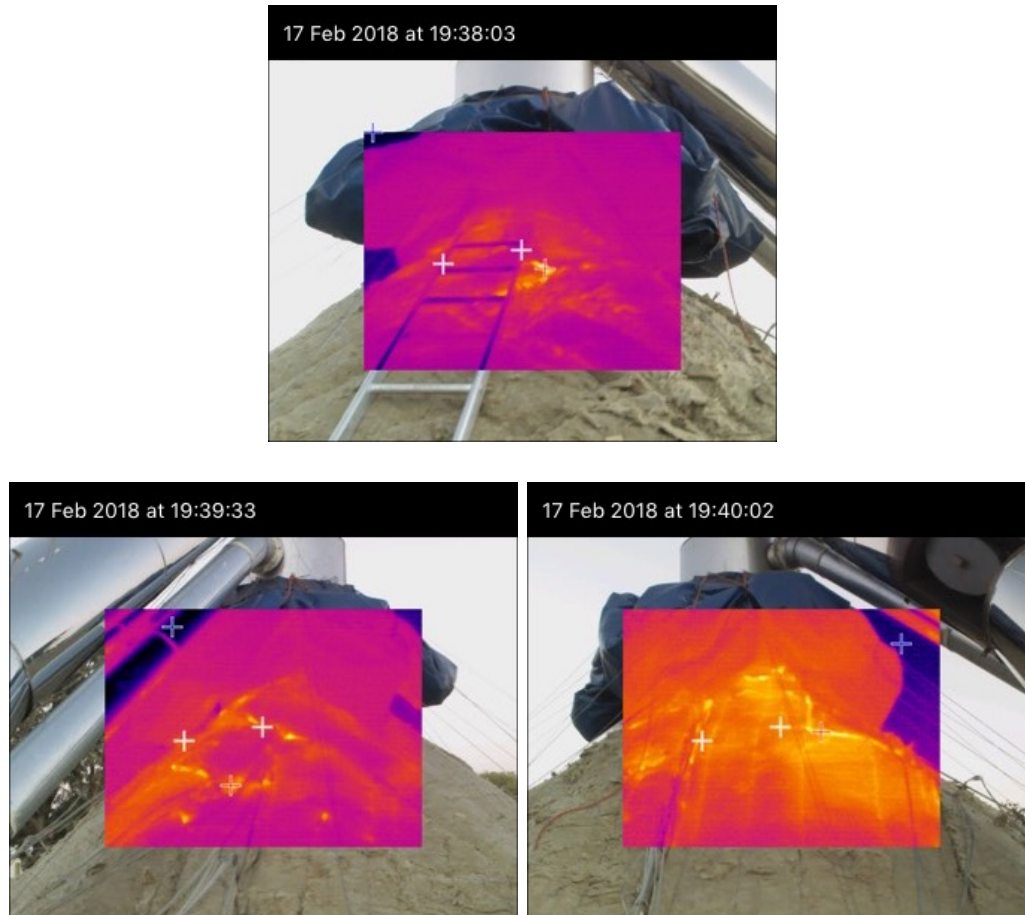


Figure 4.6: Flow leak test results

During the first experimental test campaign the insulation was once again tested for any direct leaks and it was confirmed that there were none present. The tarpaulin cover was re-installed after this confirmation to both complete the facility and allow for discharging.

Figure 4.7 presents the final dimensions, given in mm, of the completed facility.

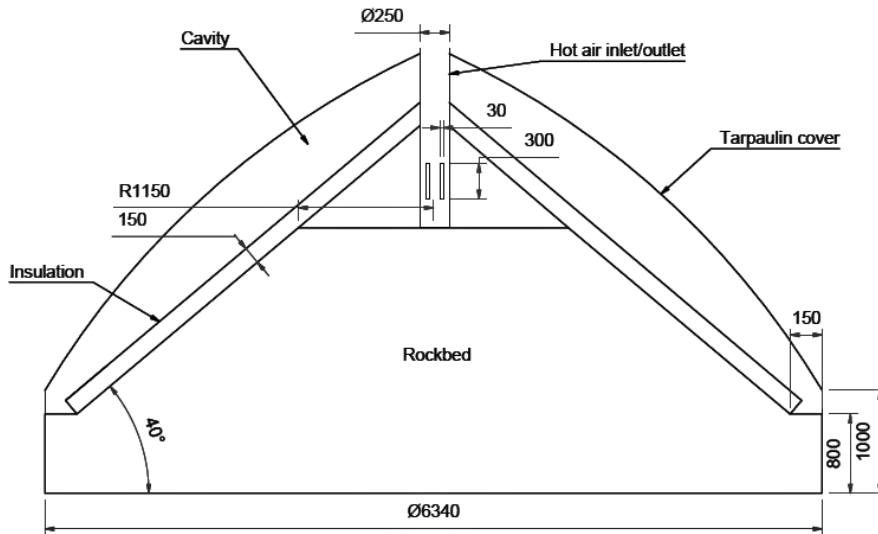


Figure 4.7: Rock bed with dimensions

4.3 Experimental Setup

Figure 4.8 gives an aerial view of the test facility, situated at the Stellenbosch University Renewable Energy Center (SUNREC) site. Displayed are the gas house, which is filled with LPG bottles, the gas train, gas burner, centrifugal fan, hot air pipe, electrical box and rock bed which is covered.

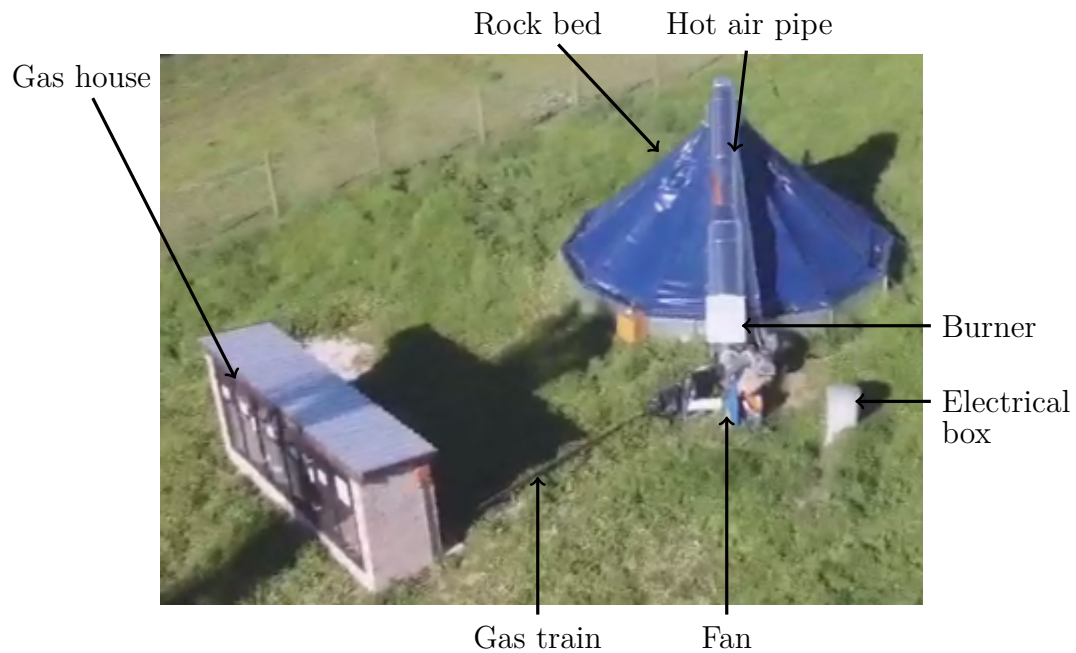


Figure 4.8: Experimental facility located at SUNREC

With the new concept, the experimental layout slightly changed with hot air entering at the top of the rock bed. The system is open, thus during charge the cold air is dumped into the atmosphere and during discharge the same is done with the hot air. Figure 4.9 and Figure 4.10 illustrate the flow diagram of the layout.

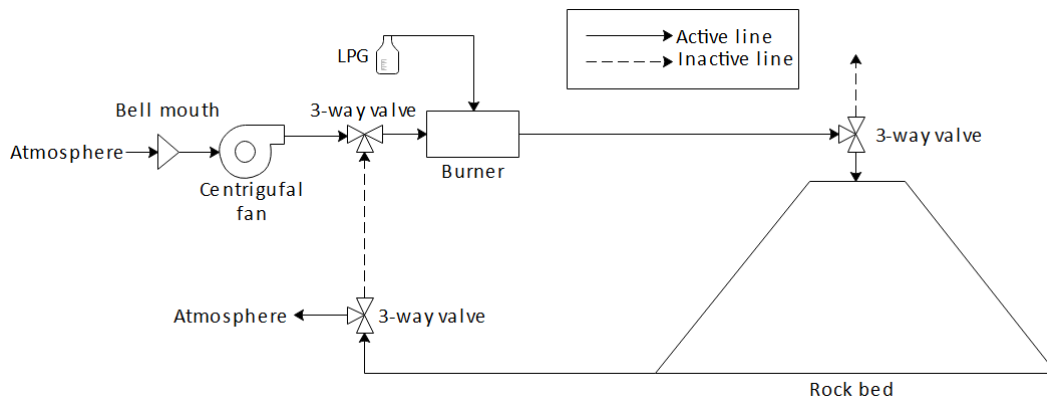


Figure 4.9: Charge cycle flow diagram

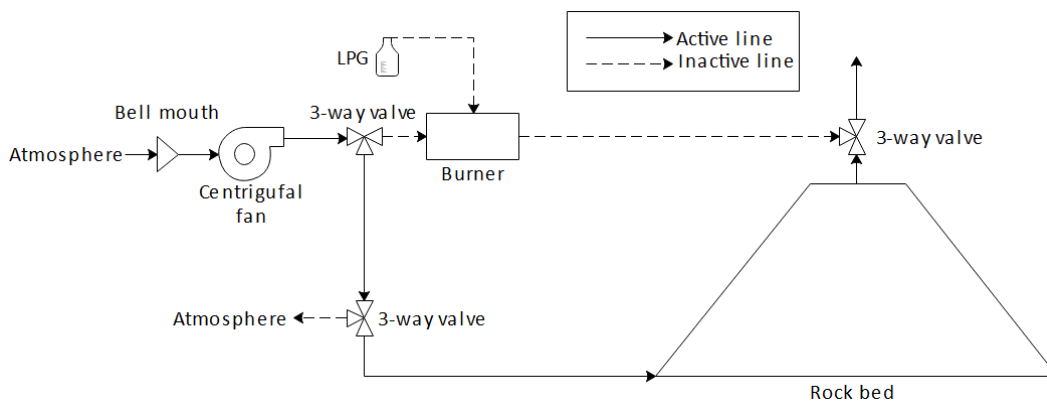


Figure 4.10: Discharge cycle flow diagram

4.4 Experimental Equipment

The monitoring of data during an experimental test campaign is conducted through the measurement of several different variables, which include temperature, pressure and flow measurements. Sections 4.4.1 and 4.4.2 explain the monitoring of each of these variables.

4.4.1 Temperature Measurement

To monitor the temperature distribution within the rock bed, Laubscher (2017) installed a grid of Type K thermocouples into the rock bed. To ensure the accuracy of the temperature profile within the rock bed, two sets of grids were installed in the west and south facing sides of the rock bed. The thermocouple layout, as well as the location of each thermocouple within the rock bed, is illustrated in Figure 4.11. A total of 50 thermocouples are installed in the rock bed, with additional thermocouples at rock bed inlet, rock bed outlet, rock bed ground surface and within the burner box.

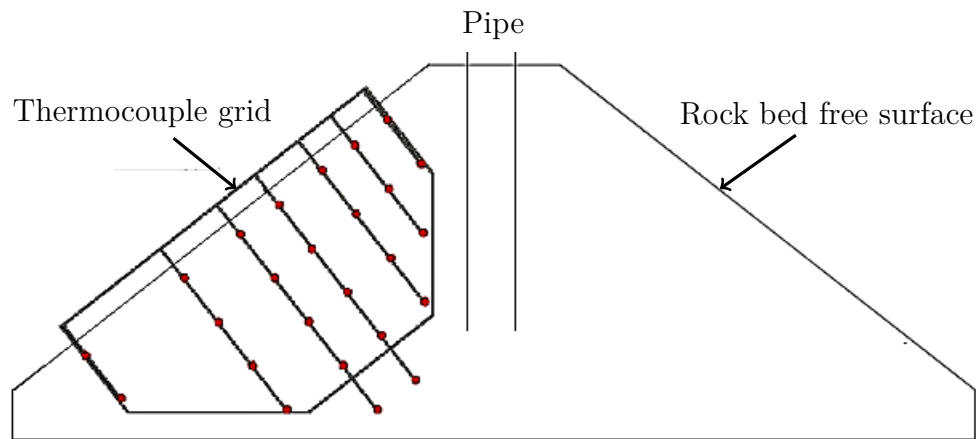


Figure 4.11: Schematic of the thermocouple layout (Adapted from Laubscher (2017))

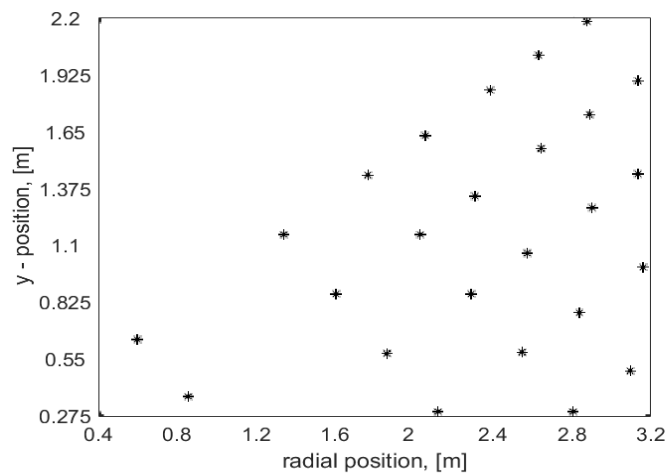


Figure 4.12: Position of the thermocouples

Figure 4.12 illustrates the positioning of each thermocouple within the rock bed, together with radial and vertical references. The average between correlating thermocouples from the west and south sides, as well as the references in Figure 4.12, are used to determine the temperature distribution within the rock bed.

4.4.2 Data and Flow Measurement

The thermocouples are monitored and the data collected through the use of a data logger, illustrated in Figure 4.13. The data logger, which makes use of an Ethernet cable to transfer the data collected directly onto a laptop, is an Agilent 34972A LXI data acquisition/switch unit type. For the laptop to receive data, software from Agilent Benchlink, specifically developed for the data logger, is used.



Figure 4.13: Data logger

The mass flow rate is measured during the charge and discharge cycles of an experiment. This is achieved by measuring the pressure drop over a bell-mouth situated at fan inlet. An Endress and Hauser pressure transducer, illustrated in Figure 4.14a, takes this measurement. Specifications of the transducer are provided in Figure 4.14b. The transducer is connected to the data logger, which allows the measured value to be transferred to the data logger software. The measured value is also displayed on the transducer's screen.



(a) Pressure transducer (b) Specifications (Laubscher, 2017)

Figure 4.14: Pressure transducer and its specifications

Figure 4.15 is used to translate the pressure drop measurement given by the pressure transducer to a mass flow rate in kg/s.

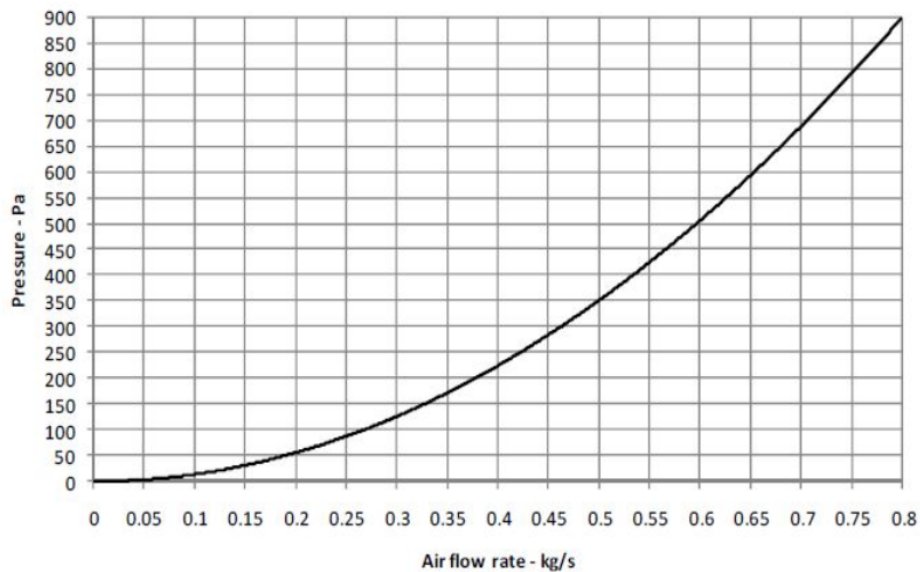


Figure 4.15: Bell mouth pressure drop over air flow rate (CFW Fans, 2016)

The pressure transducer was calibrated using a Betz micro-manometer, an instrument manufactured by ACIN (2016). The calibration entails the selection of 4 or more different pressure points within a pressure range, for example 0 Pa - 2000 Pa. The transducer is connected to both the data logger and Betz micro-manometer to produce a mADC reading for each pressure point. A curve was then fitted to these points, producing a function for the curve.

Equation 4.4.1 provides the function, with x the mADC value and P the pressure value given in Pa.

$$P = 193.34x - 848.18 \quad (4.4.1)$$

Calibration was initially performed by Laubscher (2017). The pressure transducer was not re-calibrated as an initial comparison of the zero drift suggested suitable functioning.

4.5 Efficiencies

4.5.1 Thermal Efficiency

To evaluate the performance of a TESS, there are three important efficiencies to consider. The first is called the thermal efficiency, given in equation (4.5.1). It measures the amount of useful energy extracted from the rock bed during a discharge cycle to the total energy input during the charge cycle. The useful energy is determined to be all energy extracted to a discharge temperature of 327 °C during discharge.

$$\eta_{th} = \frac{E_{out,useful}}{E_{in}} \quad (4.5.1)$$

4.5.2 Volumetric Efficiency

For thermocline storage, which the rock bed TESS is, volumetric efficiency is also an important measurement of performance. In this case, it is defined as the total amount of rock volume that is active storage material and is given in equation (4.5.2). Active refers to the action of storing heat at a temperature of 50 °C and above, the same metric as used by Laubscher (2017), to enable a comparison between the technologies.

$$\eta_v = \frac{V_{active}}{V_{total}} \quad (4.5.2)$$

4.5.3 Overall Efficiency

The overall, or round-trip, efficiency is determined in similar fashion to the thermal efficiency. However, where the thermal efficiency measures only the amount of useful energy extracted per cycle against the input, the overall efficiency measures the total energy output across all cycles against the total input across all cycles. From this it can be determined what the energy loss of the system is. Equation (4.5.3) presents the overall efficiency.

$$\eta_o = \frac{E_{out,total}}{E_{in}} \quad (4.5.3)$$

4.6 Capital Cost

The modifications introduced additional capital costs to the facility, which are listed in Table 4.2. Miscellaneous items include: Bolts, nuts, wire and silicone. The final capital cost includes the capital costs of the initial facility before modification. The capital cost does not include the LPG needed to conduct an experiment. This is regarded as an operational cost and will cost, dependent on the LPG price, approximately 1000 ZAR per 48 kg bottle. The facility can house up to 20 bottles.

Table 4.2: Updated capital cost of the facility

Material/Item	Cost, [ZAR]
Stainless steel	21 931
Insulation	26 250
Mild steel	5113
Miscellaneous	525
Initial facility	450 358
Total	504 177

Additional costs amount to 11.95 % of the initial facility costs. This implies that for a large-scale plant, the cost of insulating a TESS is approximately 12 % of the TESS capital cost without insulation. In a comparison of the experimental results between this concept and that of Gauché and Louw (2014), the cost increase can be evaluated in relation to the increase of the facility's performance.

4.7 Chapter Summary

Construction regarding the modification of the initial facility was completed, with Figure 4.7 presenting the final dimensions of the new facility. The experimental setup was described, together with the equipment that was used during testing campaigns. The chapter concludes with an update on the capital cost of the facility.

Chapter 5

Experimental Campaigns and Results¹

5.1 Introduction

Experimental test campaigns were completed on the experimental test setup discussed in Chapter 3, where-after these test results were used to validated an analytical model developed in Chapter 6. This chapter presents and discusses the results of the completed experimental test campaigns.

5.2 Procedure

The experimental test procedure is a step-by-step guideline to enable an operator to conduct experiments. The procedure includes the preparation of the test setup up until the gas system is secured after a campaign is completed. The full experimental test procedure is provided in Appendix C for future use in follow-up projects.

5.3 Experimental Campaigns

Three different experimental tests were completed on the facility to gather as much information possible to ultimately make an accurate prediction on such a facility's performance on an industrial scale. Each test focused on different aspects of a rock bed TESS and are discussed in the sections that follow. The three test campaigns and purpose are given in Table 5.1.

¹Parts of this chapter have been published in Erasmus *et al.* (2018a) and Erasmus *et al.* (2018b)

Table 5.1: Test campaigns.

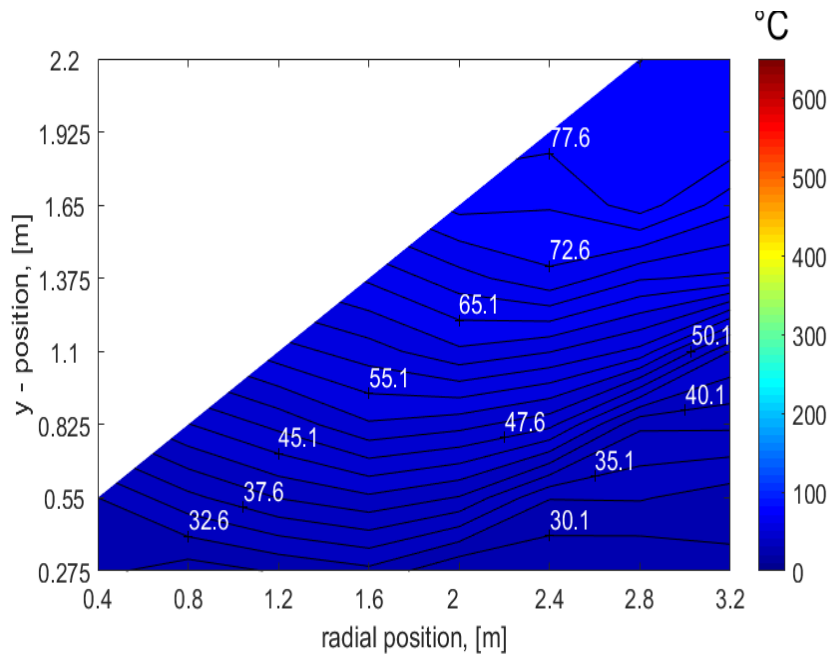
Campaign	Description
Initial test	The first test on the facility was conducted to determine the volumetric efficiency, the thermal losses and the behavior of the thermocline during a long idle period.
Charge-Discharge test	A charge-discharge cycle with no idle period was conducted. The thermal efficiency as well as a comparison of thermal losses were determined.
Multiple cycle test	A multiple cycle test was conducted. The test enabled the observation of thermocline behavior during multiple cycles, as well as effect of cycles on the efficiency of the facility.

During the data analysis of the second test, it was discovered that there is a mass flow leakage during discharge. This was not detected during the test, because in the experimental setup the flow is only measured at fan inlet. The flow leak is caused by ventilation holes situated within the tarpaulin cover, as designed by Laubscher (2017) for the initial facility. In the unlikely event that the fan would fail before discharge, these holes were to be opened for natural ventilation of the rock bed. These holes can however not be fully sealed due to their design, and thus flow leaks occur through them.

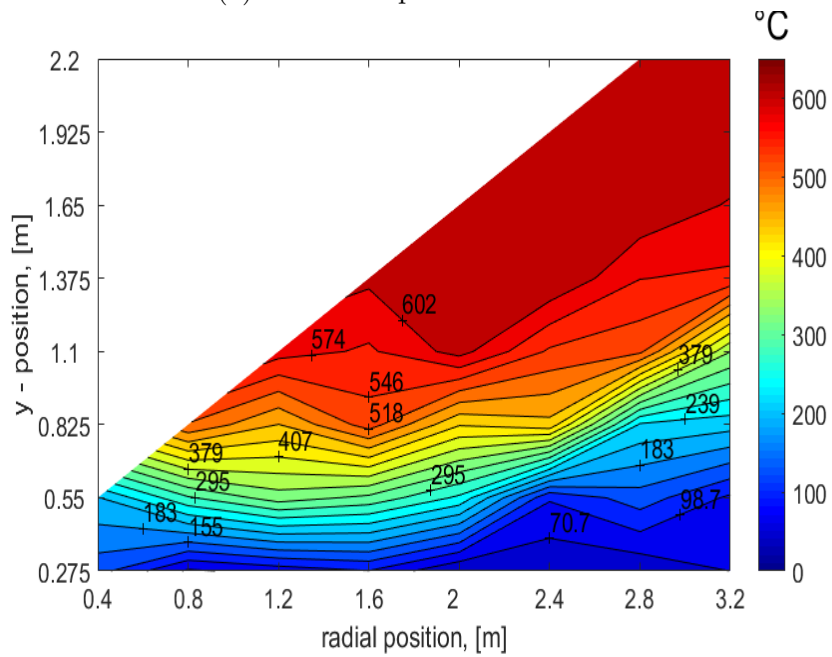
To quantify the flow leakage, cold air was blown through the cold rock bed, while an anemometer was used to determine the flow speed at discharge outlet for various inlet flow rates. Both the density and flow area were known for the cold air and were thus used to determine the mass flow rate in kg/s. Next, the measured flow rates at fan inlet were then compared with those of the anemometer, after which a 40 % flow leakage was calculated. Air density decreases with an increase in temperature, which causes the pressure to change within the system, demands that the air flow rate be increased to keep the mass flow rate constant. Due to this there is a 10 % error range applicable to the flow loss approximation. The approximation is used for all discharge calculations of each test.

5.3.1 Initial Test

The first test consisted of a single charge-discharge cycle, with a long idle period in between charge and discharge. Figures 5.1a and 5.1b illustrate the start and end of the charge cycle. The average charge cycle inlet temperature was 601 °C.



(a) Initial temperature distribution



(b) End of the charge cycle and start of idle period

Figure 5.1: Rock bed temperature distribution - Charge cycle

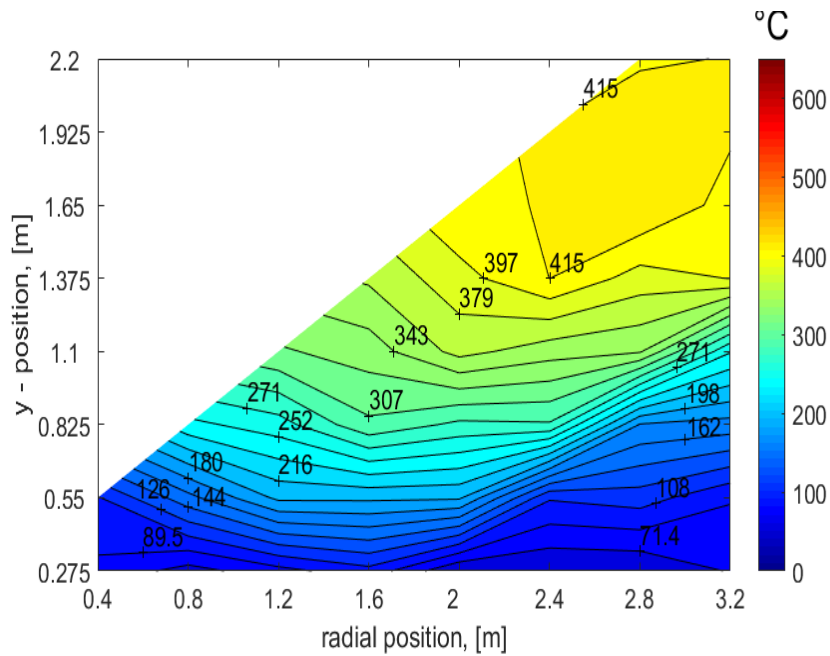


Figure 5.2: End of the idle period of 60 hours

During the idle period it can be observed from Figures 5.1b and 5.2 that there are notable thermal losses within the system. These thermal losses equated to an average temperature drop of 143 °C throughout the rock bed. It was later identified that the majority of the thermal losses occurred through the elbow of the hot air pipe, and are illustrated in Figure 5.3. These leaks were fixed between the second and last experimental campaigns.

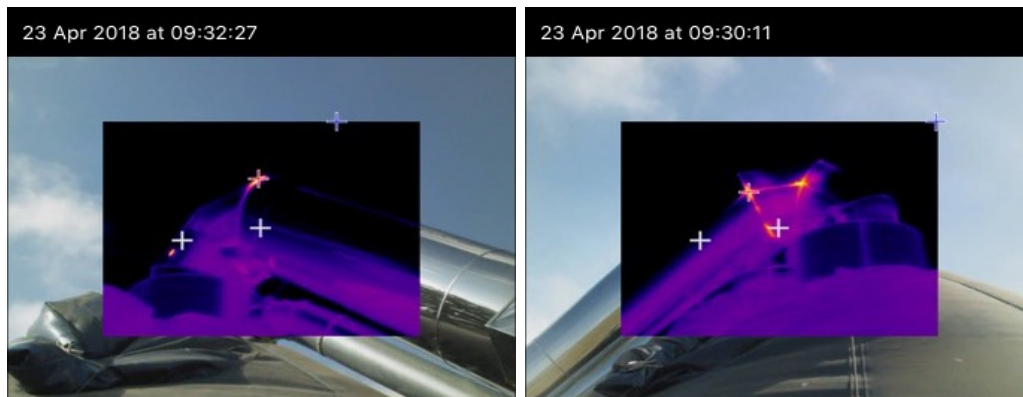


Figure 5.3: Thermal losses identified at the hot air inlet/outlet elbow

Results of the test are given in Table 5.2.

Table 5.2: Results - Initial test.

Property	Value	SI Unit
Average charge mass flow rate	0.50	kg/s
Charge temperature	601	°C
Charge duration	9.0	h
Charging capacity	330	kW _{th}
Energy input	3.02	MWh _{th}
Idle period	60.0	h
Energy loss	1.61	MWh _{th}
Total pressure drop (charge)	70.0	Pa
Volumetric efficiency	62.5	%
Overall efficiency	46.69	%

The energy loss equates to 1.61 MWh_{th} during the idle period. These losses can mainly be contributed to the thermal losses through the hot air inlet/outlet pipe, which is not sealed from the rock bed. The insulation layer was directly exposed to ambient conditions, which also contributed to thermal losses.

5.3.2 Single Charge-Discharge Test

The second test campaign consisted of a single charge-discharge cycle from cold rock bed conditions.

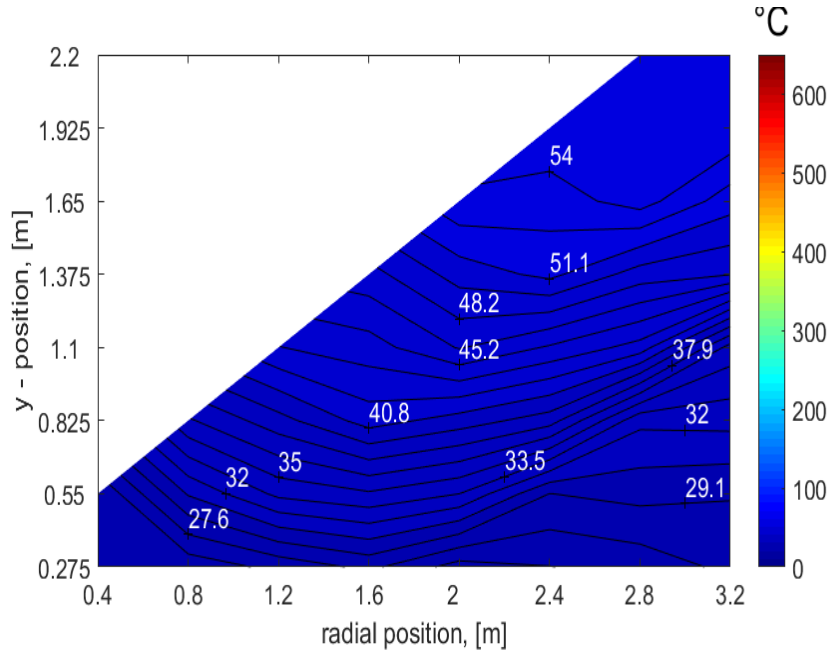
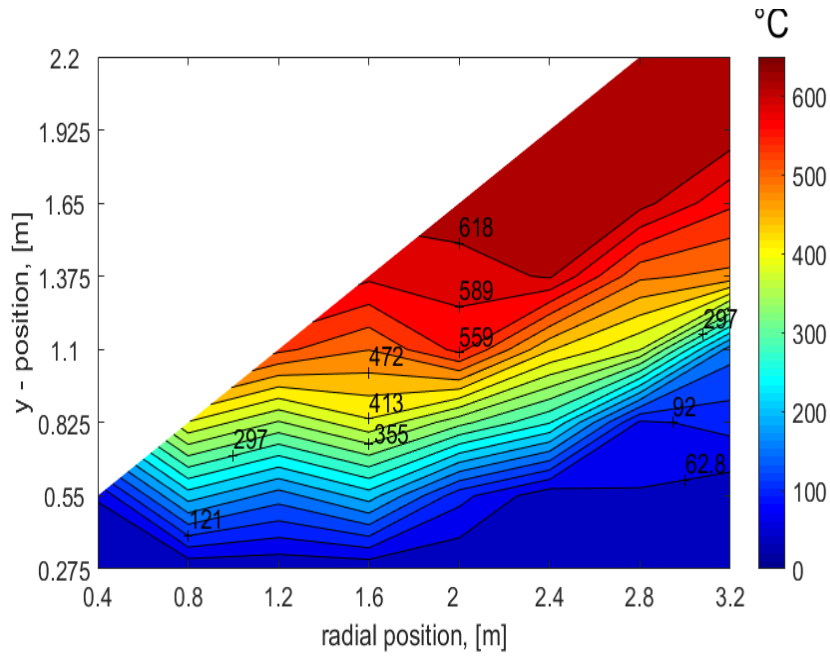
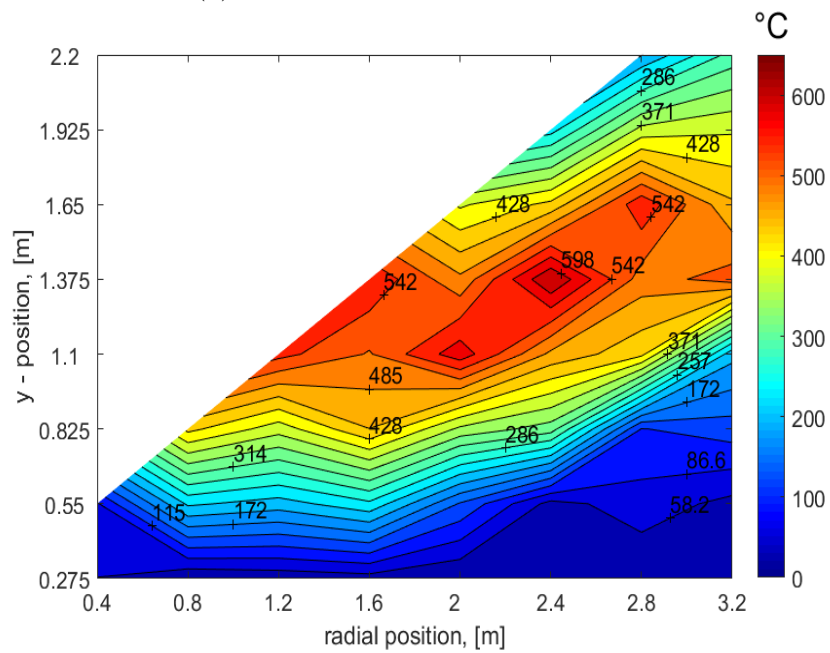


Figure 5.4: Initial temperature distribution - Test 2



(a) Distribution at 7 hours of charging



(b) Distribution at 8 hours of charging

Figure 5.5: Rock bed temperature distribution - Charge cycle

The charge cycle lasted a total of 8 hours, however 20 minutes before the end of the cycle, the LPG bottles emptied out and thus cold air got blown into the rock bed as illustrated in Figures 5.5a and 5.5b. After evaluating the data of the campaign, it was determined that it was useful and thus a repeat of the

experiment would be unnecessary. The average air temperature at rock bed inlet during the charge cycle was 618 °C. The rock bed was discharged until it reached the same state as in Figure 5.4. As discussed in Section 5.3 the flow leak was discovered during this campaign and the flow leak approximation was applied in the analysis. The total useful discharge time of 13.5 hours is due to the flow leakage.

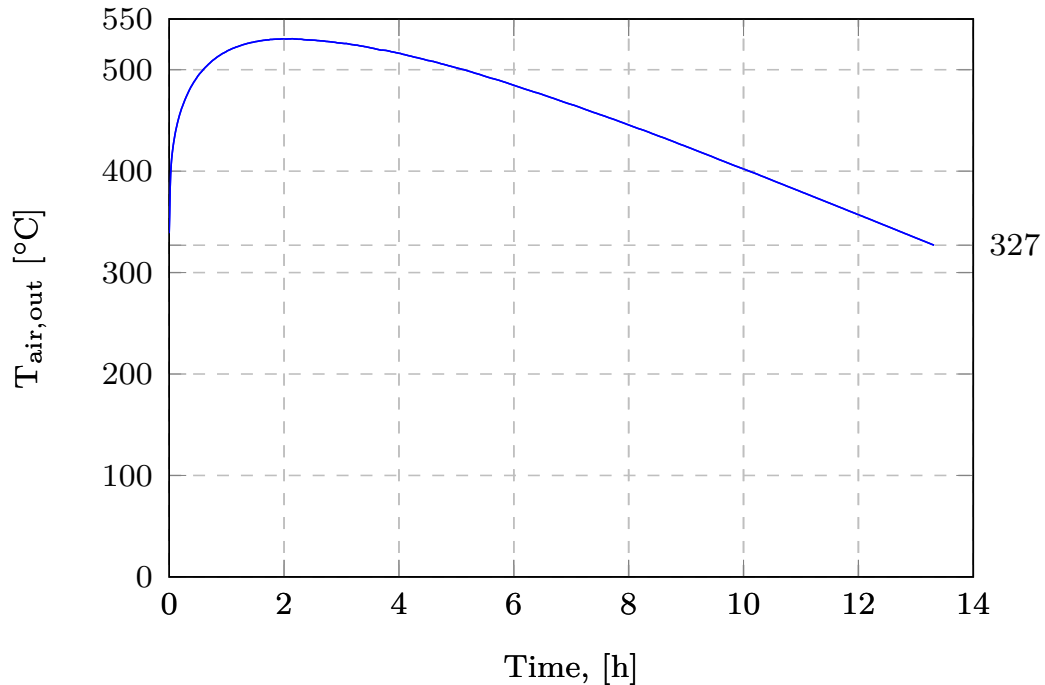


Figure 5.6: Discharge temperature over time - Second test

Figure 5.6 shows the air outlet temperature at the discharge outlet over time. Here it is illustrated that the outlet temperature exceeds 500 °C and remained above 400 °C for 10 hours. The difference between the charging temperature and maximum discharge temperature shows there is a loss in exergy, which is defined as the energy available within the system that can be used (Çengel, 2006). The thermal efficiency equated to 73.4 %. A total of 40 tons of rock was used as active storage material, giving a volumetric efficiency of 61.5 %.

Table 5.3: Results - Second test

Property	Value	SI Unit
Average charge mass flow rate	0.50	kg/s
Average charge temperature	618	°C
Charge duration	8.0	h
Charging capacity	319.91	kW _{th}
Energy input	2.56	MWh _{th}
Average discharge mass flow rate	0.30	kg/s
Discharge duration (useful)	13.5	h
Energy output	2.44	MWh _{th}
Useful energy output	1.88	MWh _{th}
Total pressure drop (charge)	14	Pa
Thermal efficiency	73.4	%
Volumetric efficiency	61.5	%
Overall efficiency	95.3	%

5.3.3 Multiple Cycle Test

Before the multiple cycle test campaign, the thermal leakage spots identified in Figure 5.3 were fixed. A scaffolding structure was erected over the facility as illustrated in Figure 5.7 to allow access to the leakage area. Figure 5.8 illustrates the area before it was fixed, with Figure 5.9 illustrating the fixed areas.



Figure 5.7: Scaffolding erected over the facility



Figure 5.8: Leakage areas



Figure 5.9: Leakage areas fixed

This test consisted of multiple charge-discharge cycles with an idle period between each charge and discharge. The test campaign was introduced to observe the behavior of the thermocline within the rock bed. It was expected that the thermal efficiency will increase as the cycles progress. All three discharge cycle

durations were governed by a minimum outlet temperature of 327 °C. The test had an average charge and discharge mass flow rate of 0.5 kg/s and 0.45 kg/s respectively.

The first charge cycle was from cold rock bed conditions as illustrated in Figure 5.10. Figures 5.11a and 5.11b illustrate the charge cycle and useful discharge cycle ends respectively. Figure 5.11a shows that a relatively thick thermocline settled within the rock bed. A difference in temperature distribution can be observed between Figures 5.11b and 5.12a, which was due to the total discharge cycle duration being longer than the useful discharge cycle duration.

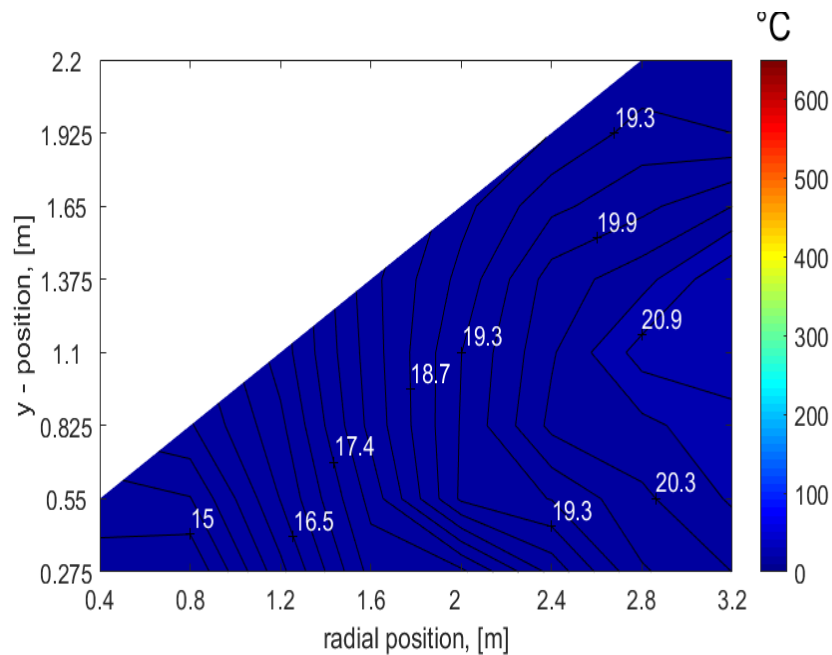
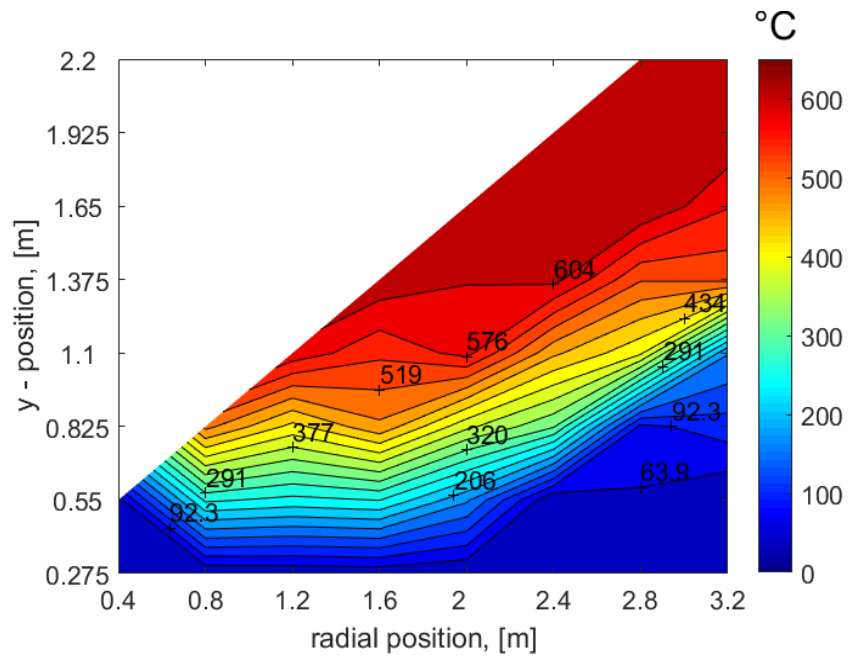
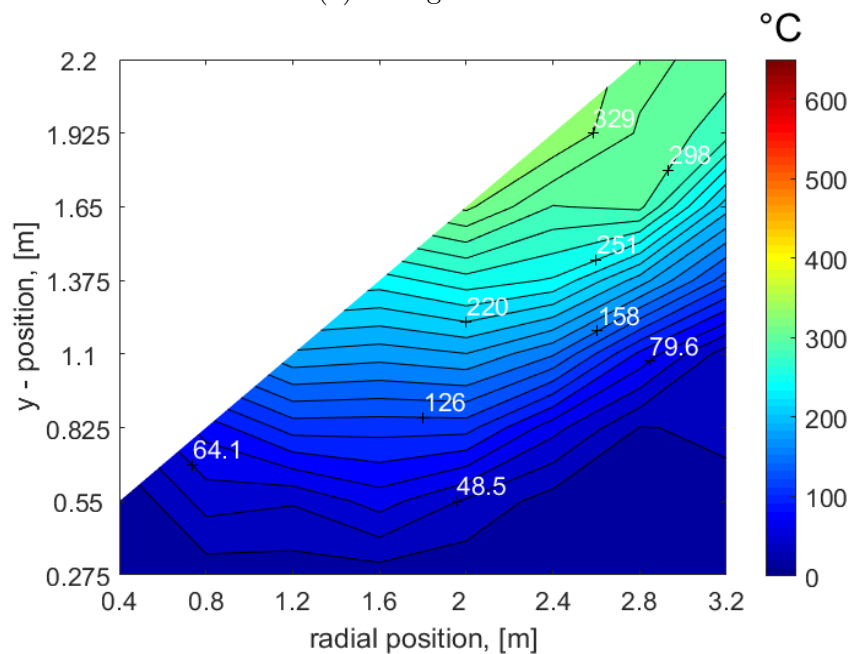


Figure 5.10: Initial temperature distribution - Multiple cycle test



(a) Charged rock bed

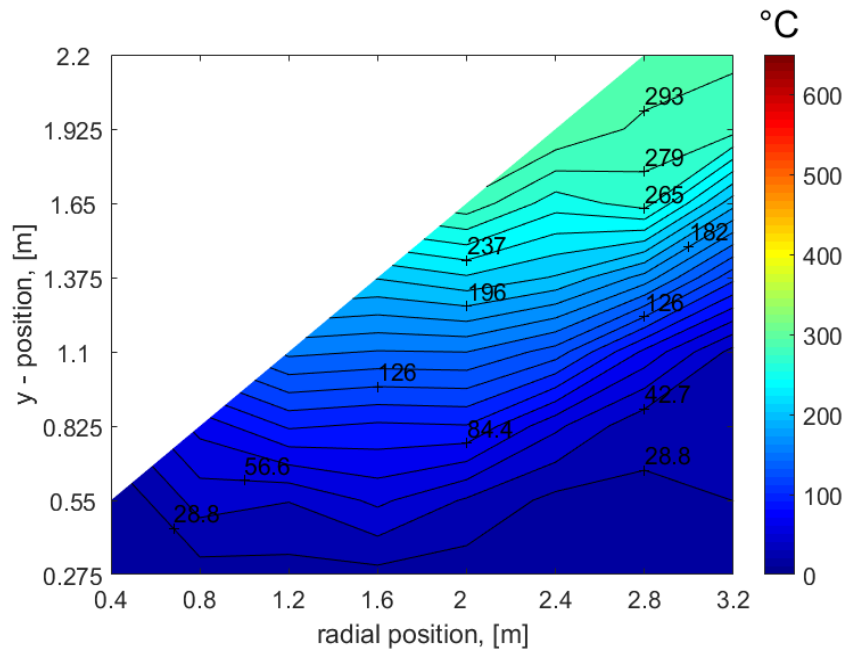


(b) Discharged rock bed to the minimum temperature

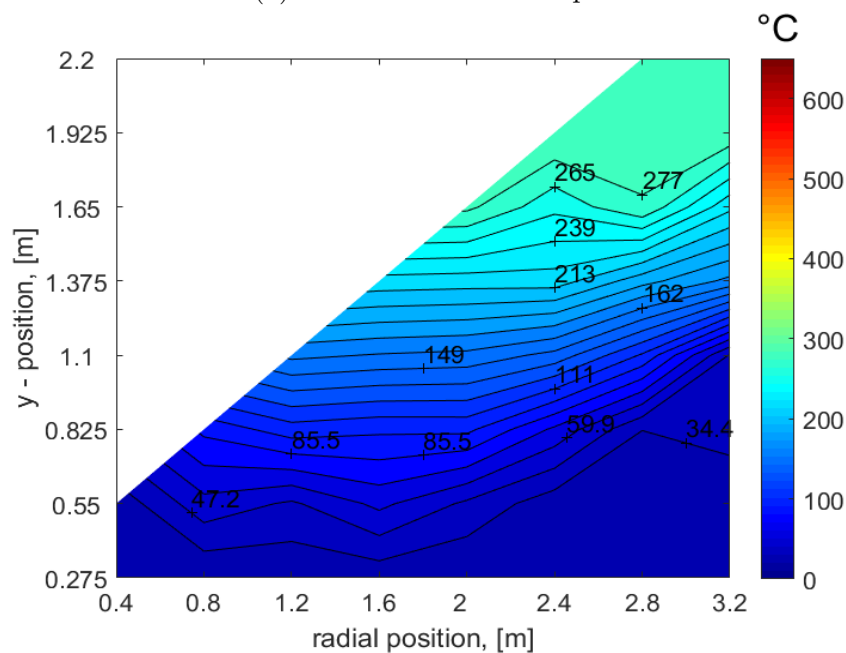
Figure 5.11: Rock bed temperature distribution - First cycle

The idle period lasted a total of 5 hours, with the temperature distribution illustrated in Figures 5.12a and 5.12b. It can be observed that the thermocline tended to settle toward a horizontal position during the idle period. The temperature slightly reduced, which is due heat that had moved up into the

hot air pipe. This can be prevented in the future by closing the rock bed off from the hot air pipe after charging is completed.



(a) Start of the first idle period

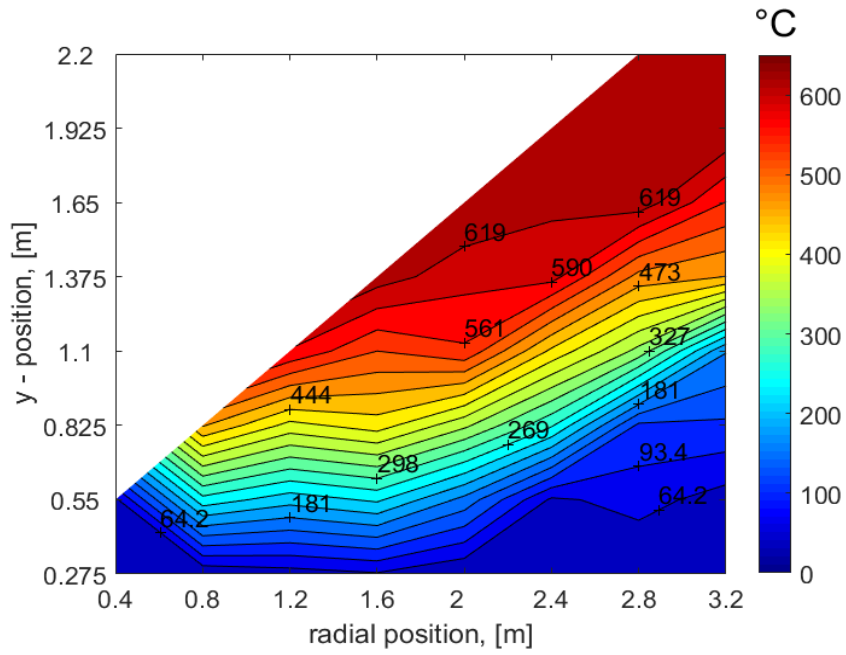


(b) End of the first idle period - 5 h

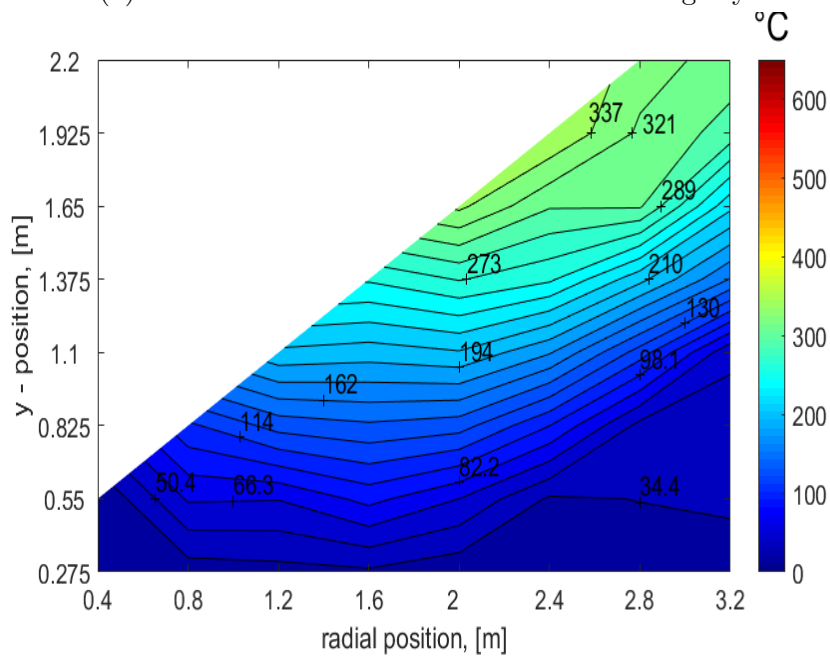
Figure 5.12: Rock bed temperature distribution - First idle period

The second charge cycle was from a pre-heated rock bed from the previous

cycle, as illustrated in Figure 5.12b. The charge cycle duration was governed by the outlet temperature at cold air outlet.



(a) Distribution at the end of the second charge cycle

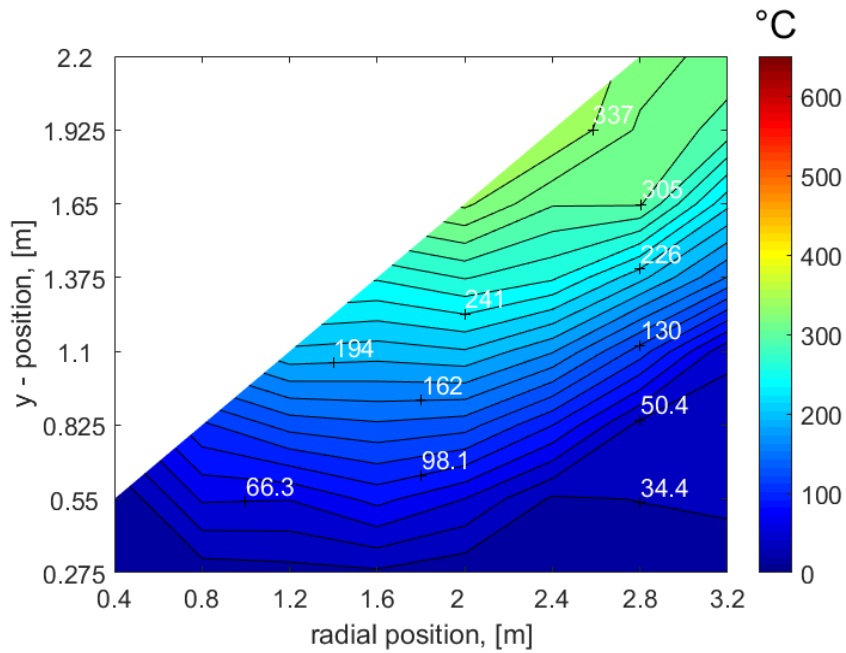


(b) Distribution at the end of the second discharge cycle

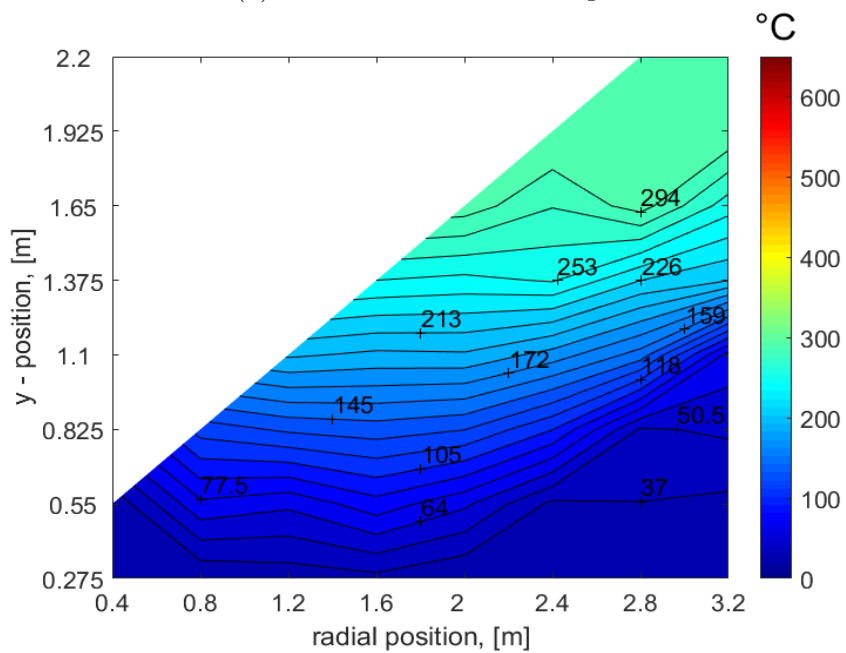
Figure 5.13: Rock bed temperature distribution - Second cycle

Figures 5.13a and 5.13b illustrate the end of the charge and discharge cycles.

Note that the thermocline remained thick throughout the second cycle. The thermocline once again settled toward a horizontal position during idle, as illustrated in Figures 5.14a and 5.14b, with the heat once again moving up into the hot air pipe and thus reducing the temperatures within the rock bed.



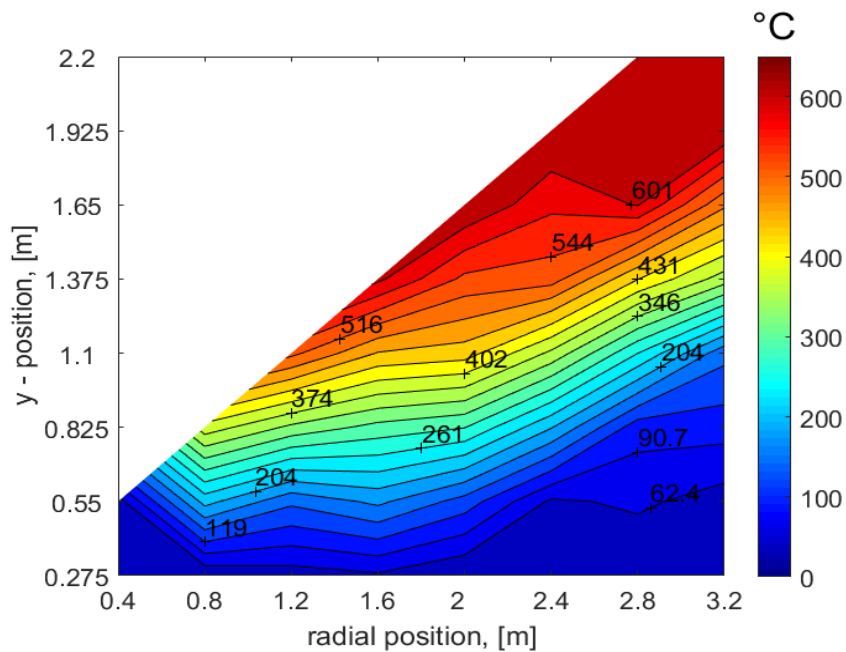
(a) Start of the second idle period



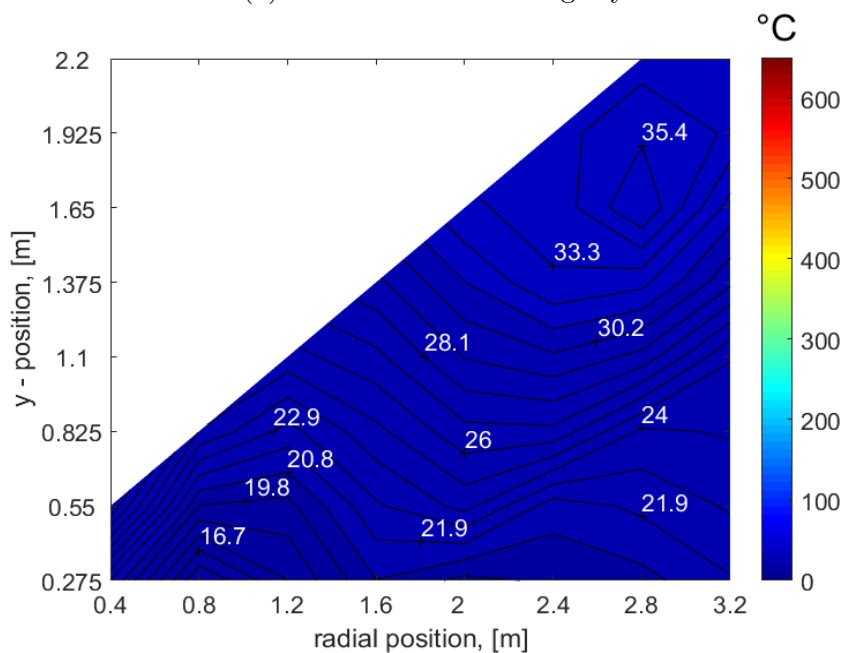
(b) End of the second idle period

Figure 5.14: Rock bed temperature distribution - Second idle period

The third charge cycle's duration was governed by the amount of LPG that remained within the bottles. Figures 5.15a and 5.15b illustrating the charge cycle and discharge cycle ends respectively. It can be observed that the charge cycle duration lasted 3.75 hours before the LPG ran out, thus a full charge was not achieved.



(a) End of the third charge cycle



(b) End of the third discharge cycle

Figure 5.15: Rock bed temperature distribution - Third cycle

Figure 5.16 compares the discharge temperature over time of each cycle. Noticeable is that the curve does not maintain a constant position at the maximum temperature as would be desired from a TESS. However, the discharge temperatures of cycle one and two remain above 400 °C for 7 hours and 6.5 hours respectively. Both the first and second cycle discharge temperatures have a near linear shape as it decreases. Although the shape is not ideal in terms of exergy, there is still a lot of energy discharged before the minimum temperature is reached. The third charge cycle could not be completed due to a limited supply of LPG, causing the rock bed to not reach a full charge state. This would explain the third discharge temperature curve's approximate linear shape. It is however noticeable that the discharge cycle still reached a maximum outlet temperature of 560 °C. The outlet temperature remained above 400 °C for a duration of 4.2 hours.

Comparing the discharge curves to those of Zanganeh *et al.* (2012), a similar behavior can be seen. Both curves have an approximate exponential shape and do not stay at the maximum discharge temperature for an extended period of time. A further study by Zanganeh *et al.* (2014) concludes that the introduction of phase-change materials (PCM) is a solution to improving the discharge temperature curve. Noticeable from Figure 5.11a, Figure 5.13a and Figure 5.15a compared to Figure 5.16 is that the maximum temperatures differ. This phenomenon is explained by the discharge temperature thermocouple's position: The thermocouple is situated within the hot air piping system, 1 m above the rock bed. This leaves an area for thermal losses, thus a drop in temperature, before the thermocouple is reached.

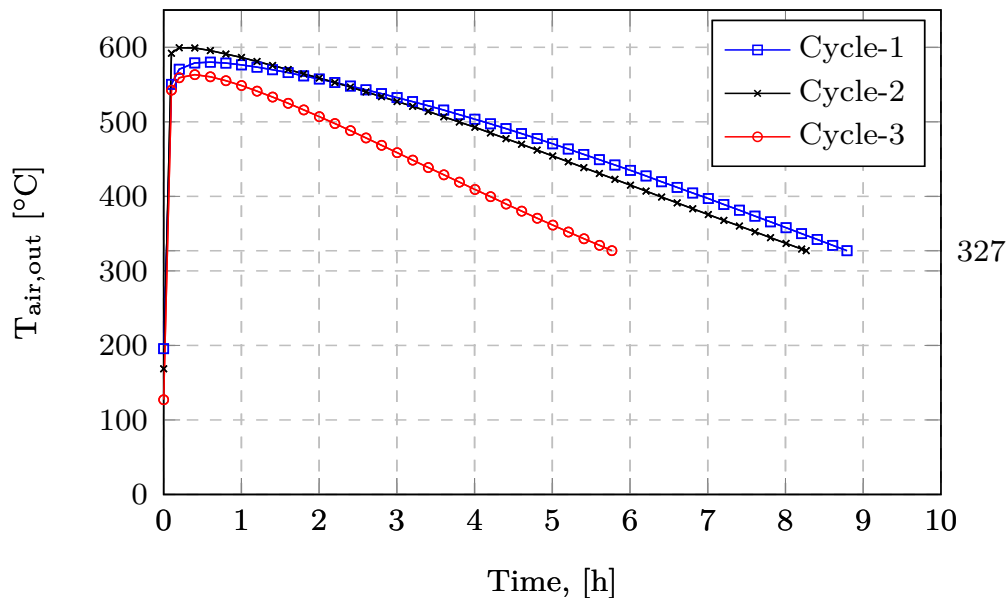


Figure 5.16: Discharge temperature over time - Multiple cycle test

Table 5.2 tabulates and compares the results of each cycle. The average charge temperature of cycle 1 was 646.8°C, energy input was 2.7 MWh_{th}, while the useful energy output was 1.9 MWh_{th}. The thermal efficiency equated to 72.75 %, which is expected considering that the first cycle occurred from cold rock bed conditions. The volumetric efficiency equated to 61.8 %.

The average charge temperature for cycle 2 was 658°C. The energy input was 1.97 MWh_{th}, while the useful energy output was 1.82 MWh_{th}. The thermal efficiency equated to 92.40 %, which is an increase of 27.01 % from the first cycle. The volumetric efficiency slightly decreased to 60.3 %.

Cycle 3 had a charge temperature of 650.56°C, energy input of 1.29 MWh_{th} and a useful energy extraction of 1.14 MWh_{th}. The thermal efficiency equated to 91.04 %, which is a decrease of 1.47 % from the second cycle. The decrease in thermal efficiency was due to a short third cycle charge, which caused the rock bed to not reach a fully charged state. The volumetric efficiency only equated to 39.1 %, due to the short charge cycle.

The pressure drop over each cycle is less than 20 Pa. Considering the large inlet area at the top of the rock bed and that the pressure measurement was taken in the middle of the rock bed, where the flow is much less, this pressure drop was expected.

Table 5.4: Multiple cycle results

Property	Cycle 1	Cycle 2	Cycle 3	SI Unit
Average charge mass flow rate	0.50	0.50	0.50	kg/s
Average charge temperature	646.80	658.00	650.56	°C
Charge duration	8.00	6.00	3.75	h
Charging capacity	337.5	336.67	348.05	kW _{th}
Energy input	2.70	1.97	1.34	MWh _{th}
Average discharge mass flow rate	0.45	0.45	0.45	kg/s
Useful discharge duration	8.50	8.30	5.77	h
Useful energy output	1.97	1.82	1.22	MWh _{th}
Total pressure drop (charge)	18.20	16.00	16.00	Pa
Thermal efficiency	72.75	92.40	91.04	%
Volumetric efficiency	61.80	60.30	39.10	%

The overall efficiency was determined by taking the total energy input over all cycles and comparing it to the total amount of useful energy output, as well as the rest of the energy output during the third discharge cycle. The overall efficiency equated to 94.24 %. This means that there was a thermal energy loss of 5.76 %, equaling 0.343 MWh_{th}.

A comparison between the results of the first cycle and the results obtained by Laubscher (2017) are listed in Table 5.5. The comparison yield an energy input increase of 1.669 MWh_{th}, a 161.88 % increase. The thermal efficiency increased by 21.25 % and the volumetric efficiency by 87.27 %. The pressure drop decreased by 261.80 Pa, which is a high decrease. The high decrease can be contributed to the fact that the inlet area of the rock bed increased from that of Laubscher (2017), which causes a lower initial pressure drop when the air enters the rock bed. The increase in the facility's performance more than justifies an additional capital cost of 11.95 %. However, it is acknowledged that there is still steps that can be taken to further improve the facility.

Table 5.5: Comparison of second-and third-generation results

Property	Cycle 1	Laubscher (2017)	SI Unit
Average charge mass flow rate	0.50	0.48	kg/s
Average charge temperature	646.80	638.00	°C
Charge duration	8.00	3.5	h
Charging capacity	337.5	318.00	kW _{th}
Energy input	2.70	1.031	MWh _{th}
Average discharge mass flow rate	0.45	0.48	kg/s
Useful discharge duration	8.50	2.75	h
Useful energy output	1.97	0.619	MWh _{th}
Total pressure drop (charge)	18.20	280.00	Pa
Thermal efficiency	72.75	60.00	%
Volumetric efficiency	61.80	33.00	%

5.4 Chapter Summary

The chapter introduced the experimental procedure, experimental campaigns and the results of these campaigns. Three tests were completed, with the final test consisting of multiple charge-discharge cycles with an idle period between each discharge and the following charge. The multiple cycle test consisted of three charge-discharge cycles, with the thermal efficiencies 72.75 %, 92.40 % and 91.04 % for each cycle respectively. The overall efficiency equated to 94.24 %. Results from the multiple cycle test will be used to validate the analytical model, presented in Chapter 6.

Chapter 6

Analytical Model and Results Comparison¹

6.1 Introduction

An analytical model of the TESS is developed to be validated by the results obtained from the experimental test campaigns. By predetermining the heat distribution throughout the rock bed through the experimental test campaigns, the analytical model's accuracy can be improved by altering the heat progression and initial conditions. Ultimately, a comparison of the two will allow for error determination between theory and practice. This will enable the concept to be simulated at various sizes, to ultimately predict the outcome of an industrial size concept without having to physically build one.

In section 6.2 the methodology regarding the analytical model is discussed. It includes the theory behind determining the heat transfer, as well as the pressure drop through the rock bed. Simulation results of the model are given and discussed.

The chapter concludes with a comparison between the experimental and analytical results, with a detailed discussion.

6.2 Methodology

The model is based on theory developed by Allen *et al.* (2015), which concentrates on the heat transfer and pressure drop over a rock bed.

¹Parts of this chapter have been published in Erasmus *et al.* (2018a) and Erasmus *et al.* (2018b)

6.2.1 Model Restrictions

The facility is represented by a one-dimensional heat transfer and pressure drop analytical model. Certain characteristics are restricted by modeling in only one dimension, such as the effect of buoyancy.

The particles (rocks) are represented by a spherical diameter approximation, due to the determination of an actual area measurement being practically impossible (Allen *et al.*, 2013). However, Allen *et al.* (2013) concluded that the approximation is adequate for the purpose of modeling the rock shape.

6.2.2 Heat Transfer

The rock bed is represented by a conical shape within the computation domain of the model. Due to this shape, the cross-sectional area differs from top to bottom. Figure 6.1 illustrates the approximation of the heat progression through the rock bed. The sloping thermocline shape is due to a larger void fraction between the rock bed free surface and the mesh, causing a preferential flow path around the edges. As the flow moves downwards through the rock bed, the flow experiences a higher relative resistance and therefore starts flowing toward the center of the rock bed. The cross-sectional area increases from the top of the rock bed to the bottom as progression takes place. The method for determining the cross-sectional area allows for flexibility in the model itself by changing α to represent different shapes of progression. The parameter L represents the direction of progression, while β is the angle of the rock bed surface. The slice thickness of each progression step is represented by ΔL .

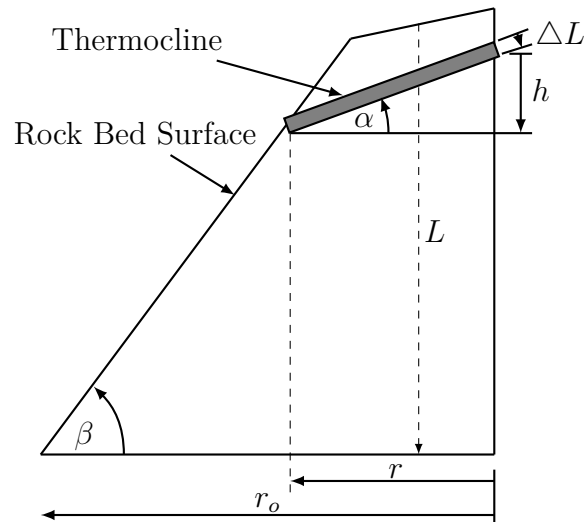


Figure 6.1: Computational domain of the cross-sectional area progression

The area is a function of the radius and height of each progression. The vertical progression is determined by the approximate diameter of a typical dolerite rock. The ratio between the height and radius of the progression is defined by α . For the simulation of this rock bed, α is approximated through observation of the thermocline progression in the experimental results. From here the height of each progression is determined by equation (6.2.1) and the cross-sectional area by equation (6.2.2). The volume of each progression step is determined by equation (6.2.3).

$$h = r \tan(\alpha) \quad (6.2.1)$$

$$A_{cs} = \pi r \sqrt{r^2 + h^2} \quad (6.2.2)$$

$$V = A_{cs} t \quad (6.2.3)$$

Forced convection is the dominant type of heat transfer that takes place during the charging and discharging cycles, with radiation and conduction negligible small compared to convection (Allen *et al.*, 2015). The heat transfer throughout the rock bed is thus calculated by making use of the effectiveness number of transfer units (e-NTU) method, originally developed by Hughes (1975), due to convection being the only heat transfer type taken into consideration. Duffie *et al.* (2003) showed that the e-NTU method is also a suitable method for predicting heat transfer in a one dimensional model.

What is different in the e-NTU method from the log mean temperature difference (LMTD) method is the use of a value known as the number of transfer units (NTU). NTU, given in equation (6.2.4), correlates with values of the computational domain namely the cross-sectional area A_{cs} and rock bed length L , as well as the computed values of the heat transfer coefficient h_v , mass flux G and specific heat of air $c_{p,a}$. The equivalent rock diameter is represented by D_v for spheres. An investigation by (Allen *et al.*, 2015) discusses the development and validation of these equations to be used for predicting the temperature profile within a packed bed. Equation (6.2.5) calculates the mass flux:

$$NTU = \frac{h_v L}{G c_{p,a}} \quad (6.2.4)$$

with

$$G = \frac{\dot{m}}{A_{cs}} \quad (6.2.5)$$

$$h_v = h_s (1 - \varepsilon) \frac{6}{D_v} \quad (6.2.6)$$

and

$$h_s = \frac{Nu k_a}{D_v} \quad (6.2.7)$$

where k_a is the thermal conductivity of air.

An added aspect of the model to the e-NTU method is the use of a time constant, making the solution time dependent. The time constant is a function of the rock density, void fraction, rock bed length, mass flow rate and the specific density of both the rocks and air. Equation (6.2.8) calculates this constant.

$$\tau = \frac{\rho_r(1 - \varepsilon)A_{cs}Lc_{p,r}}{\dot{m}c_{p,a}} \quad (6.2.8)$$

Both the Reynolds and Nusselt Numbers are non-dimensional numbers used in the e-NTU method. They are calculated using equations (6.2.9) and (6.2.10) which are simplified equations developed and validated by (Allen *et al.*, 2015). The air viscosity is represented by μ .

$$Re = \frac{GD_v}{\mu} \quad (6.2.9)$$

$$Nu_v = Re_{pv}^{0.6} \quad (6.2.10)$$

The Biot number represents the heat transfer resistances within a control volume (Incropera *et al.*, 2007). For this study, the Biot number is representative of the ratio of heat transfer resistances inside of as well as at the surface of the rocks (particles). In general, the thermal gradient is negligible when $Bi < 0.1$. From equation (6.2.11), it is observed that the Biot number is dependent on the rock pebble surface heat transfer coefficient in equation (6.2.7). In turn the heat transfer coefficient is dependent of the Reynolds number, which is calculated through equation (6.2.9). This heat transfer correlation for use in a packed bed is validated by Allen *et al.* (2015).

$$Bi = \frac{h_s D}{2k_r} \quad (6.2.11)$$

The efficiency of the heat transfer is calculated by:

$$\eta = 1 - e^{\frac{-NTU\Delta r}{(r_o - r_i)}} \quad (6.2.12)$$

For each step of progression the air and rock temperature is determined by equation (6.2.13) and equation (6.2.14). (Allen *et al.*, 2015)

$$T_{a_{i,j+1}} = T_{a_{i,j}} - \eta(T_{a_{i,j}} - T_{r_{i,j}}) \quad (6.2.13)$$

$$T_{r_{i+1,j}} = \frac{T_{a_i}(1 - \frac{\Delta t}{2\tau} \frac{L}{\Delta y} \eta) + T_{a_i}(\frac{\Delta t}{\tau} \frac{L}{\Delta y} \eta)}{1 + \frac{\Delta t}{2\tau} \frac{L}{\Delta y}} \quad (6.2.14)$$

These equations were developed by Allen *et al.* (2015) specifically for the heat transfer in packed beds between air (gas particles) and solid particles. They allow for estimation without measuring particle shape, roughness or size distribution throughout the rock bed (Allen *et al.*, 2015).

6.2.3 Energy Balance

The energy balance of the TESS is critical in understanding the efficiency of heat transfer and thermal energy storage of such a system. First however, the theory of heat transfer between a solid (the rock bed) and a fluid (the air) must be understood.

A TESS model needs to satisfy two energy balances. The first balance is that of the fluid, which acts as the carrier of the heat, and is thus defined as the heat transfer fluid. The second balance is that of the solid, which acts as the storage medium of the heat. The HTF operates within an open control volume due to the fact that it enters the control volume of the solid and then exits the control volume once heat transfer occurred. The solid operates within a closed control volume, due to no mass entering or exiting the control volume. The heating power of the fluid is calculated using equation (6.2.15), from Çengel (2006).

$$\dot{Q}_{in} = \dot{m}c_{p,a} \Delta T_f \quad (6.2.15)$$

where ΔT is the difference between the input (air) and initial (rock) temperatures, assumed to be uniform.

The total energy input is calculated by accumulation of the energy introduced into the rock bed at each time step, as depicted in equation (6.2.16):

$$E_{in} = \sum_{i=0}^t \dot{m}c_{p,a(i)} \Delta T_{f(i)} \Delta t \quad (6.2.16)$$

To determine the energy stored within the rock bed, the heating capacity of the rock bed must first be determined. The rock particle specific heat capacity ($c_{p,r}$) is defined by the function in equation (6.2.17). The function is temperature dependent and is valid up to a maximum operating temperature of 650 °C. (Allen *et al.*, 2015)

$$c_{p,r}(T_r) = -0.00129T_r^2 + 1.518T_r + 748 \quad (6.2.17)$$

From here, the total stored energy can be determined by:

$$E_{st} = \sum_{i=0}^x m_{(i)} \int_{T_{amb}}^{T_{f(i)}} c_{p,r}(T_{r(i)}) dT \quad (6.2.18)$$

The heat transfer efficiency between the HTF and rock bed is calculated by:

$$\eta_{ht} = \frac{E_{st}}{E_{in}} \quad (6.2.19)$$

6.2.4 Pressure Drop

Determining the pressure drop is important to determine the pumping power needed for the facility. Allen *et al.* (2015) identified the need to develop theory for the estimation of pressure drop through a rock bed, due to the particle shape, roughness and packing arrangement being strong influential factors. In particular for crushed rock due to it being randomly packed and of an roughly approximate spherical shape. For each progression segment, the pressure drop is calculated by making use of equations (6.2.20) to (6.2.23), developed and validated by Allen *et al.* (2015).

The superficial velocity is calculated through equation (6.2.20), and is dependent on the air mass flow rate, \dot{m} , air density, ρ_a and cross-sectional area of the segment, A_{cs} . The Reynold number, Re_v , is directly related to superficial velocity, v_s , and the air density, ρ_a . The pressure drop calculations also make use of a friction factor, f_v . Equation (6.2.22) is used for conditions where the rock diameter range is $0.009 < D_v < 0.049$ and the void fraction lies within the range $0.38 < \varepsilon < 0.48$. This rock bed satisfies these criteria.

$$v_s = \frac{\dot{m}}{\rho_a A_{cs}} \quad (6.2.20)$$

$$Re_v = \frac{\rho_a v_s D_v}{\mu(1 - \varepsilon)} \quad (6.2.21)$$

$$f_v = \frac{620}{Re_v} + \frac{13.7}{Re_v^{0.08}} \quad (6.2.22)$$

The pressure drop over each segment is calculated by equation (6.2.23), with the total pressure drop determined through equation (6.2.24).

$$\Delta p = 0.5 f_v (\Delta r \rho_a v_s^2) \left(\frac{1 - \varepsilon}{\varepsilon^3} \right) \left(\frac{1}{D_v} \right) \quad (6.2.23)$$

$$\Delta P = \sum_{i=0}^y \Delta p_i \quad (6.2.24)$$

6.3 Simulation and Result Comparison

This section discusses the simulation procedure as well as its results. The results are compared to those of the experimental test campaigns, to allow for an accurate prediction on the performance of such a concept on an industrial scale.

6.3.1 Simulation

An analytical simulation was completed and compared to the multiple cycle experimental test results. Table 6.1 lists the initial parameters of the simulation. All dimensions are in correlation with that of the experimental facility.

Table 6.1: Initial parameters

Description	Symbol	Value	SI Unit
Rock bed height	L	1.554	m
Radial progression steps	Δr	0.05	m
Horizontal progression steps	ΔL	0.042	m
Radius at top of rock bed	r_i	1.15	m
Radius at bottom of rock bed	r_o	3.0	m
Time step	Δt	30	s
rock density	ρ_r	2700	kg/m ³
Charge mass flow rate	\dot{m}_{in}	0.5	kg/s
Discharge mass flow rate	\dot{m}_{out}	0.45	kg/s
Void fraction	ε	0.43	-
Area profile	α	22.25	°
Ambient temperature	T_{amb}	28	°C

Figure 6.2, Figure 6.3 and Figure 6.4 illustrate the 2-hourly temperature distribution in the rock bed over the vertical position from the top. The marks represent each segment downwards from the top of the rock bed. Comparing the first and second cycles in Figures 6.2 and 6.3, the temperature distribution curve has changed throughout the rock bed. The distribution has reached a state where the cold area, temperatures under 327°C, has settled over a slightly thicker vertical position to a total thickness of 0.74 m, 0.04 m more than the first cycle.

However, the temperature distribution of the thermocline has also changed. From the curve shape it is observed that the thermocline has increased in temperature at each vertical position, meaning that there is more surface area at a higher temperature than after the first charge cycle. This implicates that more energy can be stored with each cycle, until an equilibrium is eventually reached after a certain number of cycles.

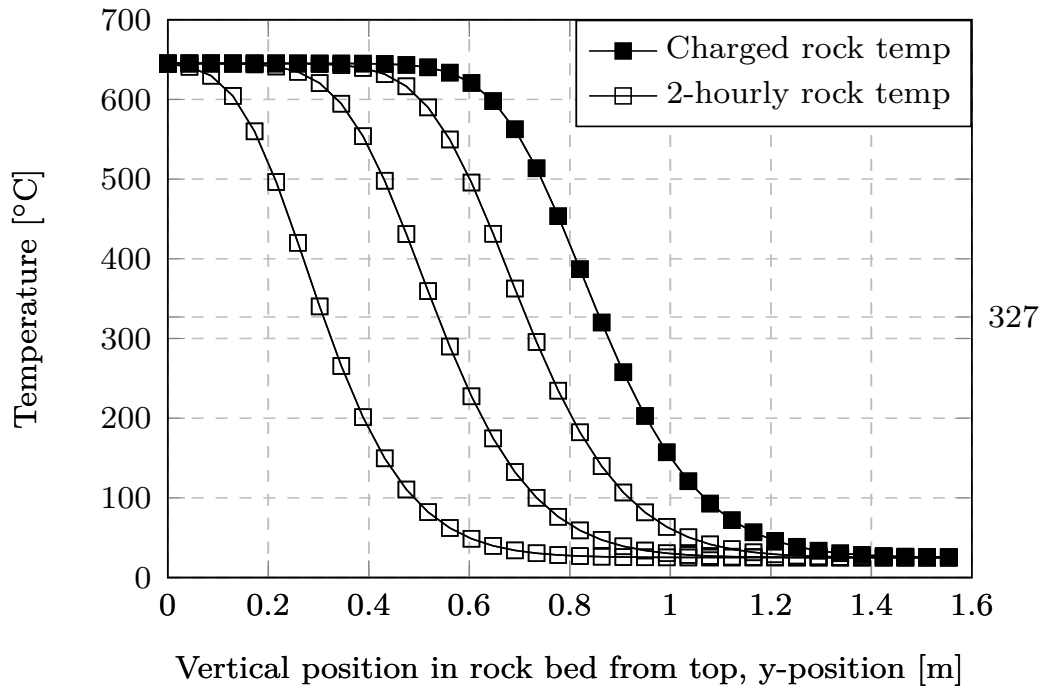


Figure 6.2: Temperature distribution over position - Cycle 1

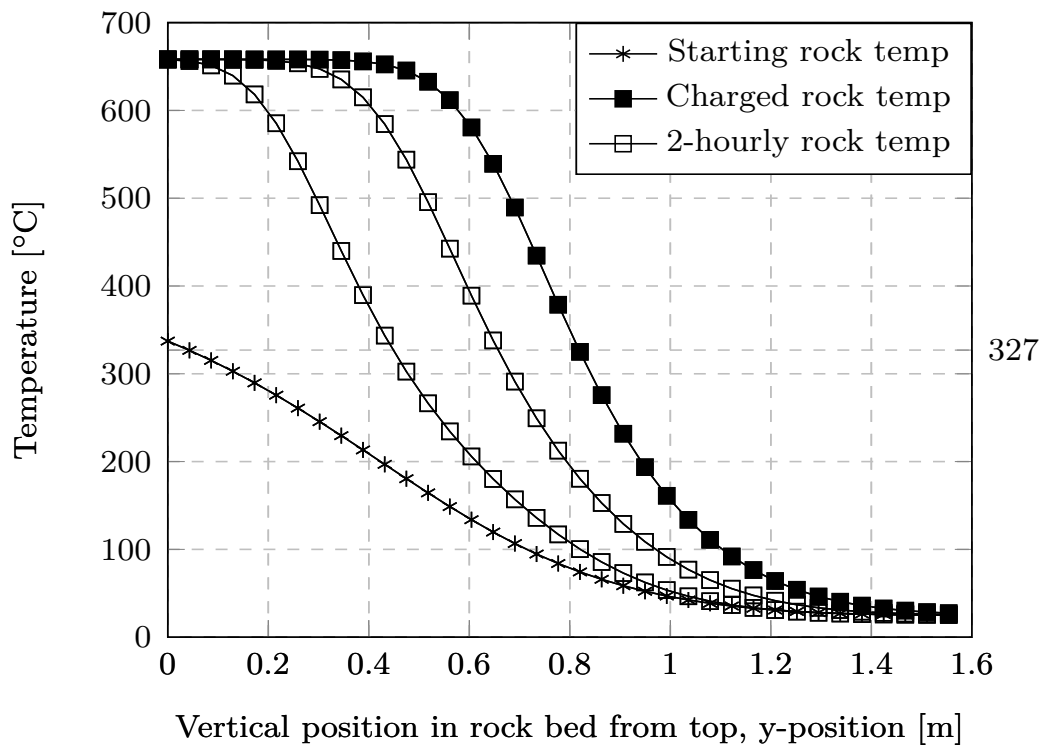


Figure 6.3: Temperature distribution over position - Cycle 2

From Figure 6.4 it is observed that the temperature distribution curve once again changed throughout the rock bed, the same behavior as observed in Figure 6.3. In this cycle the cold area distribution settles to a thickness of 0.91 m, changing the temperature distribution of the thermocline itself. This is due to the cycle not achieving a full charge state.

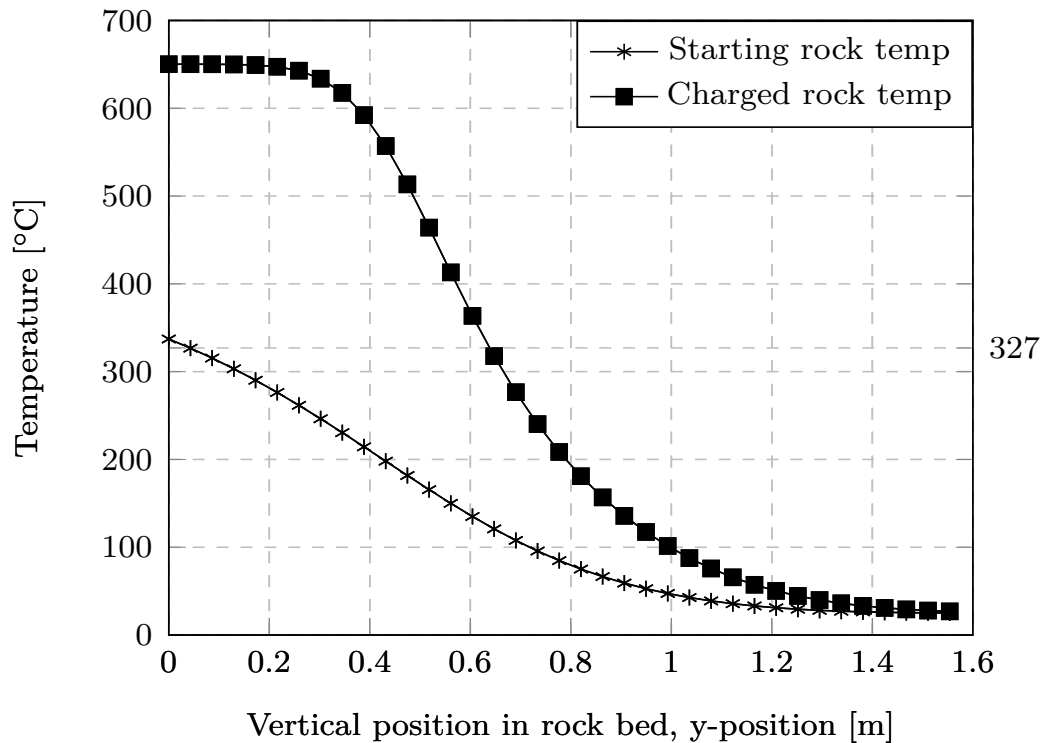


Figure 6.4: Temperature distribution over position - Cycle 3

The Biot number at the start and end of each cycle is illustrated in Figure 6.5. The Biot number is above 0.1 for the majority of the segments, with the thermal gradient negligible below 0.1. From the figure it is observed that the Biot number at each position in the rock bed increases with each cycle. Another observation is that the initial and final Biot numbers are closer to each other with each cycle. These effects are caused by the fact that the thermocline is already present in the second and third cycles.

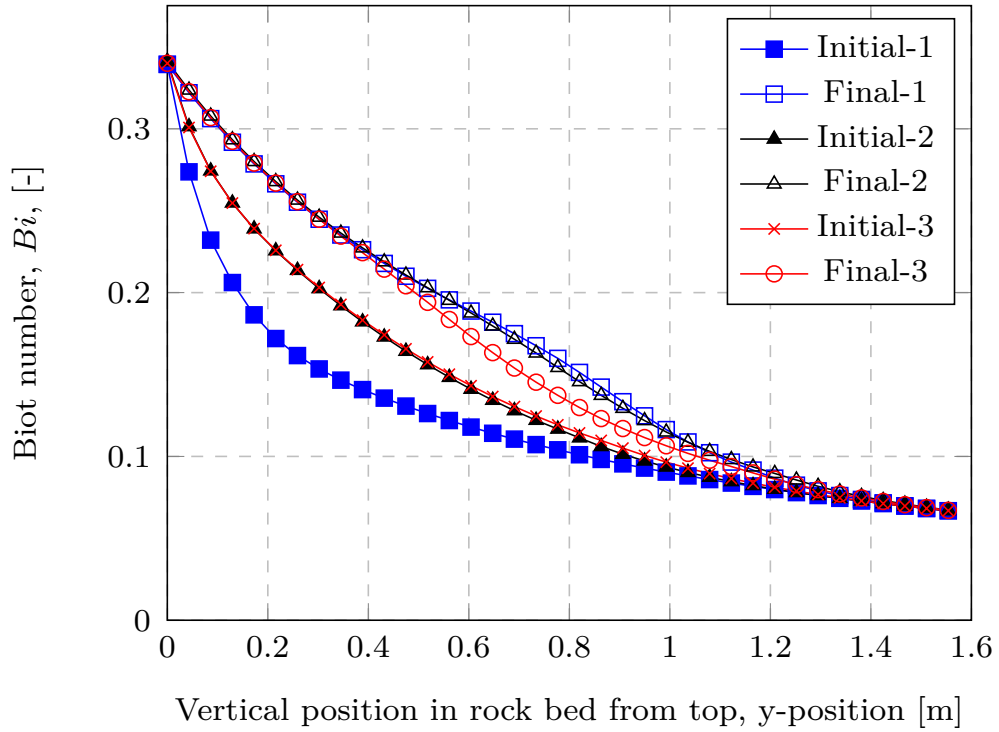


Figure 6.5: Biot number

Inspecting this phenomenon further, it is illustrated in Figure 6.6 that the Nusselt number at the start and end of each cycle also tends to come closer to each other. The Nusselt number decreases at each position with each cycle, which is expected after observing the behavior of the Biot number.

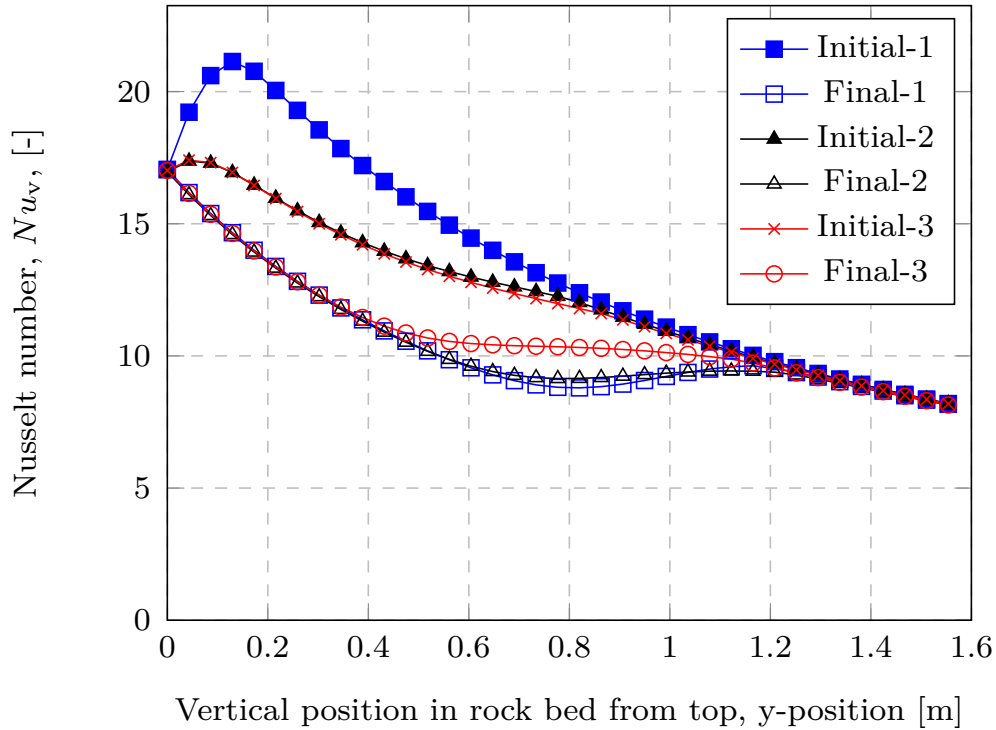


Figure 6.6: Nusselt number

Figure 6.7 illustrates the pressure gradient across the vertical position of the rock bed from the top during charge. The gradient stays relatively constant throughout the three charge cycles. As expected, the pressure gradient is largest at rock bed inlet. As the cross-sectional area increases, the pressure drop decreases. The large area at rock bed inlet, a radius of 1.15 m, causes the pressure drop at inlet to be as low as illustrated. In the case of Laubscher (2017), the hot air inlet area into the rock bed is smaller, thus the pressure drop of the previous concept is much higher than for this concept.

If it is desired to further decrease the pressure drop over the rock bed without altering the dimensions, the rock size at rock bed inlet can be increased. This will cause a higher void fraction, allowing flow to occur more easily through the rocks.

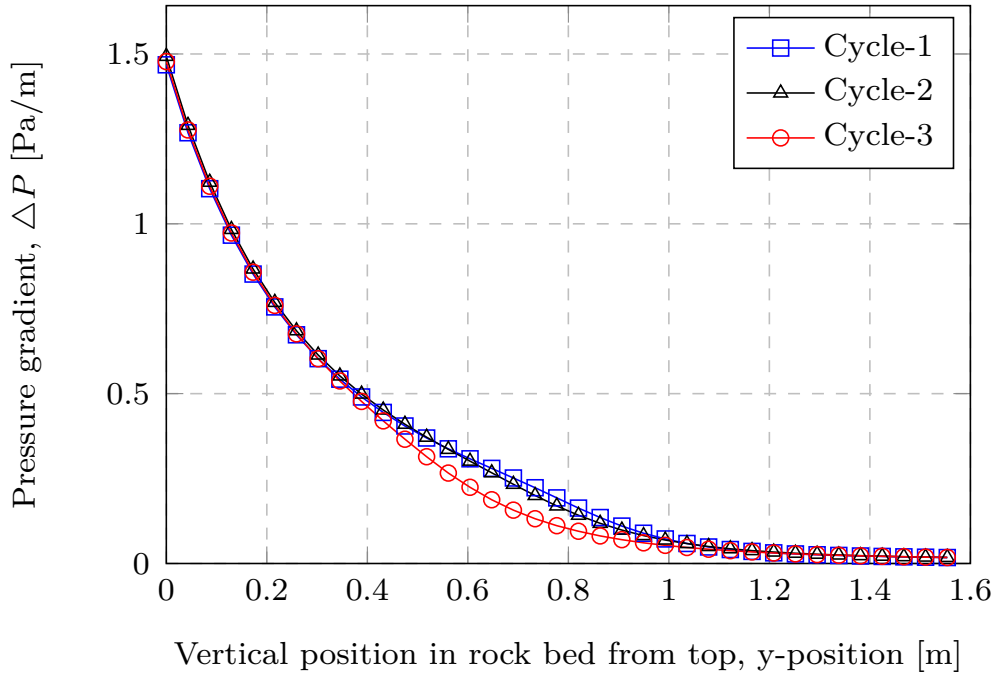


Figure 6.7: Pressure gradient

6.3.2 Comparison of Results

A comparison between the first charge-discharge cycle of the multiple cycle conditions are presented in Table 6.2. A difference of 8.00 % is calculated for the thermal efficiency between the simulation and experimental test. The pressure drop difference is 5.7 %.

Table 6.2: Comparison of the first charge-discharge cycle.

Property	Analytical	Experimental	SI Unit
Charge mass flow rate	0.50	0.50	kg/s
Charge temperature	645.00	646.80	°C
Charge duration	8.00	8.00	h
Charging capacity	327.50	337.5	kW _{th}
Energy input	2.62	2.7	MWh _{th}
Discharge mass flow rate	0.45	0.45	kg/s
Discharge duration	9.17	8.50	h
Useful energy output	2.07	1.97	MWh _{th}
Total pressure drop	12.50	18.20	Pa
Thermal efficiency	79.08	72.75	%
Volumetric efficiency	57.50	61.80	%

The simulation and experimental results of the second charge-discharge cycle are presented in Table 6.3. From the comparison the most noticeable difference is that of the thermal efficiencies. The analytical model gives an efficiency of 99.80 %, an increase of 26.20 % in reference to the first charge-discharge cycle, while the experimental results calculate a thermal efficiency of 92.40 %, an increase of 27.01 %. The difference between the simulation and experimental test is 7.41 %.

Table 6.3: Comparison of the second charge-discharge cycle.

Property	Analytical	Experimental	SI Unit
Charge mass flow rate	0.50	0.50	kg/s
Charge temperature	658.00	658.00	°C
Charge duration	6.00	6.00	h
Charging capacity	348.3	336.67	kW _{th}
Energy input	2.09	2.02	MWh _{th}
Discharge mass flow rate	0.45	0.45	kg/s
Discharge duration	8.57	8.30	h
Useful energy output	1.91	1.82	MWh _{th}
Total pressure drop	12.63	16.00	Pa
Thermal efficiency	99.80	92.40	%
Volumetric efficiency	57.50	60.30	%

The third cycle is compared in Table 6.4. The most noticeable is the model's thermal efficiency of 112.90 %, which is above 100 %. The high efficiency of the model is due to the fact that the model assumes perfect insulation, thus all heat introduced into the rock bed remains within it. As a result of this, the modeled thermocline settles in such a shape that the same rock volume at the same charge time is at a higher temperature in the next charge cycle, due to the cycle building on the heat left from the previous cycle. More heat is thus extracted from the cycle's discharge than what was introduced.

Table 6.4: Comparison of the third charge-discharge cycle.

Property	Analytical	Experimental	SI Unit
Charge mass flow rate	0.50	0.50	kg/s
Charge temperature	650.00	650.00	°C
Charge duration	3.75	3.85	h
Charging capacity	327.5	348.05	kW _{th}
Energy input	1.24	1.34	MWh _{th}
Discharge mass flow rate	0.45	0.45	kg/s
Discharge duration	5.83	5.77	h
Useful energy output	1.40	1.22	MWh _{th}
Total pressure drop	12.52	16.00	Pa
Thermal efficiency	112.90	91.04	%
Volumetric efficiency	45.7	39.1	%

The discharge temperature over time is compared in Figure 6.8. The discharge temperature is measured at the entrance of the hot air outlet pipe. With the measurement position not situated at the top of the rock bed, it is not representative of the temperature directly at the rock bed outlet. The area between the measurement point and top of the rock bed contains thermal losses. Due to this it is observed that the model has a higher discharge temperature than that of the experimental test. However, the curve has a sharper decrease than that of the experimental test.

Both the first and second cycle curves are within 20 °C of one another for the same discharge duration, with the model giving the higher temperature. Discharge duration for the model lasts 40 minutes longer for the first discharge, 16 minutes for the second discharge and 3 minutes for the last discharge cycle.

To make a more accurate comparison of the discharge temperatures curves over time, the temperature measurement at the top of the rock bed was used to make a comparison with the model. By doing this, the temperature drop between the top of the rock bed and the outlet temperature measurement position is eliminated. The comparison is illustrated in Figure 6.9.

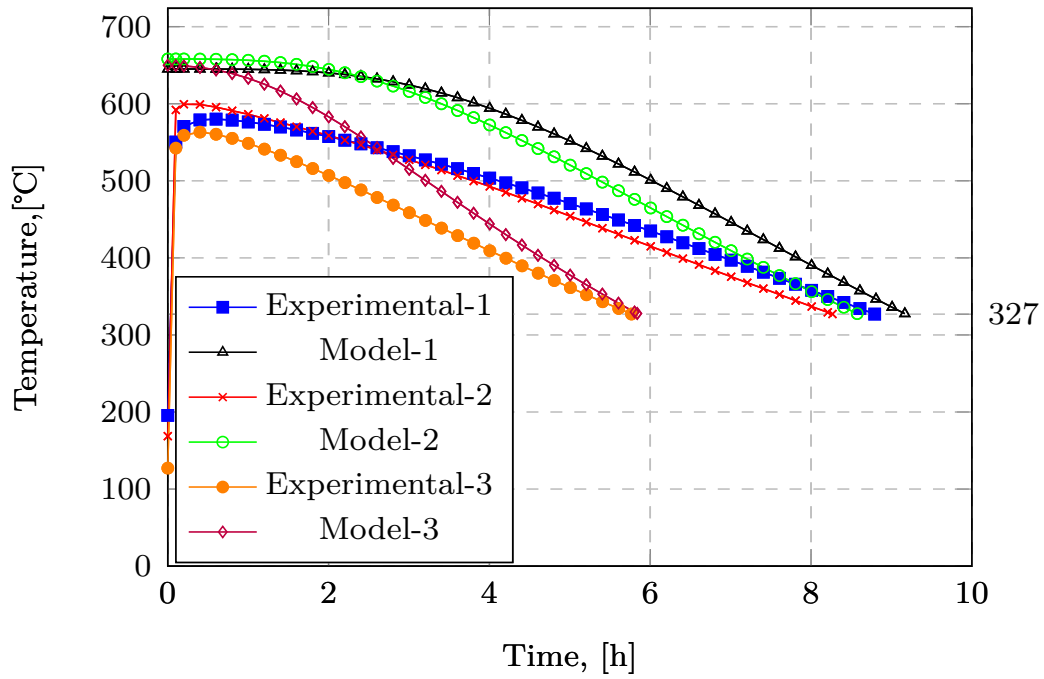


Figure 6.8: Discharge temperature over time comparison

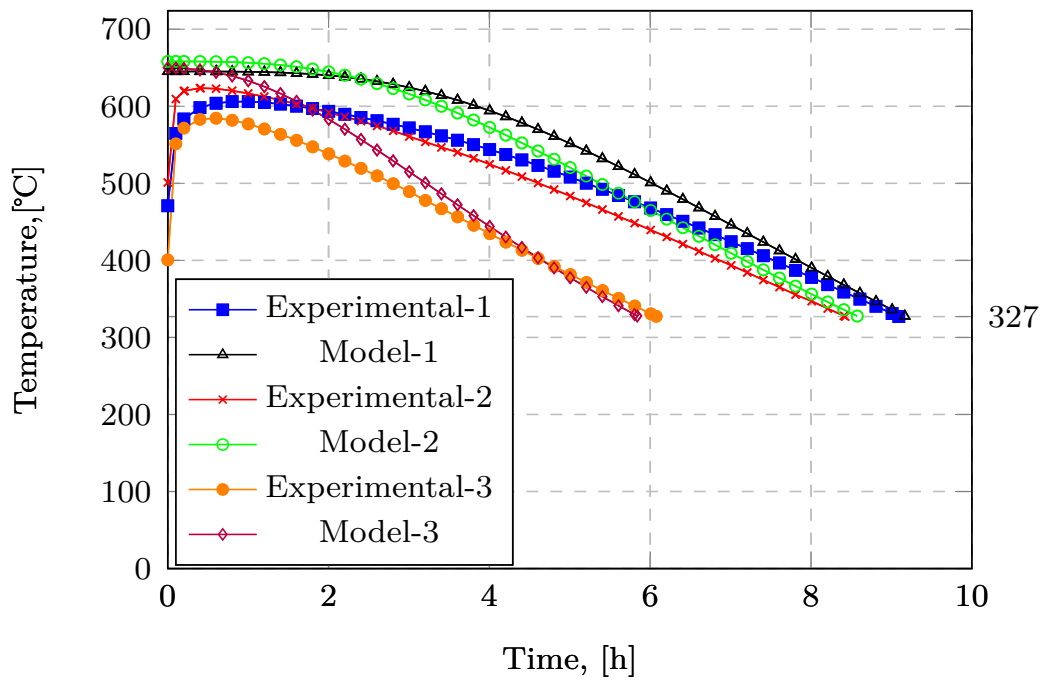


Figure 6.9: Improved discharge temperature over time comparison

From Figure 6.9 it is observed that the discharge cycles end within 10 minutes of one another. The maximum outlet temperatures are also closer to one another. The difference can be contributed to thermal losses, which are not modeled, and that the TESS never reached full charge temperature, thus discharge never started at the same point. Thermal losses are thermal energy not within the rock bed, but rather in the surrounding elements such as the spider web frame, insulation and piping.

6.4 Chapter Summary

The chapter discussed the methodology of the analytical model. The methodology includes model restrictions, heat transfer, pressure drop and energy balance discussions. The simulation represented a multiple charge-discharge cycles. The results of these simulations are presented, discussed and compared to the experimental results in detail. From the comparison it was found that there is a difference in the thermal efficiency between the experimental and simulation results of 8.00 % and 7.41 % for the first and second cycles respectively. The third cycle gave a thermal efficiency difference of 19.36 %, a result of the model assuming perfect insulation and operating conditions.

Chapter 7

Conclusion and Recommendations

7.1 Conclusion

Thermal energy storage is an integral part in concentrated solar power, allowing such plants to operate at full potential. Such storage systems however also form a large part, up to 13 % (Kolb *et al.*, 2011), of the capital cost of CSP plants. Thus, thermal rock bed TESS features as a possible low-cost solution. Studies at Stellenbosch University by Allen (2010), Kröger (2011), Gauché and Louw (2014) and Laubscher (2017) on rock bed storage has paved a way for further research within this project.

The project focused on designing and developing a next-generation concept for thermal rock bed energy storage, in Chapter 3. After the design and development stage, the concept was constructed as a modification to the existing facility. The construction is discussed in Section 4.2.

After construction, three experimental tests were completed, with the process and results discussed in Chapter 5. The multiple cycle test yielded, thermal efficiencies of 72.75 %, 92.40 % and 91.04 % for the first, second and third cycles respectively. The overall efficiency equated to 94.24 %. The volumetric efficiency was approximately 61.00 % when a full charge state was reached.

An analytical model was developed to validate the results obtained through the experimental tests, which is discussed in Chapter 6. Within Chapter 6, the results are compared to those of the experimental tests. The comparison yielded a maximum difference between the results of +8.00 % for the first two cycles. The third cycle gave a thermal efficiency difference of +19.36 %. This suggests that the model needs to be adjusted to include thermal losses in the rock bed, to allow for a more accurate comparison. In addition, the experi-

mental setup, specifically the flow measurement, is not beyond criticism. Flow leakage played a major part in the experimental test campaigns and thus had an influence in comparing the results to the analytical model.

All the objectives set out at the beginning of the project are met. An economic study is yet to determine the capital cost and LCOE of the system. It is however expected that, although the capital cost is more than that of the previous design, the improvement in efficiencies will result in a lower LCOE. The next-generation design of the rock bed TESS confirms that it is a promising technology for cheap and effective thermal energy storage systems in the future.

7.2 Recommendations

Future experimental work on the existing facility is recommended to fully understand the various phenomenons of rock bed TESS. Many lessons have been learned during the course of this project, which are listed in Appendix D. These lessons are in short:

- The cover introduced limitations that can be resolved by the introduction of a hot air fan.
- Flow should be measured both at the inlet and outlet to determine if flow losses are present.
- The rock bed should be sealed off during idle to prevent heat from entering the piping system, causing thermal losses.
- Remove the spider web structure and mesh frame to reduce preferential flow between the rock bed and the structure.

The solutions to these problems serve as recommendations for future research on the facility. The analytical model over-predicts the performance of the rock bed due to the assumptions made in the model. A model that includes the buoyancy effect, introduces thermal losses and regards radiation and convection will most likely produce a better prediction of the facility's performance. Extensive Computational Fluid Dynamics modeling of the existing facility is recommended, specifically focusing on the different void fractions throughout the rock bed to predict both the thermocline progression and thickness.

Appendices

Appendix A

Material Specification

A.1 Insulation

INSULPRO cc

52 5th STREET, BOOYSENS RESERVE, JOHANNESBURG, 2091
 P.O. BOX 38653,
 BOOYSENS 2016
 mail@insulpro.co.za

Reg. No. 1997/029725/23

TELEPHONES: 835-2127/8/9
 TELEFAX: 496-1263
 www.insulpro.co.za



SUPPLIERS OF INSULATION & ALLIED PRODUCTS

PRODUCT DATA SHEET INSULATION MATTRESS

PRODUCT NAME	ROCKWOOL MATTRESS
MANUFACTURING SPECIFICATION	BS3958 Part 3 & ASTM C592-97
BASE MATERIAL	BASALTIC ROCK MIX
PHYSICAL	WIRE MESH BACKED FIBROUS MATTRESS
BINDER	PHENOL BASED THERMOSETTING BINDER
BINDER CONTENT	± 1%
EFFECTIVE FIBRE DIAMETER	± 6 µm
THERMAL CONDUCTIVITY (35°C)	0.036 W/mK
RECOMMENDED OPERATING TEMPERATURE	< 750°C
FIRE CLASSIFICATION	NON COMBUSTIBLE
MASS DENSITY CLASSIFICATION	± 15%
DIMENTIONAL TOLERANCE	< 5%
TOTAL SHOT CONTENT	± 30%
PACKAGING	SHRINKED WRAPPED POLYETHYLENE

PRODUCT DATA SHEET
INSULATION BOARDS

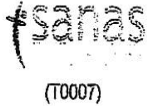
PRODUCT NAME	ROCKWOOL BATT / BOARD
MANUFACTURING SPECIFICATION	BS3958 Part 5 & ASTM C612-93
BASE MATERIAL	BASALTIC ROCK MIX
PHYSICAL	SEMI RIGID FIBROUS BOARD
BINDER	PHENOL BASED THERMOSETTING BINDER
BINDER CONTENT	± 2.5%
EFFECTIVE FIBRE DIAMETER	± 6 µm
THERMAL CONDUCTIVITY (35°C)	0.036 W/mK
RECOMMENDED OPERATING TEMPERATURE	< 750°C
FIRE CLASSIFICATION	NON COMBUSTIBLE
MASS DENSITY CLASSIFICATION	± 15%
DIMENTIONAL TOLERANCE	< 5%
TOTAL SHOT CONTENT	± 30%
PACKAGING	POLYETHYLENE BAGS

PRODUCT DATA SHEET
INSULATION LOOSE WOOL

PRODUCT NAME	ROCKWOOL LOOSE WOOL
MANUFACTURING SPECIFICATION	BS3958
BASE MATERIAL	BASALTIC ROCK MIX
PHYSICAL	LOOSE ROCKWOOL FIBRE
BINDER	UNRESINATED
BINDER CONTENT	NONE

EFFECTIVE FIBRE DIAMETER	$\pm 6 \mu\text{m}$
THERMAL CONDUCTIVITY (35°C)	0.032 W/mK
RECOMMENDED OPERATING TEMPERATURE	< 750°C (> - 200°C)
FIRE CLASSIFICATION	NON COMBUSTIBLE
MASS DENSITY CLASSIFICATION	N/A
DIMENTIONAL TOLERANCE	N/A
TOTAL SHOT CONTENT	$\pm 30\%$
PACKAGING	POLYETHYLENE BAGS

Products are made from non-combustible fibres containing inherently low levels of water leachable chlorides.



CSIR Consulting & Analytical Services

Environmental Laboratory – Pretoria

Fax: +27 +12 841-4653
Alt Tel: +27 +12 841-2261
E-mail: CAAdlem@csir.co.za

(T0007)

P O Box 395, Pretoria
Building 21, Room A107/A119
Meiring Naude Road
Brummeria, Pretoria

Vat No: 4470114283


Certificate of Analysis

Report 8638
Date Received 30-Jul-10
Sample description TCLP Leachate
No. samples received 2
Start date 02/08/2010

(Page 1 of 2)

Labnum		79251	79252
SampleId		Control	TCLP Rock-Fibre
Aluminium	mg/l Al	0.07	1.1
Antimony	mg/l Sb	<0.07	<0.07
Arsenic (inorg)	mg/l As	<0.002	<0.002
Barium	mg/l Ba	<0.03	0.06
Cadmium	mg/l Cd	<0.003	<0.003
Calcium	mg/l Ca	<0.53	178
Chloride	mg/l Cl	<5	<5
Chromium6	mg/l Cr	<0.02	<0.02
Chromium	mg/l Cr	<0.02	<0.02
Cobalt	mg/l Co	<0.03	<0.03
Copper	mg/l Cu	<0.03	<0.03
Fluoride	mg/l F	<0.2	0.38
Iron	mg/l Fe	<0.03	33
Lead	mg/l Pb	<0.02	<0.02
Magnesium	mg/l Mg	<0.46	96
Manganese	mg/l Mn	<0.03	4.2
Mercury (tot)	mg/l Hg	<0.001	<0.001
Nickel	mg/l Ni	<0.03	<0.03
Nitrate nitrogen	mg/l N	<0.2	<0.2
Potassium	mg/l K	<0.8	7
Selenium (inorg)	mg/l Se	<0.003	<0.003
Silver	mg/l Ag	<0.03	<0.03
Sodium	mg/l Na	1450	1460
Sulphate	mg/l SO4	<5	<5
Titanium	mg/l Ti	<0.03	0.03
Vanadium	mg/l V	<0.02	0.03
Zinc	mg/l Zn	<0.02	0.16
Zirconium	mg/l Zr	<0.07	<0.07

This report relates only to the samples actually supplied to CSIR CONSULTING AND ANALYTICAL SERVICES. The Operation Unit does not accept responsibility for any matters arising from the further use of these results. This certificate shall not be reproduced, except in full, without the written approval of the Laboratory Manager. No references may be made to the CSIR or any of its Operation Units or Officers in advertisements or for sale or publicity purposes without the CSIR's prior approval. All work is undertaken according to the CSIR General Conditions of Contract. Samples are discarded after 30 days from issue date of certificate.

Signed:  C. Adlem : Manager (Inorganic Chemistry)

Date: 08/09/2010



Tel: +27 +12 841 2261 /4858
 Fax: +27 +12 841-4653
 E-mail: CAclern@csir.co.za
 Email: YSingmin@csir.co.za

Consulting and Analytical services

Environmental laboratory – Pretoria

P O Box 395, Pretoria
 Building 21
 Meiring Naude Road
 Brummeria, Pretoria

Analytical Report

This report contains opinions, and discuss results etc. and is thus not covered by the accreditation certification of the chemical laboratory.

A Rockfibre sample was submitted the CSIR environmental laboratory to analyse for water soluble chloride and fluoride. The sample is highly absorbent difficult to filter using a standard vacuum system. Procedure 1 was applied to resolve the limitation.

Procedure 1:

In order to achieve a lower detection limit 100g of rock fibre was carefully saturated with 100ml of deionised water and allowed to stand for 12 hours. Due to the absorbent characteristic shaking was not a practical method. Filtration yielded only 30ml of sample. This was analysed for chloride and fluoride on a ion chromatograph first and then through the conventional accredited analyses.

Analytical procedures.

- a) Our accredited analytical methods were used namely flow injection analyses (colorimetric) for chloride and ion selective electrode analyses for fluoride content.
- b) A non - accredited method using ion chromatography for both chloride and fluoride analyses.

The results are listed in Table 1.

Table 1: Rock Fibre			
Procedure		1a	1b
Chloride in leachate	mg/l Cl	<5	0.9
Fluoride in leachate	mg/l F	2.3	2.6
Chloride leached from rock fibre	mg/kg Cl	<5	0.9
Fluoride leached from rock fibre	mg/kg F	2.3	2.6

A.2 Stainless Steel

Grade		Composition Specification (%)								
		C	Mn	Si	P	S	Cr	Mo	Ni	N
304	min.	-	-	-	-	-	17.5	-	8.0	-
	max.	0.07	2.0	0.75	0.045	0.030	19.5	-	10.5	0.10
304L	min.	-	-	-	-	-	17.5	-	8.0	-
	max.	0.030	2.0	0.75	0.045	0.030	19.5	-	12.0	0.10
304H	min.	0.04	-	-	-	-	18.0	-	8.0	-
	max.	0.10	2.0	0.75	0.045	0.030	20.0	-	10.5	-

Grade	Tensile Strength (MPa) min	Yield Strength 0.2% Proof (MPa) min	Elongation (% in 50mm) min	Hardness	
				Rockwell B (HR B) max	Brinell (HB) max
304	515	205	40	92	201
304L	485	170	40	92	201
304H	515	205	40	92	201

304H also has a requirement for a grain size of ASTM No 7 or coarser.

Grade	Density (kg/m ³)	Elastic Modulus (GPa)	Mean Coefficient of Thermal Expansion			Thermal Conductivity		Specific Heat (J/kg.K)	Electrical Resistivity (nΩ.m)
			0-100°C (μm/m/°C)	0-315°C (μm/m/°C)	0-538°C (μm/m/°C)	at 100°C (W/m.K)	at 500°C (W/m.K)		
304/L/H	7900	193	17.2	17.8	18.4	16.3	21.5	500	720

Grade	UNS No	Euronorm		Swedish SS	Japanese JIS
	No	No	Name		
304	S30400	1.4301	X5CrNi18-10	2332	SUS 304
304L	S30403	1.4307	X2CrNi18-9	2352	SUS 304L
304H	S30409	1.4948	X6CrNi18-11	-	-

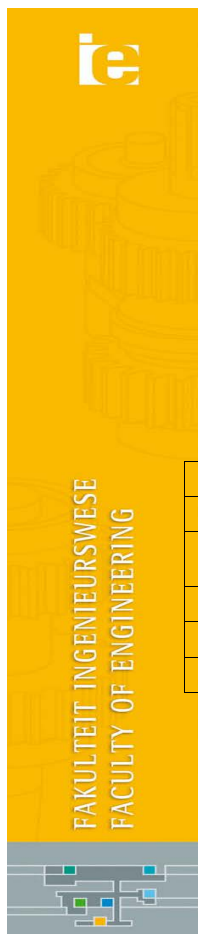
These comparisons are approximate only. The list is intended as a comparison of functionally similar materials **not** as a schedule of contractual equivalents. If exact equivalents are needed original specifications must be consulted.

Grade	Why it might be chosen instead of 304
301/L	A higher work hardening rate grade is required for roll formed or stretch formed components.
F20S	Lower cost needed in thin gauge sheet and coil. Durinox F20S also has easier fabrication.
303	Higher machinability needed; lower corrosion resistance, formability & weldability are acceptable
316	Higher resistance to pitting and crevice corrosion is required, in chloride environments
253MA	Better resistance high temperatures is needed. 253MA is optimised for temperatures to 1150°C.
430	A lower cost is required, and the reduced corrosion resistance and fabrication characteristics are acceptable.

Limitation of Liability
The information contained in this datasheet is not an exhaustive statement of all relevant information. It is a general guide for customers to the products and services available from Atlas Steels and no representation is made or warranty given in relation to this document or the products or processes it describes.

Appendix B

Safety Report



Stefaans Erasmus
18/09/2017

MEng Safety Report:

Testing of the Thermal Rock Bed Storage Pilot Plant

Date: September 2017

Supervisor: Prof TW Von Backström

Student: Stefaans Erasmus

Site Technician: Stefaans Erasmus

Emergency Contacts:

Contact	Room	Work	Cell
Mr Ferdi Zietsman	M212	4954	083 233 1646
Prof TW Von Backström	M525	021 808 4267	-
Campus Security	-	021 808 2233	-
Fire Brigade	-	887 1333	-
Ambulance	-	883 3444	-

Pressure Vessels or Pipes: No pressure vessel or pipe with a pressure in excess of 50 kPa is involved in this project

Stefaans Erasmus
18/09/2017

Site Technician (Mr Stefaans Erasmus)

Supervisor (Prof TW Von Backström)

Laboratory Manager (Mr Cobus Zietsman)

Overview:

The testing of a thermal rock bed storage plant is to be performed. The testing will be performed at Mariendahl farm outside of Stellenbosch at Elsenburg Agricultural College. The purpose of the testing is to test the thermal rock bed storage systems efficiency regarding heat recovery. The results will be used to compare to the new pilot plant as well as to other thermal storage systems.

In order to get accurate results, repeatability of testing will be required. This will allow for testing of various scenarios that the storage system will undergo.

The type of testing will include both charging and discharging cycles. Below is a description of both the equipment and approximate number of tests.

Equipment for testing:

Item	Quantity
LPG Bottle	10 x 48kg
Gas line	1
Gas Burner	1
Thermocouple	55
Fan	1
Laptop	1
Gas valve	2
Vaporizer Switch	1



Butterfly Valve	3
Gate	3
Electricity box	1
Gas House	1
Storage	1
Cover	1
Venting hole	8
Testing box	1

Activity	Quantity
Charging	10
Discharging	10

Note: Discharging excludes the following equipment: LPG Gas, Gas Burner, Gas line.

General Site Safety:

The following general site safety instructions are applicable:

- Closed shoes must be worn at all times.
- During construction, a hard hat must be worn at all times.
- No loose clothing.
- Follow the testing procedure carefully during testing.
- Leave the site neat and tidy, as found.
- Always be aware of your surroundings.
- Stay clear of extracted heat during discharging cycle.
- Wear protective heat gloves during discharging cycle.
- Always be accompanied by second person.



Stefaans Erasmus
18/09/2017**Activity based risk assessment:**

Activity	Risk	Risk Type	Likelihood	Exposure	Consequence	Risk Score	Mitigating Steps
Entering site	Hand injuries at the gate	P	3	3	1	9	Be cautious when opening and closing the gate
Moving around site	Stepping into a hole	P	3	3	7	63	Be cautious of where you walk
Opening the gas house gate	Hand injury	P	3	3	1	9	Be careful of sharp edges
Opening the gas bottles	Hand injury	P	3	3	1	9	Support the bottle with one hand while opening with another
Starting the vaporiser	Hand injury	P	3	3	1	9	Be careful of clamping your hand
Opening gas valves	Hand injury	P	3	3	1	9	Be careful of any sharp edges



Switch on the mains	Tripping the electrical supply	E	3	2	7	42	Make sure there are no open cables or wet spots where the cable/switch is
	Shocking yourself	P	1	1	40	40	Be sure to wear rubber soles and safety gloves.
Connecting the fan with the electrical box	Electrical short	E	0.5	2	7	7	Ensure the plug is clean of any dirt
Purge	Spontaneous combustion	E	3	1	40	120	Ensure that the burner is switched off during purging
Moving between fan and data box	Tripping over gas line	E	3	3	1	9	Be aware of where you walk
Open/closing of butterfly valves	Hand injury	P	3	3	1	9	Wear safety gloves
Open/closing of butterfly valves	Pressure build up tearing cover apart	E	3	2	7	42	Ensure the outlet valve is open
Being on site	Sunburn	P	6	3	1	18	Apply sunscreen

LPG Bottles	Explosion	E	0.2	3	100	60	Carefully follow experimental procedure and do not operate flames/sparks near LPG bottles
Los of electricity	Melting/damaging of cover	E	3	2	7	42	Open the vents in the cover to ventilate
Removing the hot pipe outlet	Burning your hands	P/E	3	3	1	9	Wear safety gloves
Climbing the ladder	Falling	P	3	3	1	9	Ensure the ladder is stable

Testing Procedure

Below a detailed description of both test procedure for both the charging and discharging cycles.

1.1 Charging Cycle

- Open the gas house.
- Open all the LPG bottles.
- Start the vaporiser to allow it to warm up.
- Open all the valves on the gas line.
- Open the valve to the hot pipe as well as the exit valve.
- Close the valve between the fan and the cold pipe.
- Switch on the main switch in the electricity box.
- Connect the fan to the electricity box.
- Switch on the fan and let it run for at least 5 minutes for purge purposes.
- Switch on the burner after purging is complete. Testing will now begin.

1.2 Discharge Cycle

- Switch off the burner.
- Close the gas line valves.
- Switch off the vaporiser.
- Close all the LPG bottles.
- Let the fan run for approximately 5 minutes through the hot pipe.
- Open the outlet of the hot pipe.
- Open the valve to the cold pipe and close both the other valves.



- Note the temperature of the burner box. If it rises above 32°C, open the valve to the hot pipe 1/8 to cool down the burner box until the temperature is below 28°C and then close the valve.

1.3 Switching off the system

- This occurs after discharge
- Open the hot valve 1/8 and reduce the fan speed.
- Close the cold valve.
- Let the cold air cool down the burner box.
- Switch off the fan after approximately 5min.
- Open the cold valve exit ¼ to allow all access air to leave the storage.
- Close the outlet of the hot pipe.
- Disconnect the fan and switch off the mains.



Appendix C

Operation Manual

For operation of the Rock Bed TESS, there are certain procedures that need to be followed, ensuring a successful test as well as a safe environment. Here follows a detailed manual, listing all components and explaining the correct procedure in operating the system during charge and discharge.

C.1 Components

Table C.1 lists all components needed to operate the TESS, with a brief description of each component's function. Other components not listed include: Local Area Network (LAN) cable, electric cable and a multiple port adapter. A detailed safety report is set out in Appendix B.

Table C.1: TESS components

Component	Function Description
Gas bottles	Contains Liquefied Petroleum Gas (LPG) that is in the burner.
Vaporizer	Warms the LPG to the desired state for burning
Gas train	The pipeline which transports the gas to the burner. Consists of multiple components
Burner	Burns the gas, heating air in the process
Centrifugal fan	Supplies air at a user defined flow rate
Variable speed drive (VSD)	Allows the user to define a flow rate for the air supplied by the fan
Electrical box	Houses all the on/off switches of each component
Data box	Houses the data cards
Data cards	Allows the user to collect the thermocouple temperatures
Burner control panel	Gives feedback regarding the burner performance and houses the controls of the burner
Pressure transducer	Supplies data regarding the air flow rate and pressure drop of the system
Data Logger	Logs all data received from the data cards
Laptop	Collects and saves all data logged by the data logger

C.2 Charge Cycle Procedure

The charge cycle procedure is explained in the array of figures that follow, with an explanation under each. Following the procedure is critical. An important point to keep in mind is that 480 kg of LPG allows for a charge time between 17 hours and 18 hours for an inlet mass flow rate of 0.5 kg/s.

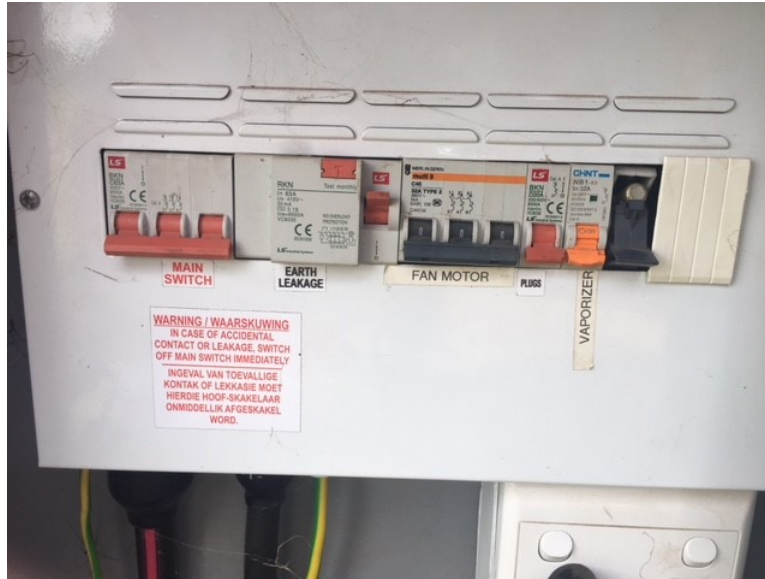


Figure C.1: The electrical box housing all main switches

Figure C.1 shows the main switches setup of the electrical box. The main switch on the far left should be switched on before any other. The switch on the far right, as indicated, is the burner switch. It contains a fuse that must be pushed into the box to switch on the burner controls, illustrated in Figure C.12.



Figure C.2: Vaporizer Switch

A very important step towards activating the facility is to switch on the vaporizer to warm up. By the time all other activations are completed the vaporizer should be warm enough. The vaporizer switch is illustrated in Figure C.2 and is situated against the gas house wall.



Figure C.3: The main setup that runs the cycles

Figure C.3 illustrates the centrifugal fan, burner box, electrical box, gas train and piping system of the facility. Notice the cable connecting the VSD to the centrifugal fan



Figure C.4: The valve setup for a charge cycle

The valve setup for a charge cycle to be commence is illustrated in Figure C.4 and explained from left to right. Valve 1 is open to allow airflow from the

centrifugal fan to the burner. Valve 2 is closed to prevent any air to flow from the fan to the cold pipe. Valve 3 is open to allow air to exit the cold pipe and into the atmosphere.



Figure C.5: VSD that controls the centrifugal fan

The VSD illustrated in Figure C.5 controls the speed of the centrifugal fan. The controls are easy: up increases the speed, down decreases the speed, green is start and red is stop. The speed is displayed in Hz, with the fan capable of a speed of up to 50 Hz. Start the fan to run at a speed of 18 Hz.



Figure C.6: Gas train



Figure C.7: Gashouse housing the LPG bottles

Figure C.7 shows the building which houses all the LPG bottles. The vaporizer, illustrated in Figure C.8 is also situated in this building. make sure all the LPG bottles are open.



Figure C.8: The vaporizer



Figure C.9: Gas valve 1



Figure C.10: Gas valve 2

Open the valve shown in Figure C.9, which is situated between the LPG bottles and the vaporizer. Next open the valve situated below the vaporizer, illustrated in Figure C.10. Figure C.11 shows the third valve that need to be open. This valve is situated outside the building in the gas line that leads up to the gas train.



Figure C.11: Valve 3

Once the vaporizer has warmed up, the next step is to switch on the burner. The burner controls are illustrated in Figure C.12. Switch to "auto" as in-

licated on the control panel. In approximately 40 seconds the first stage will switch on, in which case the centrifugal fan speed must be increased to 25 Hz, or any other speed above 18 Hz depending on the mass flow rate is desired. The second stage of the burner should start up once the temperature reaches 400 °C and above. In the case where the first stage switches off after 2-3 seconds, turn the switch to "0", push the reset button for 3 seconds and then switch the burner to "auto". Repeat this sequence in the case where the burner switches off again. Remember that the burner can only start at speeds of 16-18 Hz, any faster than that and the first stage will not be able to fire.



Figure C.12: Burner Control Panel

When fully functional, both stages of the burner will operate until the temperature reaches 625 °C. The second stage will then switch off, the temperature will climb slightly before dropping to below 600 °C, where the second stage will switch back on again. The effect of this will be a sinus wave, with an average input temperature of between 615 °C and 640 °C.

C.3 Discharge Cycle Procedure

For the discharge procedure, the procedure will be discussed, with references to the figures in section C.2.

First, the burner should be switched off using the switch displayed in Figure C.12. Immediately after this is done, lower the fan speed to 18 Hz. Next, open the hatch illustrated in Figure C.13. Wear heat protective gloves and be careful, the steel is hot. Once the hatch is open, switch off the fan and insert the deflector scoop. Once this is completed, switch the valves around in Figure C.4, thus the open valves need to be closed and vice versa. To commence the discharge cycle, switch on the fan and set the desired speed. The hot air will now exit the rock bed through the hatch. While the discharge cycle is running, switch off the vaporizer at the switches illustrated in Figures C.1 and C.2. Also close gas valves 1, 2 and 3. The gas train is now closed and secure.



Figure C.13: Hatch

To switch off the whole system, switch off the fan and close the pipe valves. After making sure all data is collected and saved, switch off the mains and lock the electrical box and gas house.

Appendix D

Lessons Learned

During the course of this project many lessons were learned in regards to rock bed TESS and the infrastructure thereof. Avoidance or fixing of these problems/features are necessary for progress in the research of rock bed TESS. Each section discusses the problem/feature and suggests a solution.

D.1 Tarpaulin Cover

The use of a cover over the rock bed led to mass flow losses during discharge. It was identified that the mass flow losses occurred through the openings within the cover. These openings were designed during the previous project to be opened in the event of fan failure.

The cover is a major restriction to the facility. Remove the cover as a feature of the facility by introducing a hot fan that sucks the hot air out of the rock bed during discharge. By this introduction the rock bed outlet temperature during charge is not governed by the temperature rating of the cover, allowing for a charge up until $T_{in} = T_{out}$, reaching a fully charged rock bed. It will also eliminate all flow losses currently present in the system.

D.2 Flow Measurement

The mass flow measurement is done by measuring the pressure drop over the bell-mouth at fan inlet. Once it was identified that there is a flow leakage during discharge, the importance of measuring flow at various point became clear. This will allow for high accuracy.

When designing a piping system, install a section that consists of either a venturi or orifice. By measuring the pressure drop over the flow meter, the mass flow rate can be determined at two points in the system.

D.3 Hot Air Pipe

During the idle period there were thermal losses within the rock bed. These thermal losses occurred through the hot air pipe elbow which is situated at the top of the rock bed.

Introduce a valve that closes the hot air pipe during the idle period. This will keep the heat within the rock bed itself, minimizing heat losses as a result.

D.4 Mesh Frame

A larger void between the mesh and the rock bed free surface caused the heat to distribute within the rock bed as illustrated in Chapter 6. This limited the use of rock volume, together with the restriction of the tarpaulin cover.

There are a few options to rectify the problem. Firstly, the mesh frame can be removed as an element. This will allow the insulation to be situated directly onto the rock free surface, eliminating the void. Secondly, a larger mesh grid, together with the elimination of the steel structure, can be used to allow the rocks to fit into the mesh. Thirdly, the installation procedure can be altered. The mesh frame can be installed with a layer of insulation on the inside and then the rocks can be introduced into the mesh frame. Lastly, a finer rock can be introduced to the outside of the rock bed free surface to create a smaller void fraction, thus restricting flow in the area.

To increase the volumetric efficiency without altering the frame mesh, a one-way valve can be introduced within the hot air pipe. The idea is that during charge the valve will allow a certain amount of heat to travel down the hot air pipe to the bottom of the rock bed where it will be released. During discharge the valve will be closed and all the heat will be extracted through the top of the rock bed.

List of References

- ACIN (2016). Betz Micromanometer Manual.
Available at: <http://www.acin.nl/wp-content/uploads/2016/06/Betz-manual-NL-EN-web.pdf>
- Allen, K.G. (2010). Performance characteristics of packed bed thermal energy storage for solar thermal power plants. pp. 1–130.
- Allen, K.G. (2014). Rock bed thermal storage for concentrating solar power plants. pp. 1–205.
- Allen, K.G., Von Backström, T.W., Joubert, E.C. and Gauché, P. (2016). Rock bed thermal storage: Concepts and costs. *AIP Conference Proceedings*, vol. 1734, pp. 0–8. ISSN 15517616.
- Allen, K.G., Von Backström, T.W. and Kröger, D.G. (2013). Packed bed pressure drop dependence on particle shape, size distribution, packing arrangement and roughness. *Powder Technology*, vol. 246, pp. 590–600.
- Allen, K.G., Von Backström, T.W. and Kröger, D.G. (2015). Rock bed pressure drop and heat transfer: Simple design correlations. *Solar Energy*, vol. 115, no. Supplement C, pp. 525–536. ISSN 0038-092X.
- Çengel, Y.A. (2006). *Heat Transfer: A Practical Approach*. 3rd edn. McGraw-Hill, New York. ISBN 9780073250359.
- CFW Fans (2016). Centrifugal Fan Manual.
- Duffie, J.A., Beckman, W.A. and Worek, W.M. (2003). *Solar Engineering of Thermal Processes, 4th ed.*, vol. 116. ISBN 1118418123. [arXiv:1011.1669v3](https://arxiv.org/abs/1011.1669v3).
- EAI (2017). CSP, concentrated solar power, solar thermal, power plants, steam rankine, parabolic dish, trough, power tower, linear fresnel, thermal energy storage-Energy Alternatives India - EAI.in.
- EPRI, Black & Veatch, National Renewable Energy Laboratory, Sandia National Laboratories and Purdue University (2010). Solar Thermocline Storage Systems: Preliminary Design Study. Tech. Rep., Electric Power Research Institute, Palo Alto, California.

- Erasmus, S.J., Von Backström, T.W., Lubkoll, M. and Dinter, F. (2018*a*). Design and Development of a Next Generation Thermal Rock Bed Storage Experimental Facility. In: *SASEC 2018*.
- Erasmus, S.J., Von Backström, T.W., Lubkoll, M. and Dinter, F. (2018*b*). Design and Development of a Next Generation Thermal Rock Bed Storage Experimental Facility. In: *SolarPACES 2018*.
- Esence, T., Bruch, A., Molina, S., Stutz, B. and Fourmigué, J.F. (2017). A review on experience feedback and numerical modeling of packed-bed thermal energy storage systems. *Solar Energy*, vol. 153, pp. 628–654. ISSN 0038092X.
- Faas, S.E., Thorne, L.R., Fuchs, E.A. and Gilbertsen, N.D. (1986). 10 Mwe Solar Thermal Central Receiver Pilot Plant - Thermal storage subsystem evaluation - Final report. Tech. Rep..
- Gauché, P. and Louw, A.D.R. (2014). Cone rock bed thermal energy storage system, South African Provisional Patent, 2014/03555, Stellenbosch University. Available at: <http://www.innovus.co.za/assets/files/TechnologiesEnglish/CONEROCKBEDTHERMALENERGYSTORAGESYSTEM.pdf>
- Hallet, R.W.J. and Gervais, R.L. (1977). Central receiver solar thermal power system - Phase 1 - CDRL ITEM 2 - Pilot Plant Preliminary Design Report - Vol V - Thermal Storage Subsystem. Tech. Rep..
- Herrmann, U., Kelly, B. and Price, H. (2004). Two-tank molten salt storage for parabolic trough solar power plants. *Energy*, vol. 29, no. 5-6, pp. 883–893. ISSN 03605442. arXiv:1011.1669v3.
- Hoffmann, J.-F., Fasquelle, T., Goetz, V. and Py, X. (2016). A thermocline thermal energy storage system with filler materials for concentrated solar power plants: Experimental data and numerical model sensitivity to different experimental tank scales. *Applied Thermal Engineering*, vol. 100, pp. 753–761. ISSN 1359-4311. Available at: <https://www.sciencedirect.com/science/article/pii/S1359431116300606>
- Hollands, K.G.T. and Sullivan, H.F. (1984). Pressure drop across rock bed thermal storage systems. *Solar Energy*, , no. 32, pp. 343–348.
- Hughes, P.J. (1975). *The Design and Predicted Performance of Arlington House*. Ph.D. thesis, University of Wisconsin-Madison.
- Incropera, F., DeWitt, D., Bergman, T. and Lavine, A. (2007). *Introduction to Heat Transfer*. 5th edn. John Wiley & Sons, Inc., Hoboken, NJ, USA. ISBN 9780471457282.
- International Renewable Energy Agency (IRENA) (2018). *Renewable capacity statistics 2018*. ISBN 9789295111905.
- Kolb, G.J., Ho, C.K., Mancini, T.R. and Gary, J.A. (2011). Power Tower Technology Roadmap and cost reduction plan. , no. April. ISSN 9781620814239.

- Kröger, D.G. (2011). SUNSPOT: The Stellenbosch UNiversity Solar POver Thermodynamic cycle. pp. 1–3. ISSN 0717-6163. [arXiv:1011.1669v3](https://arxiv.org/abs/1011.1669v3).
- Kröger, D.G. (2013). Packed rockbed thermal storage facility, South African Provisional Patent, 2013/03068, Stellenbosch University.
- Laubscher, H.F. (2017). *Developing and testing a cost effective thermal rock bed storage system*. Master's Thesis, Stellenbosch University.
- McDonnell Douglas Astronautics Company (1986). 10 MWe Solar Thermal Central Receiver Pilot Plant Mode 5 (Test 1150) and Mode 6 (Test 1160) Test report, Sandia National Laboratories. Tech. Rep..
- Pacheco, J.E., Showalter, S.K. and Kolb, W.J. (2002). Development of a molten-salt thermocline thermal storage system for parabolic trough plants. *Solar Energy Engineering*, pp. 153–159.
- Schumann, T.E.W. (1929). Heat transfer: A liquid flowing through a porous prism. *Journal of the Franklin Institute*, vol. 208, no. 3, pp. 405–416. ISSN 0016-0032. Available at: <https://www.sciencedirect.com/science/article/pii/S0016003229911868>
- Shewen, E.C., Sullivan, H.F., Hollands, K.G.T. and Balakrishnan, A.R. (1978). A heat storage subsystem for solar energy - Final Report - Phase 2, STOR - 6. Tech. Rep..
- SolarGIS (2015). South-Africa-DNI-solar-resource-map. Available at: <https://solargis.com/maps-and-gis-data/download/south-africa/>
- Stine, W.B. and Geyer, M. (2001). *Power From The Sun*. Available at: <http://www.powerfromthesun.net>
- Trieb, F., Schillings, C., Sullivan, M.O., Pregger, T. and Hoyer-klick, C. (2009). Global Potential of Concentrating Solar Power. In: *SolarPACES*, vol. 0, pp. 1–11. ISBN 9781420083699.
- Von Backström, T.W., Allen, K.G. and Joubert, E.C. (2012). Rock Bed Thermal Storage: Pilot Plant Concept Design and Application (Report 2). vol. 5, no. 1, pp. 1–16.
- Von Backström, T.W., Erasmus, S.J. and Laubscher, H.F. (2017). Next-Generation Thermal Rock Bed Energy Storage Concept, Provisional Patent.
- Wait But Why (2014). Energy. Available at: <http://waitbutwhy.com/2014/03/energydummies.html>
- Zanganeh, G., Commerford, M., Haselbacher, A., Pedretti, A. and Steinfeld, A. (2014). Stabilization of the outflow temperature of a packed-bed thermal energy storage by combining rocks with phase change materials. *Applied Thermal Engineering*, vol. 70, no. 1, pp. 316–320. ISSN 13594311.

Zanganeh, G., Pedretti, A., Zavattoni, S., Barbato, M. and Steinfeld, A. (2012). Packed-bed thermal storage for concentrated solar power - Pilot-scale demonstration and industrial-scale design. *Solar Energy*, vol. 86, no. 10, pp. 3084–3098. ISSN 0038092X.